



UNIVERSIDADE ESTADUAL DE CAMPINAS
INSTITUTO DE GEOCIÊNCIAS

DOUGLAS TEIXEIRA MARTINS

A DECRATONIZAÇÃO NA GÊNESE DOS DEPÓSITOS DE FERRO NO
SUDOESTE DA PROVÍNCIA BORBOREMA E NOROESTE DO CRÁTON SÃO
FRANCISCO

DECRAZTONIZATION IN THE GENESIS OF IRON DEPOSITS IN THE SOUTHEAST OF
THE BORBOREMA PROVINCE AND NORTHWEST OF THE SÃO FRANCISCO
CRATON

CAMPINAS

2024

DOUGLAS TEIXEIRA MARTINS

A DECRATONIZAÇÃO NA GÊNESE DOS DEPÓSITOS DE FERRO NO
SUDOESTE DA PROVÍNCIA BORBOREMA E NOROESTE DO CRÁTON SÃO
FRANCISCO

DECRAZONIZATION IN THE GENESIS OF IRON DEPOSITS IN THE SOUTHEAST OF
THE BORBOREMA PROVINCE AND NORTHWEST OF THE SÃO FRANCISCO
CRATON

TESE APRESENTADA AO INSTITUTO DE
GEOCIÊNCIAS DA UNIVERSIDADE
ESTADUAL DE CAMPINAS PARA
OBTENÇÃO DO TÍTULO DE DOUTOR
EM CIÊNCIAS NA ÁREA DE GEOLOGIA
E RECURSOS NATURAIS

THESIS PRESENTED TO THE INSTITUTE
OF GEOSCIENCES OF THE UNIVERSITY OF
CAMPINAS TO OBTAIN THE DOCTOR IN
SCIENCIES IN AREA OF GEOLOGY AND
NATURAL RESOURCES

ORIENTADOR: PROF. DR. WAGNER DA SILVA AMARAL

ESTE EXEMPLAR CORRESPONDE À
VERSÃO FINAL DA TESE DEFENDIDA PELO
ALUNO DOUGLAS TEIXEIRA MARTINS E
ORIENTADA PELO PROF. DR. WAGNER DA
SILVA AMARAL.

CAMPINAS

2024

Ficha catalográfica
Universidade Estadual de Campinas (UNICAMP)
Biblioteca do Instituto de Geociências
Marta dos Santos - CRB 8/5892

Martins, Douglas Teixeira, 1990-
M366d A decratonização a gênese dos depósitos de ferro no sudoeste da Província Borborema e Noroeste do Cráton São Francisco / Douglas Teixeira Martins. – Campinas, SP : [s.n.], 2024.

Orientador: Wagner da Silva Amaral.
Tese (doutorado) – Universidade Estadual de Campinas (UNICAMP), Instituto de Geociências.

1. Ferro - Minas e mineração. 2. Sistema mineral. 3. Província Borborema. I. Amaral, Wagner da Silva, 1979-. II. Universidade Estadual de Campinas (UNICAMP). Instituto de Geociências. III. Título.

Informações Complementares

Título em outro idioma: Decratonization in the genesis of iron deposits in the southeast of the Borborema Province and northwest of the São Francisco Craton

Palavras-chave em inglês:

Iron - Mines and mining

Mineral system

Borborema Province

Área de concentração: Geologia e Recursos Naturais

Titulação: Doutor em Geociências

Banca examinadora:

Wagner da Silva Amaral [Orientador]

João Paulo Araújo Pitombeira

Felipe Grandjean da Costa

David Jozef Cornelius Debruyne

Emilson Pereira leite

Data de defesa: 24-06-2024

Programa de Pós-Graduação: Geociências

Identificação e informações acadêmicas do(a) aluno(a)

- ORCID do autor: <https://orcid.org/0000-0001-6543-1336>

- Currículo Lattes do autor: <http://lattes.cnpq.br/6979584389458681>



UNIVERSIDADE ESTADUAL DE CAMPINAS
INSTITUTO DE GEOCIÊNCIAS

AUTOR: Douglas Teixeira Martins

A DECRAVONIZAÇÃO NA GÊNESE DOS DEPÓSITOS DE FERRO NO SUDOESTE DA
PROVÍNCIA BORBOREMA E NOROESTE DO CRÁTON SÃO FRANCISCO

ORIENTADOR: Prof. Dr. Wagner da Silva Amaral

Aprovado em: 24 / 06 / 2024

EXAMINADORES:

Prof. Dr. Wagner da Silva Amaral - Presidente

Prof. Dr. Emilson Pereira Leite

Prof. Dr. David Jozef Cornelius Debruyne

Prof. Dr. João Paulo Araújo Pitombeira

Dr. Felipe Grandjean da Costa

*A Ata de Defesa assinada pelos membros da Comissão Examinadora consta no processo de
vida acadêmica do aluno.*

Campinas, 24 de junho de 2024.

SÚMULA/BIOGRAFIA

Douglas Teixeira Martins é geólogo, formado em 2014, e mestre em Geologia, concluído em 2017, ambos pela Universidade Federal do Ceará. Possui especialização em Inteligência Artificial e Machine Learning pela Universidade Cruzeiro do Sul (2024). Desde 2014, atua como professor de Geologia no Instituto Federal de Educação, Ciência e Tecnologia do Piauí (IFPI), onde ministra as disciplinas de Geoprocessamento, Pesquisa Mineral e Geologia Estrutural. Tem experiência no uso de Sistemas de Informações Geográficas (SIG) aplicados à exploração mineral, com enfoque no uso de técnicas de Aprendizado de Máquina para análise espacial. Sua pesquisa concentra-se no Orógeno Riacho do Pontal e no Terreno Granjeiro, localizados na Província Borborema, com foco no mapeamento prospectivo de minerais metálicos. Atualmente coordena o projeto Modelagem de Potencial Mineral para identificação de minério de Manganês na região de Paulistana - Piauí (EDITAL 6/2023 - PROPI/REI/IFPI - PIBIC EM CNPq – 2023) e contribui com o projeto Potencial de elementos terras-raras em depósitos de manganês e fosfato (UFC). Além disso, participa dos grupos de pesquisa Recursos Naturais e Educação do Nordeste (RENEDU - IFPI) e Evolução Crustal e Metalogênese (UNICAMP).

AGRADECIMENTOS

Gostaria de expressar a minha gratidão ao Prof. Dr. Wagner Amaral pelo seu constante empenho na minha trajetória acadêmica, desde a graduação até o doutorado, pela compreensão e, sobretudo, pela paciência ao longo de todo o doutorado. Sua orientação e conhecimento foram de suma importância para a elaboração desta tese, assim como para o meu crescimento moral.

Agradeço profundamente ao Instituto Federal do Piauí pelo estímulo à minha trajetória acadêmica através do meu afastamento e apoio ao longo deste tempo.

Aos meus amigos de universidade e de vida, Felipe Holanda, Evilarde, João Paulo e Daniel, que têm sido meus companheiros desde a graduação e mestrado, exercendo influência direta no meu conhecimento geológico.

Agradeço aos professores e servidores do IG que me acompanharam, Ticiano, Erica, Elson, Vinícius, Emilson, Gelvam e Alessandro Batezelli.

Aos amigos que fiz ao longo deste tempo, Robert, Ana Clara, Vínicus, Diógenes, José Henrique, Poly, Igor, Cleberson, André, Bruno, Laura e Josué, agradeço a companhia e o apoio.

Por fim, mas não menos relevante, agradeço à minha família e à minha esposa Mariana pelo apoio que tive durante todos esses anos de doutorado.

RESUMO

Nesta tese, discorremos, sob a perspectiva da hipótese de "decratonização" do Paleocontinente São Francisco (PSF), a origem e controle das mineralizações de ferro de alto teor associados às formações ferríferas (FF). Para isso, investigamos duas áreas: a primeira no noroeste do Cráton São Francisco (CSF), Complexo Sobradinho; a segunda no sudoeste da Província Borborema (PB), Terreno São Pedro. Depósitos de alto teor de ferro resultam da substituição gradual dos minerais primários de ferro e da remoção da sílica, influenciados pela percolação de fluidos hipogênicos e supergênicos. Neste sistema mineralizador, o contexto geodinâmico desempenha um papel crucial, por regular desde a sedimentação até o enriquecimento dos minerais. Para testar a hipótese de correlação entre as áreas de estudo, separadas durante a fragmentação do paleocontinente, e traçar os ambientes deposicionais do protominério, utilizamos gravimetria de satélites. Estes dados serviram para mapear estruturas crustais profundas, suas características geométricas e continuidades laterais. Além disso, utilizamos lineamentos gravimétricos para compreender os mecanismos de transporte dos fragmentos crustais. Em seguida, datamos, por U-Pb em zircão, rochas do embasamento coletadas ao longo das anomalias gravimétricas. Nossos dados revelaram uma conexão significativa entre as duas regiões de estudo, especialmente na distribuição de rochas plutônicas mesoarqueanas e o neoarqueanas, e sedimentações com idades máximas de deposição no Estateriano. Para compreender a influência da decratonização na formação dos depósitos, estudamos em escala regional o controle estrutural do Distrito Ferrífero de Curral Novo. Identificamos, por meio de dados litoestratigráficos disponíveis na literatura, levantamentos estruturais e sensoriamento remoto, quatro eventos deformacionais que atuaram na gênese do minério. O evento D1, relacionamos a colisão, que originou intensa atividade magmática em torno de 2.8-2.7 Ga e possíveis magmatismos anorogênicos em 2.6 Ga, causando circulação de fluidos hidrotermais. O evento D2 envolveu as rochas arqueanas do embasamento durante a colisão Transamazonica, conforme indicado pelas idades das bordas dos zircões e dados geoquímicos. Durante D3, por volta de 1.8-1.6 Ga em um contexto extensional, houve a preservação dos depósitos minerais e a circulação de fluidos hidrotermais. O evento D4, relacionamos ao desenvolvimento e reativações de zonas de cisalhamento durante o neoproterozoico, que influenciaram na circulação de fluidos hipogênicos e na geometria dos corpos de minério.

Palavras-chave: Decratonização; Depósitos de ferro; Cráton São Francisco; Província Borbo- rema.

ABSTRACT

In this thesis, we discuss, from the perspective of the "decratonic" hypothesis of the São Francisco Paleocontinent (PSF), the origin and control of high-grade iron mineralizations associated with iron formations (FF). To do this, we investigate two study areas: the first in the northwest of the São Francisco Craton (CSF), Sobradinho Complex; the second in the southwest of Borborema Province (BP), São Pedro Terrain. High-grade iron deposits result from the gradual replacement of primary iron minerals and the removal of silica, influenced by the percolation of hypogene and supergene fluids. The geodynamic context is crucial in this mineralizing system, regulating everything from sedimentation to mineral enrichment. We used satellite gravimetry to test the hypothesis of correlation between the study areas, separated during the fragmentation of the paleocontinent, and to delineate the depositional environments of the protore. These data were used to map deep crustal structures, geometric characteristics, and lateral continuities. Additionally, we used gravimetric lineaments to understand the mechanisms of crustal fragment transport. We then dated basement rocks collected along the gravimetric anomalies using U-Pb on zircon. Our data revealed a significant connection between the two study regions, especially in mesoarchean and neoarchean plutonic rocks distribution and sedimentations with maximum deposition ages in the Ectasian. To understand the influence of decratonic on deposit formation, we studied the structural control of the Curral Novo Iron District at a regional scale. We identified four deformational events that acted on ore genesis through available lithostratigraphic data in the literature, structural surveys, and remote sensing interpretations. Event D1 relates to collision, which originated intense magmatic activity around 2.8-2.7 Ga and possible anorogenic magmatism around 2.6 Ga, causing hydrothermal fluid circulation. Event D2 involved Archean rocks of the basement during the Transamazonian collision, as indicated by zircon rim ages and geochemical data. During D3, mineral deposits were preserved around 1.8-1.6 Ga in an extensional context, and hydrothermal fluids circulated. Event D4 relates to developing and reactivating neoproterozoic shear zones, which influenced hypogene fluid circulation and ore body geometry.

Keywords: Decratonic; Iron deposits; São Francisco Craton; Borborema Province.

LISTA DE ILUSTRAÇÕES

Figura 1.1 – Contexto geológico regional simplificado da Província Borborema e Cráton São Francisco, indicando as áreas de estudos. Dados obtidos e compilados do Repositório Institucional de Geociências (RIGEO) do Serviço Geológico do Brasil.....	16
Figura 2.1 – Anomalia Bouguer do Modelo EGM2008 para o território brasileiro. Em destaque a área de estudo.....	19
Figura 2.2 – Definicao geometrica do angulo de inclinacao. $\frac{\partial f}{\partial x}$ = derivada do campo na direção x, $\frac{\partial f}{\partial y}$ = derivada na direção y, $\frac{\partial f}{\partial z}$ = derivada na direção z, $\frac{\partial f}{\partial h}$ = gradiente horizontal do campo. O ângulo de inclinação, θ , é medido em relação à horizontal. Modificado de Miller & Singh (1994).....	20
Figura 3.1 – Distribuição espaço temporal das formações ferríferas e sua relação com a variação das atividades de plumas mantélicas (A)(segundo Abbott & Isley (2002)) e os níveis de oxigênio na atmosfera (linha tracejada em B)(modificado de Klein (2005)).....	22
Figura 3.2 – Ocorrências das FF quanto aos tipos deposicionais e suas distribuições globais em relação aos cráttons pré-cambrianos. Modificado de Beukes & Gutzmer (2008).....	23
Figura 3.3 – Tipos de ambientes deposicionais e relação espaço-temporal de Formações Ferríferas. (A) Classificação das FF em relação ao ambiente deposicional (modificado de Gross (1980)); Distribuição temporal dos números (B) e quantidades (C) de FF em relação ao ambiente de deposição ao longo do Pré-cambriano - modificado de Beukes & Gutzmer (2008)).....	24
Figura 3.4 – Modelo de fácies deposicionais de James (1954).....	25
Figura 3.5 – Elementos críticos de um Sistema Mineral. Modificado de McCuaig & Hronsky (2014).....	28

LISTA DE TABELAS

Tabela 3.1 – Principais minerais presentes na classificação das fácies de FF segundo James (1954).....	25
--	----

SUMÁRIO

1 Introducao.....	12
1.1 Area de estudo.....	14
1.1.1 Distrito Ferrifero de Curral Novo do Piaui.....	14
1.1.2 Formacoes Ferriferas de Sao Raimundo Nonato.....	15
1.2 Objetivo e Metas.....	17
2 Materiais e métodos.....	18
2.1 Gravimetria de Satelite.....	18
2.1.1 Filtragem dos dados.....	18
2.2 Levantamentos geologicos de campo.....	20
2.3 Datacoes U-Pb.....	20
3 Formacoes Ferriferas e Sistema Mineral de depositos de Fe.....	22
3.1 Formacoes Ferriferas.....	22
3.1.1 Ambientes de deposicao de FF.....	23
3.1.2 Classificação.....	25
3.1.3 Mineralogia e metamorfismo.....	26
3.2 Sistema mineralizador.....	27
3.2.1 Controles geotectonicos e origem dos fluidos.....	28
3.2.2 Controle estrutural.....	29
3.2.3 Modelos de depositos de Fe.....	30
4 Resultados.....	31
4.1 Exploring the Gravimetric and Geochronological Links in Ancient Terranes of the Sao Francisco Craton and Borborema Province, NE-Brazil.....	32
4.2 Sao Francisco Paleocontinent Construction, Fragmentation, and Reworking in the Mineral System Evolution of the Curral Novo Iron District.....	55
5 Discussão e Conclusões.....	89
Bibliografia.....	91
ANEXO I.....	106
ANEXO II.....	107
ANEXO III.....	108

1. Introdução

Existem duas principais unidades geológicas que compõem a superfície dos continentes: os crátions e os cinturões orogênicos. Os crátions ([Şengör et al. 2021](#)), ao contrário dos cinturões orogênicos, são áreas estáveis da litosfera continental que permaneceram rígidas por pelo menos 1 Ga ([Hoffman 1988; Hoffman 2014; Yoshida & Yoshizawa 2021](#)) e são cobertos por camadas significativas de rochas sedimentares. A estabilidade dos crátions está relacionada a raízes litosféricas mais espessas ([Sleep 2005; Peslier et al. 2010; Lee et al. 2011; Yoshida & Yoshizawa 2021](#)). Dois principais mecanismos explicam essa espessura: o empilhamento de litosferas oceânicas por acreção e por atuação de plumas mantélicas ressurgentes (subcreção da pluma) ([Arndt et al. 2009; Aulbach 2012; Griffin et al. 2003; Lee 2006; Pearson & Wittig 2008; Aulbach et al. 2007](#)). Essa litosfera mais espessa, embora empobrecida por fusão, confere maior flutuabilidade aos crátions arqueanos em comparação com a litosfera continental proterozoica ([Boyd 1989; Sleep 2005; Snyder et al. 2017](#)).

No entanto, é importante salientar que alguns crátions, considerados estáveis, passaram por eventos episódicos de rejuvenescimento ao longo de sua história ([Holdsworth et al. 2001; Lee et al. 2011; Wu et al. 2019; Kusky et al. 2014](#)). Esse processo de rejuvenescimento envolve a destruição dos crátions, conhecida como decratonização ([Gao et al. 2004; Menzies et al. 2007; Wu et al. 2019](#)), que é um fenômeno raro e foi bem estudado no Cráton do Norte da China (CNC) ([Yang et al. 2008](#)) e no Cráton do Wyoming ([Snyder et al. 2017; Kusky et al. 2014](#)). Vários modelos têm sido propostos para explicar o processo de decratonização ([Wu et al. 2019](#)), por exemplo, a erosão termomecânica ([Davies 1994; Ruppel 1995](#)) e química ([Bedini et al. 1997](#)), e delaminação ([Bird 1978; Bird 1979; Kay & Kay 1993](#)).

No Cráton do Norte da China (CNC), onde há um avanço considerável no entendimento da decratonização, dois modelos são usados para explicar o afinamento da litosfera durante o Mesozoico ([Wu et al. 2019; Li & Santosh 2014](#)). O modelo de erosão termomecânica ([Griffin et al. 1998; Menzies & Xu 1998; Li & Santosh 2014](#)), atribui a reciclagem da astenosfera e a ascensão da pluma do manto como a principal causa da erosão na base da litosfera. Em contrapartida, o modelo de delaminação ([Deng et al. 2004; Gao et al. 2002; Li & Santosh 2014](#)), que é a remoção da parte inferior da litosfera, particularmente do material eclogítico denso, que afunda no manto devido à sua alta densidade. Em ambos os modelos, as margens cratônicas e os limites entre microblocos são identificados como áreas de fraqueza que estão sujeitas à erosão termomecânica ou delaminação ([Li & Santosh 2014](#)).

Dentre os crátions da plataforma sul-americana, o Cráton São Francisco (SFC)

(Almeida et al. 1981), localizado no nordeste do Brasil, é notável por uma extensa pesquisa que abrange aspectos geocronológicos, geofísicos e evolutivos (Heilbron et al. 2017). O embasamento do SFC é constituído por núcleos arqueanos que registram eventos magmáticos entre 2,8-2,7 Ga (Teixeira et al. 2017). Durante a orogenia Rhyaciana-Orosiriana, esses núcleos foram aglutinados (Trompette et al. 1992; Barbosa & Sabaté 2004; Teixeira et al. 2017; Brito Neves 2011). O CSF é circundado por sistema orogênicos desenvolvidos entre sua colisão e de sua contraparte africana o Cráton do Congo, os crátions Amazônico e São Luiz-África Ocidental (Brito Neves et al. 2000).

Entre estes sistemas orogênicos destaca-se a Província Borborema (PB) (Almeida et al. 1981) que é constituída por blocos de núcleos arqueanos retrabalhados no Paleoproterozóico, os quais foram intrudidos por granitos neoproterozóicos e recobertos por bacias neoproterozóicas (Caxito et al. 2020). O CSF e o PB compartilham semelhanças pré-brasilianas, como a presença de rochas arqueanas, rochas siderianas, riftes intermitentes e eventos magmáticos intraplaca entre 1,78 e 1,50 Ga (Neves 2021). Devido a essas semelhanças, alguns pesquisadores sugerem a possibilidade de que os terrenos antigos do PB sejam produto da fragmentação do CSF, em um processo de decratonização (Neves 2021; Ganade et al. 2021), embora seus mecanismos ainda não estejam estabelecidos.

Os crátions e suas margens são conhecidos por conterem altas concentrações de depósitos minerais (Groves & Santosh 2021). Embora alguns trabalhos explorem a relação entre o processo de decratonização e a gênese de depósitos minerais, por exemplo, Li & Santosh (2014), Yang et al. (2022), Yang et al. (2021), Yang & Santosh (2020) e Li et al. (2022), estes abordam principalmente depósitos de ouro. Neste trabalho, procuramos entender, a partir da hipótese de decratonização do Cráton São Francisco (CSF), conforme discutido em Neves (2021) e Ganade et al. (2021), como este processo influenciou na formação dos depósitos de ferro associados às formações ferríferas da margem noroeste do CSF e no sudoeste da Província Borborema. Assim, a pergunta central é: de que modo a decratonização controlou a formação e distribuição regional desses depósitos de ferro?

Formações Ferríferas (FF) são rochas sedimentares químicas, que exibem camadas de ferro, com teores entre 20 e 30%, intercaladas por SiO₂ (James 1954; James 1983) e possuem ampla distribuição espaço-temporal, com registros do Arqueano ao Fanerozoico (Gross 1983; Klein 2005). A deposição destas rochas resultou da complexa interação entre processos mantélicos, tectônicos, oceanicos e biosféricos (Bekker et al. 2010). As FF pré-cambrianas foram divididas em dois tipos, o Tipo Superior e o Tipo Algoma, com base em suas características deposicionais e associações litológicas (Gross 1965; Gross 1980).

As FF do Tipo Superior foram depositadas em ambientes de margens passivas e hoje

são encontradas associadas a sequências plataformais cratônicas. Elas estão intercaladas com carbonatos, quartzo-arenitos, folhelhos negros e restritas rochas vulcânicas (Gross 1965; Gross 1980). Já as FF do Tipo Algoma estão associadas a sequências vulcanossedimentares em terrenos granito-*greenstone belts*. Sua gênese está relacionada a processos hidrotermais exalativos (Gross 1980; James 1983; Beukes & Gutzmer 2008; Bekker et al. 2010; Bekker et al. 2014).

O sistema mineralizador responsável pelo enriquecimento das FF é complexo e envolve a atuação conjunta de processo sin- e pós-deposicionais (Hagemann et al. 2016; Angerer & Hagemann 2010). Processos sin-deposicionais definem a fertilidade de ferro nas FF e estão relacionados a estratigrafia e características geodinâmicas dos ambientes deposicionais. Os processos pós-deposicionais são responsáveis pela dissolução da sílica e envolvem a percolação de fluidos hipogênicos e supergênicos, favorecida pela permeabilidade em varias escalas. Além disto estruturas geológicas atuam na exumação, geometria, preservação e modificação dos corpos mineralizados (Thorne et al. 2014).

Diante disso, o conhecimento geodinâmico regional assume papel fundamental na descoberta, exploração e desenvolvimento de depósitos de ferro associados a formações ferríferas. A compreensão da relação entre o processo de decratonização do CSF e a formação e distribuição dos depósitos é fundamental para o nosso estudo.

1.1. Área de estudo

Este projeto investigará duas formações ferríferas geograficamente correlatas, localizadas no nordeste do Brasil no estado do Piauí, porém situadas em diferentes contextos geológicos (Figura 1.1). A unidade investigada corresponde as rochas que hospedam o Distrito Ferrífero de Curral Novo (DFCN) (Sato 2011), situado no Terreno São Pedro (TSP) (Brito Neves et al. 2023), Zona Transversal da Província Borborema. A outra unidade corresponde as formações ferríferas do Complexo Sobradinho no município de São Raimundo Nonato, limite noroeste do Cráton São Francisco.

1.1.1. Distrito Ferrífero de Curral Novo do Piauí

O Distrito Ferrífero de Curral Novo (DFCN) (Sato 2011) localiza-se no setor sul do Terreno Granjeiro (TGS) no estado do Piauí. O Terreno São Pedro faz parte da Zona Transversal da Província Borborema (Figura 1). Esse terreno possui duas áreas de exposição (Vasconcelos &

Gomes 1998; Delgado et al. 2003): a primeira aflora no estado do Ceará; e a segunda abrange os estados do Piauí e Pernambuco. A continuidade entre esses dois setores está encoberta pela Bacia do Araripe.

O arcabouço tectônico do Terreno São Pedro é formado pelo embasamento, denominado Complexo Granjeiro e pela Sequência Metavulcanossedimentar Arrojado. O Complexo Granjeiro é constituído por gnaisses para- e ortoderivados de valores εNd positivos e idades modelo TDM Nd de 2, 65 e 2,55 Ga (Silva et al. 1997). A Sequência Metavulcanosedimentar Arrojado é composta por formações ferríferas, xistos, quartzitos, mármore, calcissilicáticas, metacherts, metabasitos anfibolitizados e metatufos félsicos e máficos (Vasconcelos & Gomes 1998; Gomes & Vasconcelos 2000) com idade de sedimentação entre 2.7 - 2.5 Ga (Ancelmi 2016).

O TSP apresenta três unidades o embasamento TTG, sequências metavulcanosedimentares e intrusões sienograníticas. O embasamento é formado por uma suíte TTGs gnáissico-migmatítica de idade paleoarqueana (Martins 2017; Vale 2018; Pitarello et al. 2019). As formações ferríferas estão associadas a sequências metavulcanosedimentares, intercaladas por unidades metamáficas e metaultramáficas (Costa 2010). Essas duas unidades foram intrudidas por sinenogranitos com idades de 2.6 Ga (Martins 2017; Vale 2018; Pitarello et al. 2019).

1.1.2. Formações Ferríferas de São Raimundo Nonato

A segunda área de estudo localiza-se no extremo noroeste do Cráton São Francisco e faz limite com a Província Parnaíba a oeste. Nessa região os litotipos podem ser divididos em três grandes grupos: o embasamento arqueano, os granitóides paleoproterozoicos e os sedimentos paleozoicos da Bacia do Parnaíba. O embasamento arqueano do cráton, formado pelos Complexo Sobradinho-Remanso (Souza et al. 1979), Lagoa da Ema (Souza et al. 1979) e Lagoa do Alegre (Angelim et al. 1997). Essas rochas são intrudidas pelos granitos paleoproterozicos Fartura do Piauí e Monte Alegre (Augusto et al. 2017).

As FF objeto de estudo fazem parte do Complexo Lagoa do Alegre. Esse complexo formado pelas unidades Minadorzinho e Macambira (Angelim et al. 1997). A Unidade Mina-dorzinho corresponde a rochas metavulcanosedimentar caraterizadas por micaxistas, gnaisses e quartzitos, além de metabasitos, mármore e formações ferríferas. A Unidade Macambira é constituída por metamáficas, metaultramáficas (talcoxistas), silexitos, paragnaisse e, menos frequentemente, metavulcânicas ácidas, calcários cristalinos, rochas calcissilicáticas e quartzitos (Augusto et al. 2017).

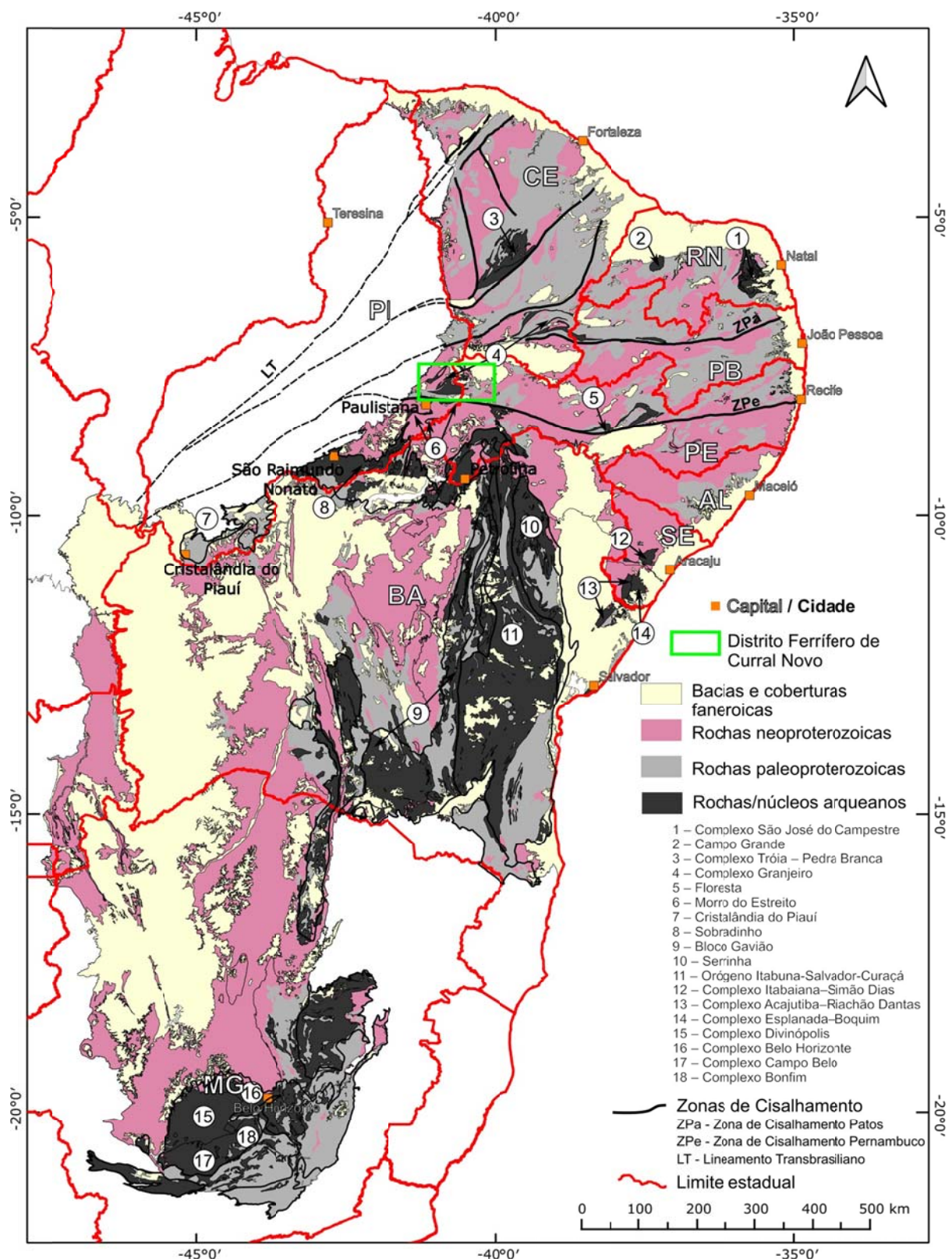


Fig. 1.1 – Contexto geológico regional simplificado da Província Borborema e Cráton São Francisco, indicando as áreas de estudos. Dados obtidos e compilados do Repositório Institucional de Geociências ([RIGEO](#)) do Serviço Geológico do Brasil.

1.2. Objetivo e Metas

O objetivo deste estudo foi investigar o papel da decratonização na influência na formação e distribuição dos depósitos de ferro localizados na região noroeste do Cráton São Francisco e no sudoeste da Província Borborema.

Metas de trabalho

- Estabelecer relação entre os blocos do embasamento do noroeste do CSF e sudoeste da Província Borborema;
- Definir a função das estruturas geológicas nos processos de enriquecimento dos protomínérios e na geometria das mineralizações;
- Investigar a possível correlação genética entre as FF que ocorrem em São Raimundo Nonato e as que hospedam o minério de ferro em Curral Novo do Piauí.
- Criar um modelo prospectivo regional de minério de ferro como base nos dados obtidos.

2. Materiais e métodos

2.1. Gravimetria de Satélite

Os dados gravimétricos de satélite são fundamentais para estudar as estruturas profundas da crosta terrestre, uma vez que informam sobre a geometria, direção, cinemática e continuidade laterais entre diferentes blocos crustais. Nesta tese, utilizamos os dados gravimétricos do modelo EGM2008 (Modelo Gravitacional da Terra de 2008 - *Earth Gravitational Model 2008*) para investigar os blocos crustais arqueanos-paleoproterozoicos remanescentes do Paleocontinente São Francisco, das margens NW do CSF e SW da Província Borborema.

O modelo EGM2008 é composto por grades médias com uma resolução de 2.5x2.5 minutos de arco, criadas a partir de uma combinação de dados gravimétricos terrestres, aéreos e de satélite (ITG-GRACE03S) ([Pavlis et al. 2012](#)). Este modelo tem uma abrangência até o grau 2190 e a ordem 2159, o que permite capturar variações extremamente precisas e detalhadas no campo gravitacional da Terra, tanto em termos de mudanças radiais quanto angulares ([Pavlis et al. 2012](#)). Isso resulta em uma representação precisa e detalhada da gravidade em várias regiões do planeta. A anomalia Bouguer Total utilizada foi obtida do *Bureau Gravimétrique International* (BGI), cujas correções são computadas em escalas regionais usando o método FA2BOUG ([Fullea et al. 2008](#)). A correção topográfica é aplicada em uma faixa de até 167 km, usando o modelo digital de terreno de 1 minuto de arco, ETOPO1, e densidade de redução de 2.67 g/cm³. A figura

[2.1](#) apresenta a anomalia Bouguer Total do território brasileiro, com destaque na área de estudo.

2.1.1. Filtragem dos dados

Para separar as fontes rasas e profundas da anomalia Bouguer Total, usamos o método de [Spector & Grant \(1970\)](#), que envolve a análise da inclinação da curva do espectro de potência. Aplicamos um filtro gaussiano com desvio padrão de 0.005 rad/km para separar o componente regional (baixa frequência) do componente residual (alta frequência). Utilizamos os softwares GMT e Oasis Montaj para realizar o processamento dos dados.

As componentes regional e residual da anomalias Bouguer foram realçadas usando ângulo de inclinação *Tilt angle* (Eq. [2.1](#)) ([Miller & Singh 1994](#)). Esse método extrai o ângulo tangente da razão entre a derivada vertical e horizontal ([Miller & Singh 1994](#)) (Fig. [2.2](#)), permitindo

individualizar anomalias de grande e pequenas amplitudes (varia entre $-\pi/2$ e $+\pi/2$). O ângulo de inclinação proporciona uma melhor visualização de fontes profundas, que, muitas vezes, são obscurecidas por fontes mais superficiais (Miller & Singh 1994), além de melhorar a delimitação de suas extensões laterais. Godin & Harris (2014), por exemplo, aplicaram o ângulo de inclinação aos dados de gravidade Bouguer do EGM2008 para identificar as direções dos campos potenciais que estão associados às estruturas geológicas regionais transversais aos Himalaias, interpretando-as como falhas cruciais.

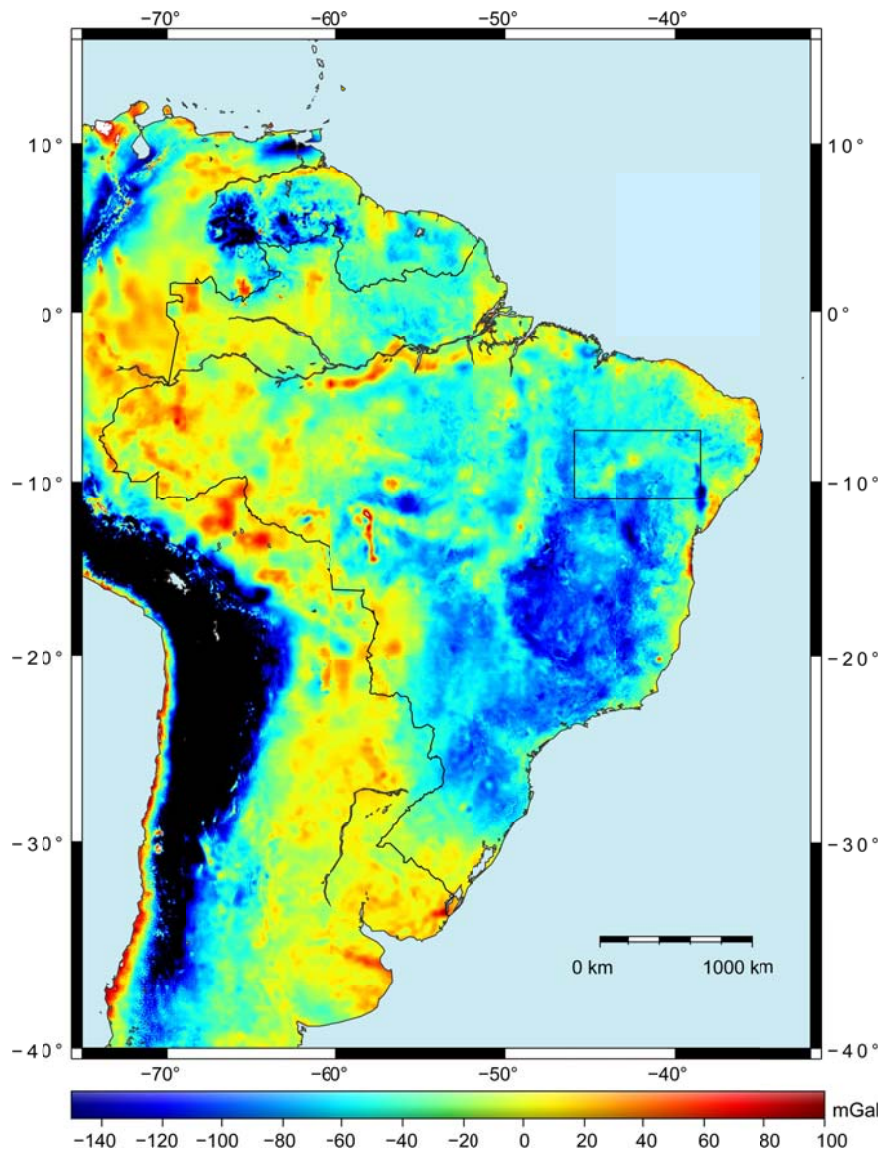


Fig. 2.1 – Anomalia Bouguer do Modelo EGM2008 para o território brasileiro. Em destaque a área de estudo.

$$\text{Tilt angle} = \tan^{-1} \left(\frac{\frac{\partial f}{\partial z}}{\sqrt{\left(\frac{\partial f}{\partial x}\right)^2 + \left(\frac{\partial f}{\partial y}\right)^2}} \right) \quad (2.1)$$

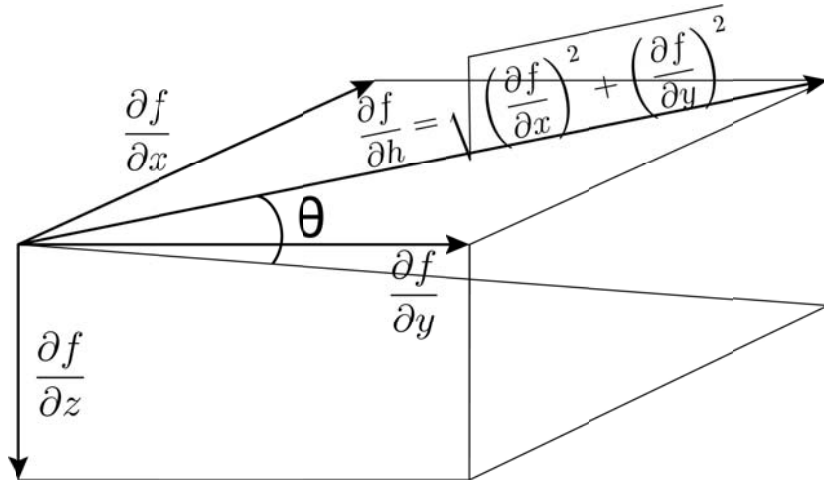


Fig. 2.2 – Definição geométrica do ângulo de inclinação. $\frac{\partial f}{\partial h}$ = derivada do campo na direção x, $\frac{\partial f}{\partial x}$ = derivada na direção y, $\frac{\partial f}{\partial y}$ = derivada na direção z, $\frac{\partial f}{\partial z}$ = gradiente horizontal do campo. O ângulo de inclinação, θ , é medido em relação à horizontal. Modificado de Miller & Singh (1994).

2.2. Levantamentos geológicos de campo

Esta etapa consistiu na definição dos litotipos metavulcanossedimentares encaixantes das mineralizações, suas relações de contato, discordâncias e empilhamento litoestratigráfico. Para isso foram realizados o levantamento bibliográfico e cartográfico das áreas de estudo, e o processamento e interpretação de imagens Landsat 8 - OLI (*Operational Land Imager*) (<https://earthexplorer.usgs.gov/>), o modelo de superfície digital Copernicus DSM GLO- 30 (<https://scihub.copernicus.eu/>) e ocorrências minerais disponibilizadas pelo Serviço Geológico do Brasil (<http://geosgb.cprm.gov.br/>). Essas informações serviram de base para o mapeamento das unidades geológicas.

2.3. Datações U-Pb

Investigamos cinco amostras por geocronologia U-Pb LA-ICP-MS: duas do Bloco Gran- jeiro, SMD-011 (3A) e RPW-04; duas do embasamento da Faixa Ri- acho do Pontal, RPE-27 (3C) e RPB-22 (3E); e uma coletada ao longo do Lineamento Pernambuco no Domínio Itaizinho, RPB-25 (3F). As análises foram realizadas no Instituto de Geociências da Universidade de Campinas – UNICAMP e os resultados obtidos podem ser visualizados no material suplementar em anexo.

Os zircões examinados foram extraídos de cerca de 5kg de rocha. As amostras foram moídas, bateada e os grãos concentrados através de separador magnético isodinâmico Frantz. Separamos o concentrado através de microscópio binocular, e os grãos selecionados colados em mounts epoxy, polidos e limpos com ácido nítrico 3%. Em seguida, imageamos os grãos por catodoluminescência (CL) e elétrons retroespalhados (BSE) utilizando microscópio de varredura eletrônica LEO 430i e EDS. Usamos estas imagens para descrever a morfologia e textura dos zircões e definir os pontos de análise.

Os dados isotópicos foram coletados em spots de 25 μm durante tempo de aquisição de 60 segundos, em um sistema Photon Machines Excite 193 equipado com célula de ablação HelEx acoplada a ICP-MS Thermo Scientific Element XR. O sistema operou com frequência de 10Hz, fluência de 4, 74 J/cm⁻² e quantificação dos isótopos 204Pb, 206Pb, 207Pb, 232Th, 235U e 238U. A correção do fracionamento elementar baseou-se no padrão primário 91500 ([Wiedenbeck et al. 1995](#)), e para o controle de qualidade o padrão secundário Peixe ([Navarro et al. 2017](#)). Os resultados foram reduzidos usando o software Iolite, versão 2.5 Visual Age (2014.10), na plataforma Igos-Pro 6.3.7.2 ([Paton et al. 2010](#); [Petrus & Kamber 2012](#)). Finalmente, usamos o pacote IsoplotR ([Vermeesch 2018](#)) e o software DensityPlotter ([Vermeesch 2012](#)) para gerar os gráficos.

3. Formações Ferríferas e Sistema Mineral de depósitos de Fe

3.1. Formações Ferríferas

Formação ferrífera (FF) é o termo litológico e estratigráfico usado para denominar rochas sedimentares químicas que exibem altos teores de ferro (Trendall 1983; Trendall 2002). Estas rochas possuem ampla distribuição temporal, indo desde do Arqueano até o Fanerozoico (Gross 1983; Klein 2005) (Fig. 3.1), e sua gênese está relacionada a uma complexa interação entre o manto, processos tectônicos, oceânicos e biosféricos (Bekker et al. 2010). As grandes deposições de FF no Paleocambriano, por exemplo, estão associadas a liberação de Fe em oceanos anóxicos devido ao aumento de atividades mantélicas (Bekker et al. 2010; Bekker et al. 2014; Abbott & Isley 2002) (Fig. 3.1A). Por outro lado, o menor registro no Fanerozoico pode estar associado tanto as mudanças no estilo da tectônica de placas (Lascelles 2013), quanto ao aumento da oxigenação (Cloud 1973; Holland 1973; Holland 1978; Holland 1984) (Fig. 3.1B).

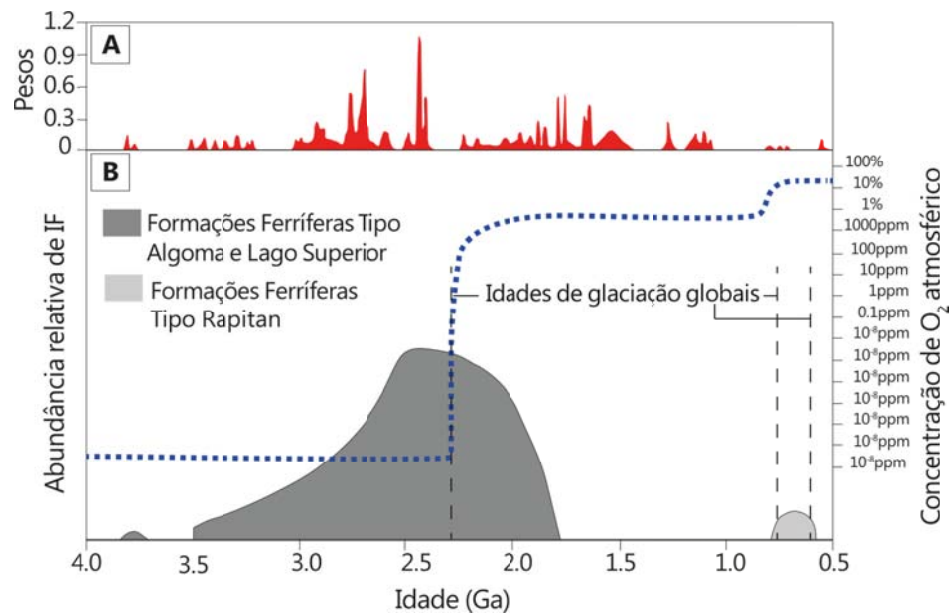


Fig. 3.1 – Distribuição espaço-temporal das formações ferríferas e sua relação com a variação das atividades de plumas mantélicas (A) (segundo Abbott & Isley (2002)) e os níveis de oxigênio na atmosfera (linha tracejada em B) (modificado de Klein (2005)).

Além de serem importantes registros paleoambientais, as FF têm relevância econômica, sendo responsáveis pelas maiores reservas mundiais de minério de ferro com alto teor (> 60%) (Beukes et al. 2003; Kock et al. 2008). Esses depósitos se formam pela lixiviação da sílica e substituição de minerais primários por magnetita e hematita (Hagemann et al. 2016). A seguir,

serão apresentadas definições gerais sobre os ambientes deposicionais e mineralogia das FF, o Sistema Mineralizador e os elementos críticos essenciais para a formação das mineralizações, bem como os critérios mapeáveis que geram as variáveis preditoras para os modelos prospectivos.

3.1.1. Ambientes de deposição de FF

As FF são rochas sedimentares químicas que possuem teores de ferro entre 20-30% e podem apresentar ou não intercalações de SiO₂ (James 1954; James 1983). Essas rochas são classificadas em três grupos com base em suas características deposicionais e associações litológicas: tipo Algoma, tipo Superior e tipo Rapitan (Gross 1965; Gross 1980). Os tipos Algoma e Superior correspondem a idades arqueanas-paleoproterozoicas, enquanto o tipo Rapitan está restrito ao Neoproterozoico e ocorre associado a diamictitos glaciais (Klein & Beukes 1993; Klein 2005; Beukes & Gutzmer 2008) (Fig. 3.2).

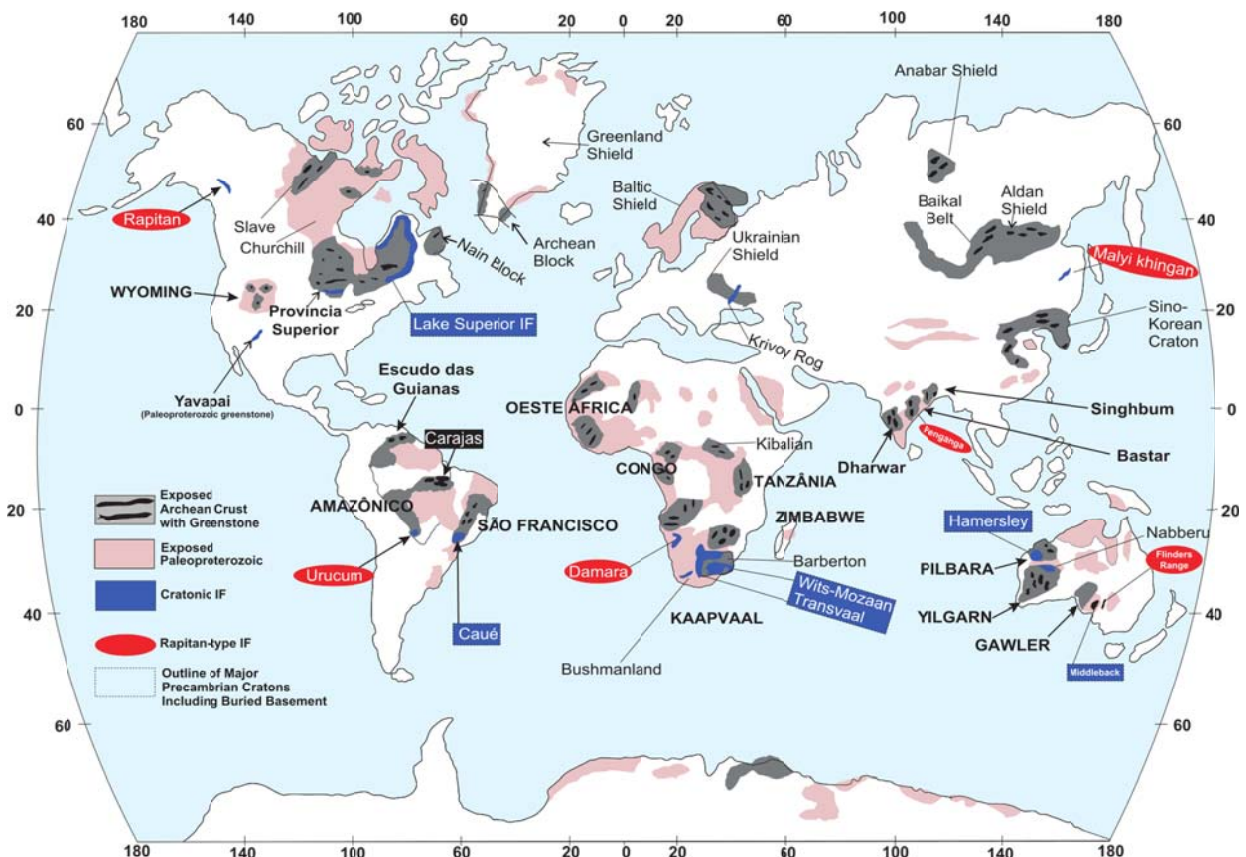


Fig. 3.2 – Ocorrências das FF quanto aos tipos deposicionais e suas distribuições globais em relação aos crátons pré-cambrianos. Modificado de Beukes & Gutzmer (2008).

As FFs do Tipo Algoma possuem idades que variam do Eoarqueano ao Paleoproterozoico e estão intercaladas a sequências vulcanossedimentares hidrotermais exalativas marinhas em

terrenos *greenstone belts* (Gross 1980; James 1983; Beukes & Gutzmer 2008; Bekker et al. 2010; Bekker et al. 2014; Goodwin 1973) (Fig. 3.3A). Elas exibem o maior número de depósitos e distribuição geográfica (Figura 3.3B), entretanto de menores espessuras e extensão quando comparados as FF do tipo Superior (Beukes & Gutzmer 2008), raramente excedendo 10^7 Mt (Huston & Logan 2004) (Fig. 3.3 C). Alguns autores ressaltam (Bekker et al. 2010; Gole & Klein 1981) que as atuais dimensões geométricas dessas rochas podem não refletir as originais, pois a maioria dos registros estão intensamente deformados e tectonicamente desmembrados.

As FF do Tipo Superior foram depositadas em margens passivas a partir do Mesoarqueano até o Proterozoico. Elas são tipicamente intercaladas a carbonatos, quartzo arenitos e folhelhos negros, com pouca presença de rochas vulcânicas (Gross 1965; Gross 1980) (Fig. 3.3A). Comparadas às FF do Tipo Algoma, essas formações são consideravelmente maiores, apresentando extensas continuações laterais e contendo valores superiores a 10^8 Mt de ferro a 15% em peso de Fe (James 1983; Isley 1995) (Fig. 3.3B e C).

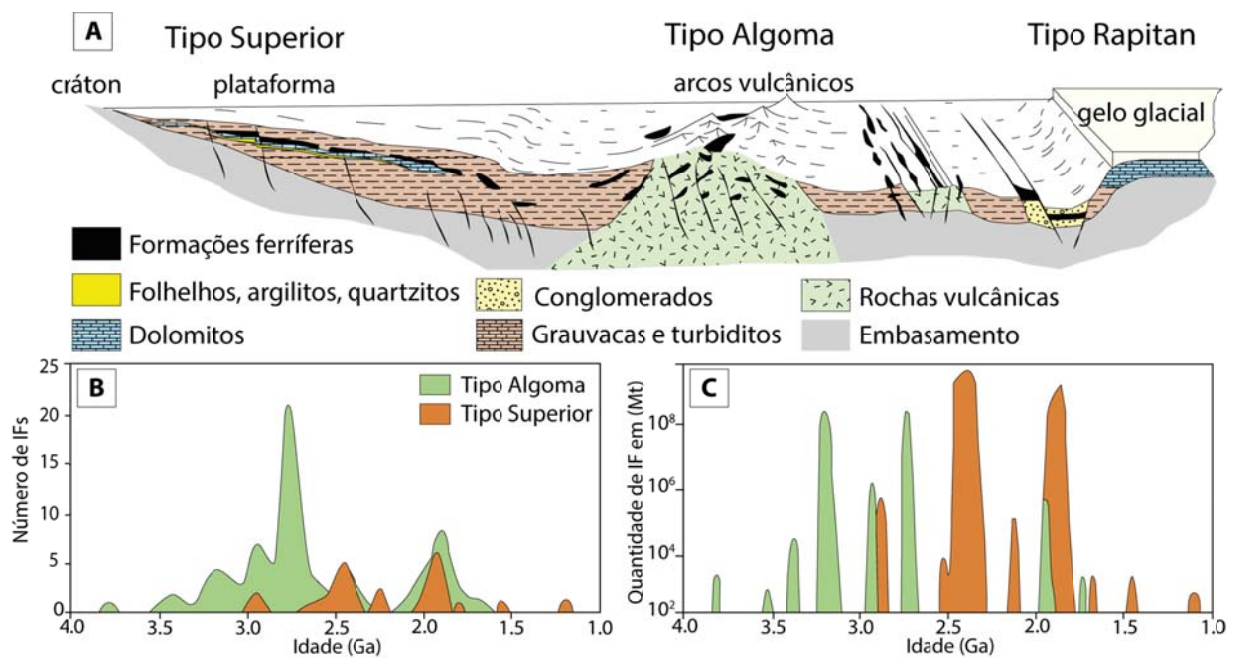


Fig. 3.3 – Tipos de ambientes deposicionais e relação espaço-temporal de Formações Ferríferas. (A) Classificação das FF em relação ao ambiente deposicional (modificado de Gross (1980)); Distribuição temporal dos números (B) e quantidades (C) de FF em relação ao ambiente de deposição ao longo do Pré-cambriano - modificado de Beukes & Gutzmer (2008)).

3.1.2. Classificação

A classificação das FFs é baseada na mineralogia e textura das rochas. James (1954) propôs uma classificação mineralógica, baseada nas descrições das rochas da região do Lago Superior no Canadá, que divide as FFs em quatro fácies: silicato, óxido, carbonato e sulfetos (Tabela 3.1). De acordo com o autor, essa classificação reflete a sequência deposicional, sendo o potencial de oxidação um dos principais fatores que influenciam na formação das fácies (Fig. 3.4).

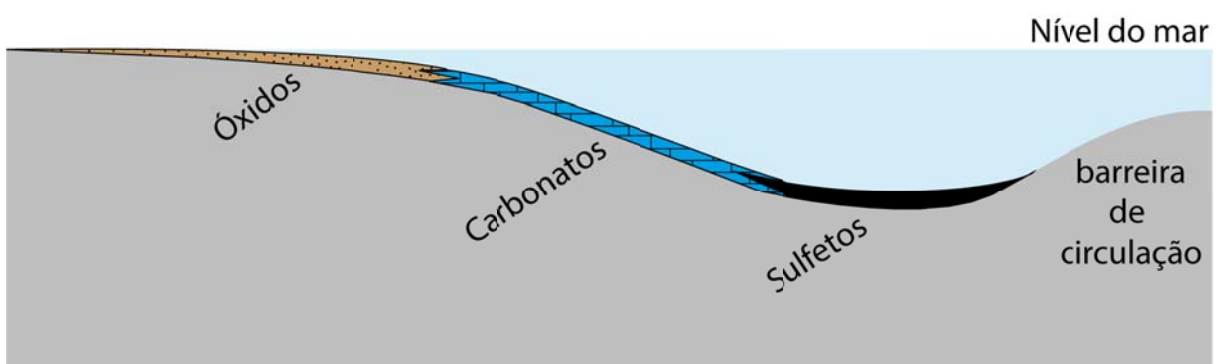


Fig. 3.4 – Modelo de fácies deposicionais de James (1954).

Embora a fácie sulfeto esteja incluída na classificação de FF, ela consiste em sedimentos piríticos e não é considerada uma FF *stricto sensu* (Bekker et al. 2014). Essas rochas podem estar relacionadas à deposição de depósitos VMS (*Volcanogenic Massive Sulfide* - Sulfetos Maciços Vulcanogênicos) ou formações ferríferas com enriquecimento hidrotermal, e frequentemente hospedam importantes depósitos de ouro em terrenos arqueanos (Ohmoto et al. 2006; Groves et al. 1987; Gourcerol et al. 2016).

Tabela 3.1 – Principais minerais presentes na classificação das fácies de FF segundo James (1954).

Fácie silicato	Fácie óxido	Fácie carbonato	Fácie sulfeto
greenalita $\text{Fe}_6\text{Si}_4\text{O}_{10}(\text{OH})_8$	magnetita Fe_3O_4	siderita FeCO_3	pirita FeS_2
minnesotaite $2 \text{Fe}_3\text{Si}_4\text{O}_{10}(\text{OH})_2$	hematita Fe_2O_3	dolomita - anquerita $\text{CaMg} \longleftrightarrow \text{CaFe}(\text{CO}_3)_2$	
stilpnometano $\text{Fe}_{2.7}(\text{Si},\text{Al})_4(\text{O},\text{OH})_{12} \cdot \text{xH}_2\text{O}$			

As FF são divididas em dois tipos texturais, que refletem estilos deposicionais diferentes (Beukes & Gutzmer 2008). As formações ferríferas bandadas (BIF) são dominantes no Arqueano

e aleoproterozoico Antigo (Beukes & Gutzmer 2008). Elas são compostas por lâminas alternadas ou camadas de precipitados químicos de *chert* (40-50%) e minerais de ferro (20-30%), incluindo óxidos, carbonatos e silicatos (James 1954; James 1983; Simonson 2003; Beukes & Gutzmer 2008). As formações ferríferas granulares (GIF) são mais comuns no Novo Paleoproteozoico e são compostas por camadas centimétricas relacionadas a áreas sedimentadas em ambientes proximais e rasos (Simonson 2003; Simonson 1985).

3.1.3. Mineralogia e metamorfismo

De acordo com Klein (2005), as FF do tipo Algoma e Superior são semelhantes em termos mineralógicos, apresentando principalmente chert (ou quartzo - SiO_2), magnetita (Fe_3O_4), hematita (Fe_2O_3), Fe-silicatos e siderita (FeCO_3). Essas fases não refletem a mineralogia primária, mas são resultado de sobreposições diagenéticas e metamórficas. Acredita-se que os silicatos presentes nos FFs sejam provenientes de géis hidratados ou coloides com composições próximas à greenalita ($\text{Fe}^{+2}\text{Si}^{+4}\text{O}_4(\text{OH})_4$) e ao stilpnomelano ($\text{Fe}^{+2}\text{Si}^{+4}\text{O}_4(\text{OH}(\text{Na},\text{K},\text{Al}))$) (Klein 2005; Li et al. 2017). Já os carbonatos presentes são misturas de CO_2 , Fe^{2+} , Mg^{2+} e Ca^{2+} . É importante ressaltar que essas fases são resultado de processos diagenéticos e metamórficos e não refletem a mineralogia primária das FF (Klein 2005).

A hematita pode ter se formado de diversas maneiras, incluindo a desidratação de hidróxidos de ferro (Fe(OH)_3) precipitados em zonas fóticas (Kappler et al. 2005), a oxidação enzimática e a oxidação por O_2 derivado de cianobactérias (Planavsky et al. 2014). Em relação à origem da magnetita, existem duas linhas de raciocínio em discussão. A primeira defende que esse mineral foi formado por processos diagenéticos (Krapež et al. 2003; Ewers & Morris 1981). Já a segunda linha de raciocínio sugere que a magnetita foi formada por redução dissimilatória de Fe(III) (DIR - Dissimilatory Fe(III) Reduction), que ocorreu por biomineralização a partir de sedimentos inicialmente ricos em Fe^{+3} (Li et al. 2013; Li et al. 2017).

Segundo Klein (1983), Klein (2005) e Miyano & Klein (1983), existem três graus metamórficos que são utilizados para classificar as formações ferríferas pré-cambrianas: diagenético ou baixo grau, médio grau e alto grau. O metamorfismo age de forma progressiva nos minerais silicáticos e carbonáticos, e em todos os intervalos, é possível encontrar quartzo, magnetita e hematita, que aumentam a granulação com o aumento do grau do metamorfismo (Klein 2005). Os registros de FF com assembleias típicas de baixo grau, como sub-xisto verde e xisto verde, são raros e os melhores exemplos estão restritos à Bacia de Hamersley, na Austrália, e ao Cráton Kaapval, na África do Sul. Em Hamersley, as temperaturas de metamorfismo variam entre 200 e 300°C, com

pressão máxima de 1,2 kbar (Klein 2005). Já para o Cráton Kaapval, as temperaturas foram estimadas entre 100 e 150°C (Klein 2005).

Durante os estágios de baixo a médio grau de metamorfismo, ocorre a reação entre a greenalita, stilpnometano, quartzo e carbonatos, formando a minnesotaite. Além disso, outras fases metamórficas podem estar presentes, como minerais do grupo da clorita (chamosita e ripidolita), anfíbolio (riebeckita) e biotita (ferri-anita) (Klein 2005). Quando a metamorfismo atinge os estágios de médio a alto grau, nas zonas de granada e estaurolita, cianita e silimanita, carbonatos e quartzo reagem para originar anfibólios ricos em ferro da série cummingtonita- grunerita. Em estágios mais elevados de metamorfismo (zona da silimanita), podem ocorrer cummingtonita, grunerita, granada e outras fases como piroxênios e fayalita, formadas por reações de altas temperaturas (Klein 2005; Bekker et al. 2014).

3.2. Sistema mineralizador

O conceito de Sistema Mineral aborda os depósitos minerais como expressões em pequena escala de processos geodinâmicos ocorridos em diferentes escalas temporais e espaciais (Wyborn et al. 1994). Neste conceito, os sistemas minerais são formados pela combinação de quatro elementos críticos, que são: a arquitetura da litosfera, a geodinâmica favorável, fertilidade e preservação da zona de deposição primária (McCuaig et al. 2010; Groves et al. 2022) (Fig. 3.5). A ideia de Sistema Mineral foi inspirada no bem-sucedido conceito de Sistema Petrolífero utilizado na indústria de exploração do petróleo (Wyborn et al. 1994).

Na exploração mineral, o uso de Sistema Mineral envolve identificar os fatores críticos necessários para a formação de um depósito mineral (McCuaig et al. 2010). A aplicação prática deste conceito consiste em analisar gradualmente os elementos do sistema investigado, traduzindo-os em informações úteis e que sejam mapeáveis, para a identificação de alvos (McCuaig et al. 2010; Yousefi et al. 2019; McCuaig & Hronsky 2014). Em outras palavras, o objetivo é compreender os fatores fundamentais que levaram à formação do depósito mineral e usá-los para orientar a exploração mineral de forma mais eficiente. As incertezas ao traduzir os componentes de um sistema mineral incluem, a qualidade da representatividade dos critérios, a falta de compreensão dos processos que controlam a mineralização e a dependência de escala dos critérios mapeáveis (McCuaig et al. 2010; Ford & McCuaig 2010).

De acordo com Angerer et al. (2015), a formação e preservação de depósitos de minério de ferro em FF requerem cinco elementos críticos: (i) presença de fertilidade em ferro nas FF; (ii) fluxos de fluidos que possam dissolver a sílica presente; (iii) alta permeabilidade em várias escalas;

(iv) exumação e modificação supergênica dos corpos de minério; (v) preservação dos corpos de minério de ferro. Esses elementos podem ser resumidos como o cenário tectônico de deposição do protominério, a trajetória dos fluidos e as alterações minerais (Hagemann et al. 2016). O controle estrutural é fundamental para o enriquecimento e transformação do minério em baixo e alto teor de ferro, uma vez que favorece a percolação dos fluidos que causam alterações hipogênicas e supergênicas, originando diferentes tipos de minérios de ferro e preservando os corpos de minério (Hagemann et al. 2016; Thorne et al. 2014; Dalstra & Rosière 2008; Rosière et al. 2001; Dalstra 2014).

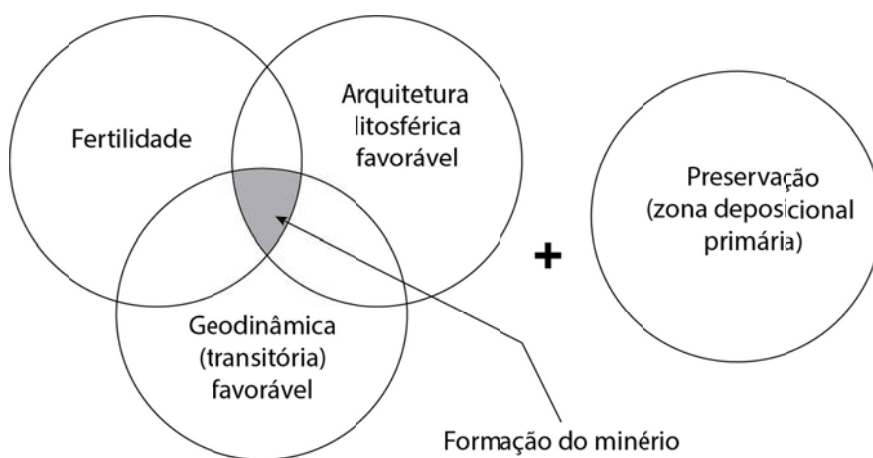


Fig. 3.5 – Elementos críticos de um Sistema Mineral. Modificado de McCuaig & Hronsky (2014).

3.2.1. Controles geotectônicos e origem dos fluidos

Os depósitos de ferro hospedados em FF são formados em três configurações geodinâmicas (Hagemann et al. 2016): as FF arqueanas-paleoproterozóicas do Tipo Algoma e Lago superior e FF neoproterozoicas do tipo Rapitan. O fluxo de fluidos hidrotermais hipogênicos nestes cenários são controlado por estruturas geológicas regionais, conhecidas como estruturas ativas, que permitem a ascensão de fluidos e a mineralização hipogênica (Hagemann et al. 2016; Dalstra & Rosière 2008; Groves & Santosh 2021; Angerer et al. 2012; Thorne et al. 2014). Por outro lado, estruturas passivas de alta permeabilidade, como fraturas, favorecem a geração de alterações supergênicas pela percolação descendente de água meteórica (Thorne et al. 2014).

As margens cratônicas são locais propícios para a formação de depósitos de ferro de alto teor (Groves & Santosh 2021). Nessas regiões, ocorre o desenvolvimento de falhas extensionais

profundas, que criam bacias sedimentares nas margens continentais, onde as FF são depositadas. Essas bacias sedimentares são permeáveis e permitem a circulação de fluidos, que posteriormente atuam na formação do minério. Além disso, a litosfera espessa e flutuante associada às margens de crátons preserva grandes depósitos minerais (Groves & Santosh 2021).

O tipo de fluido presente nos depósitos é controlado pelo cenário geotectônico (Evans et al. 2013). No caso dos depósitos do tipo Algoma, a mineralização é formada por fluidos magmáticos, enquanto nos depósitos do tipo Lago Superior, os fluidos são salmouras hipersalinas de alto pH (>9) (Evans et al. 2013) que substituem bandas de chert por carbonatos. Em ambos os casos, ocorrem processos de enriquecimento supergênico causados pela percolação descendente de água meteórica.

Neste sistema mineral, são identificados quatro estágios de mineralização hipogênica e um estágio supergênico (Hagemann et al. 2016). O primeiro estágio é caracterizado pela lixiviação de sílica e formação de magnetita e carbonatos. No segundo estágio, ocorre oxidação da magnetita para hematita, acompanhada da dissolução de quartzo e formação de carbonatos, martitização e substituição de silicatos de ferro por hematita. O terceiro estágio envolve a formação de novas microplacas de hematita e hematita especular, além da dissolução de carbonatos. Já o quarto estágio é observado em minérios de ferro metamorfizados, onde ocorrem recristalização da hematita e formação de textura granoblástica de magnetita/hematita, além do desenvolvimento de xistosidade em zonas de cisalhamento e porfiroblastos de óxido de ferro (martita). O estágio de alteração supergênica é marcado pela substituição de magnetita e carbonatos por goethita, bem como a formação de quartzo fibroso e argilominerais.

3.2.2. Controle estrutural

Hagemann et al. (2016) dividem as estruturas envolvidas na formação e preservação de depósitos de minério de ferro, associados a BIF, em três grupos: pré-mineralização, sin-mineralização e pós-mineralização.

As estruturas pré-mineralização são aquelas que se desenvolvem antes da mineralização e podem atuar na formação do minério de ferro passivamente, como as vias de fluido, ou ativamente, quando reativadas durante a fase sin-mineralização. As estruturas sin-mineralização, por sua vez, se desenvolvem durante a gênese do minério e podem ser ativas, como as falhas normais, ou passivas, como as brechas de colapso de porosidade. Já as estruturas pós-mineralização facilitam o fluxo de fluidos, causam modificações texturais e/ou mineralógicas e moldam e preservam os corpos de minério existentes. Entre as estruturas que favorecem o fluxo de fluidos estão as foliações, zonas de cisalhamento dúctil, falhas e fraturas.

As estruturas pós-mineralização também podem ser subdivididas em três grupos. O primeiro grupo inclui as estruturas que preservam ou expõem corpos de minério de ferro após sua formação, como horsts e grabens ou impulsos. O segundo grupo consiste em estruturas que segmentam os corpos de minério de ferro existentes, como falhas de deslizamento. Por fim, o terceiro grupo é formado pelas estruturas que causam modificações texturais e/ou mineralógicas em corpos de minério existentes. É importante ressaltar que, devido à natureza de múltiplos estágios da formação de minério em qualquer depósito, pode haver estruturas pertencentes ao mesmo subtipo, mas formadas em idades diferentes.

3.2.3. Modelos de depósitos de Fe

Com base nos critérios mencionados anteriormente, [Hagemann et al. \(2016\)](#) propõem quatro modelos discretos de depósitos de minério de ferro associados a FF: Carajás, Hamersley, Urucum e Capanema. Cada um desses modelos é controlado por diferentes tipos de fluidos e estruturas geológicas. O modelo Carajás, por exemplo, é hospedado em terrenos granito-greenstone belts e é controlado por zonas de cisalhamento. Os fluidos que originam o minério são de origem hipogênica, com significativa contribuição de enriquecimento supergênico. O modelo Hamersley é uma bacia sedimentar controlada por zonas de falhas normais, com os fluidos envolvidos sendo salmouras primitivas e águas meteóricas. O modelo Urucum, por sua vez, é controlado por grabens precoces e FF de baixo grau. Finalmente, o modelo Capanema é caracterizado por um minério goethítico sem evidência de enriquecimento hipogênico.

É importante destacar que esta é uma classificação baseada na gênese de depósitos. Essa nova classificação se sobrepõe à classificação Superior-Algoma-Rapitan, baseada no ambiente deposicional. Por exemplo, o modelo de depósito do tipo "Carajás", encontrado em granito-greenstone belts, também é classificado como um BIF Algoma segundo a classificação de [Gross \(1980\)](#).

4. Resultados

Os resultados desta tese estão organizados nos seguintes capítulos:

- Artigo 1 - **Exploring the Gravimetric and Geochronological Links in Ancient Terranes of the São Francisco Craton and Borborema Province**

Neste capítulo, nosso objetivo foi investigar conexões entre os blocos do embasamento arqueano-paleoproterozoico das faixas marginais do noroeste do Cráton São Francisco e sudoeste da Província Borborema. Para isto utilizamos dados gravimétricos de satélite e geocronologia U-Pb em zircão.

- Artigo 2 - **São Francisco Paleocontinent Construction, Fragmentation, and Reworking in the Mineral System Evolution of the Curral Novo Iron District**

Neste estudo, investigamos a influência das estruturas geológicas regionais nas fases de enriquecimento mineral no Distrito Ferrífero de Curral Novo do Piauí. Relacionamos estas fases com o processo de fragmentação do Paleocontinente São Francisco e retrabalhamento dos blocos crustais remanescentes na Província Borborema.

4.1. Exploring the Gravimetric and Geochronological Links in Ancient Terranes of the São Francisco Craton and Borborema Province, NE-Brazil

WILEY

My Submissions Douglas ▾

Start a new submission for *Terra Nova*

Start submission →

My Submissions

Journal

All Journals ▾

Submission Status

All Submission Statuses ▾

Author Role

Submitting Author Only ▾

Terra Nova
Research Article

Exploring the Gravimetric and Geochronological Links in Ancient Terranes of the São Francisco Craton and Borborema Province, NE-Brazil

Submission Status Under Review

Submitted On 9 May 2024 by Douglas Martins

Submission Started 30 April 2024 by Douglas Martins

This submission is under consideration and cannot be edited. Further information will be emailed to you by the journal editorial office.

Submission overview →

Need help choosing a journal?

We've put together some resources and tools to help you find the right journal for your research.

Find a Journal

Exploring the Gravimetric and Geochronological Links in Ancient Terranes of the São Francisco Craton and Borborema Province, NE-Brazil

Douglas Teixeira Martins^{1,2*}, Wagner da Silva Amaral¹, Felipe Holanda dos Santos³, Evilarde Uchôa Filho^{3,4}

¹*Instituto de Educação Ciência e Tecnologia do Piauí (IFPI), Paulistana, PI, Brazil;*

²*Department of Geology and Natural Resources, Institute of Geosciences, University of Campinas, Campinas, SP, Brazil;*

³*Department of Geology, University of Ceará, CE, Brazil;*

⁴*Geological Survey of Brazil, Fortaleza, CE, Brazil;*

*Corresponding author: douglas.teixeira@ifpi.edu.br

<https://orcid.org/0000-0001-6543-1336>

ABSTRACT

This study aimed to map ancient terrane fragments from decratonization in the São Francisco Craton in northeastern Brazil. We mapped deep crustal fragments and their structural lineaments using satellite gravimetric data. Additionally, we dated rocks from the São Pedro Terrane, the Borborema Province Transversal Zone, and the Sobradinho Complex, forming the northwest basement of the São Francisco Craton. Our findings reveal a strong connection between these regions, highlighting significant granitic rock generation between the Mesoarchean and Neoarchean and sediment deposition dating back to the Statherian period. Neoproterozoic regional shear zones, likely from the Transbrasiliano Lineament, were crucial in transporting these crustal fragments.

Keywords: Decratonization; São Francisco Craton; Borborema Province; Statherian.

1. Introduction

Various studies have underscored the dynamic nature of seemingly stable cratonic regions, highlighting rejuvenation processes throughout their extensive geological histories (Holdsworth *et al.*, 2001; Lee *et al.*, 2011; Wu *et al.*, 2019). Decratonization mechanisms, often associated with these rejuvenations, remain a subject of interest (Foley, 2008; Lee *et al.*, 2011; Wu *et al.*, 2019), with lithospheric dynamics, thermal gradients, magmatism, tectonics, and deformation identified as critical triggers (Lee *et al.*, 2011; Wu *et al.*, 2019).

While petrological studies and surface geology have yielded valuable insights into decratonization mechanisms (Foley, 2008; Liu *et al.*, 2021; Lee *et al.*, 2011; and references therein), challenges persist in resolving issues concerning cratonic crustal architecture. Integrating geophysics, such as satellite gravimetry, with field data and geochronology can enhance our understanding of cratonic areas and associated decratonization processes.

We examined a geological area south of the Borborema Province (BP), located at the northern limit of the São Francisco Craton (SFC), to discover the tectonic processes that trigger the decratonization and remodeling of previously stable regions of the Earth crust. The BP is made up of several terranes, probably derived from the SFC, and had its final structuring during the Pan-African Brasilian Orogeny around 630 to 500 Ma (Santos and Brito Neves, 1984; Van Schmus *et al.*, 1995; Van Schmus *et al.*, 2008; Van Schmus *et al.*, 2011; Brito Neves *et al.*, 2000; Trompette, 1994).

Recent studies suggest that decratonization of the SFC northern margin occurred through extensional events between 1.0–0.92 and 0.9–0.82 Ga, followed by basin inversion around 0.60 Ga (Ganade *et al.*, 2021; Neves, 2021). However, our findings indicate older Paleoproterozoic crustal reworking events initiated decratonization at least 700 million years earlier, extending the SFC limits into the BP (Neves, 2021). This work aims to understand fragmentation mechanisms and investigate reworking processes, revealing tectonic and thermal evolution from the Archean to the Mesoproterozoic.

2. Geological settings

Among the cratons on the South American shelf, the SFC in northeastern Brazil has been extensively studied in geochronological, geophysical, and evolutionary terms (Almeida *et al.*, 1981; Heilbron *et al.*, 2017). Its basement comprises Archean nuclei documenting tectonothermal events around 2.8-2.7 Ga, which were subsequently amalgamated during the Rhyacian-Orosirian orogeny (Trompette *et al.*, 1992; Barbosa and Sabaté, 2004; Teixeira *et al.*, 2017; Brito Neves, 2011). Neoproterozoic orogenic belts developed along the SFC's margins due to collisions between the São Francisco- Congo paleocontinent, Amazonian, and São Luiz-West Africa, forming part of the Gondwana Supercontinent (Trompette, 1994; Arthaud *et al.*, 2008; Caxito *et al.*, 2020; Van Schmus *et al.*, 2008).

The BP is one such orogenic system resulting from these collisions (Almeida *et al.*, 1981; Santos and Brito Neves, 1984; Brito Neves *et al.*, 2000). It comprises Archean nuclei reworked in the Paleoproterozoic, intruded by neoproterozoic granites, and covered by neoproterozoic basins (Caxito *et al.*, 2020). Regional shear zones divide the province into three segments: North, Transversal, and South sub-province, subdivided into domains (Vauchez *et al.*, 1995). This study investigates a region encompassing parts of the Sobradinho Block, Riacho do Pontal, and Rio Preto orogens, along with the São Pedro Terrane (Teixeira *et al.*, 2017; Caxito *et al.*, 2017; Caxito *et al.*, 2016; Barros *et al.*, 2020; Brito Neves *et al.*, 2023).

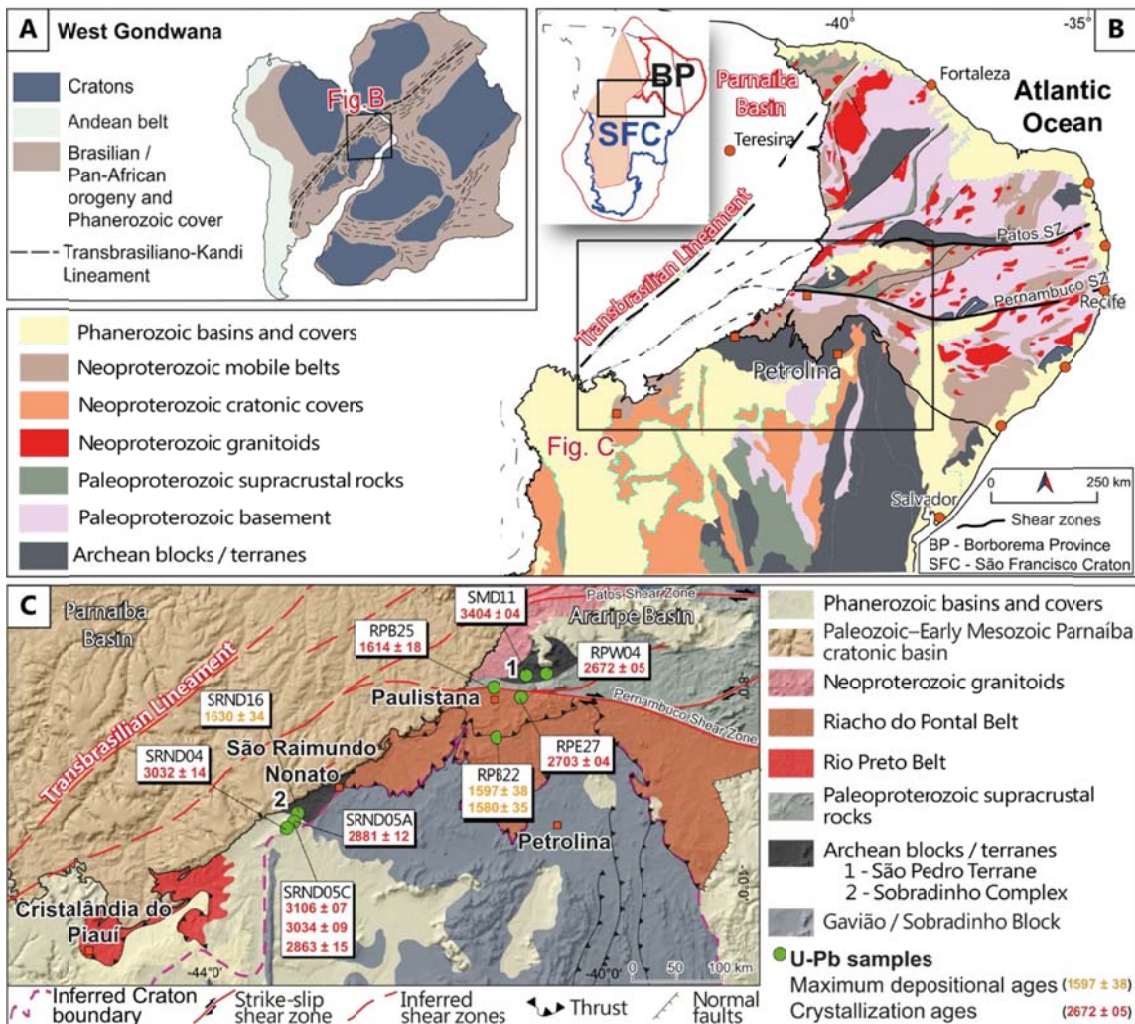


Figure 1. Location of the study area. (A) – Location of the study area in the context of West Gondwana. (B) – Location of the study area at the Borborema Province and the São Francisco Craton. In Figure B, in the upper left frame, the boundary of the São Francisco Paleocontinent proposed by [Neves \(2021\)](#). (C) – Simplified map of the main tectonic units in the study area and the location of geochronology samples. Modified from [Bizzi et al. \(2003\)](#).

3. Satellite gravity

3.1. Data and processing

We utilized the EGM2008 ([Pavlis et al., 2012](#)) model' Bouguer gravimetric anomaly data to analyze deep blocks and shallow structures, focusing on their horizontal continuity, geometry, and kinematics. This model, known for identifying deep crustal structures, uses mean grids with a 2.5x2.5 arc-minute resolution derived from a combination of terrestrial, aerial, and satellite gravimetric data (GRACE03S) ([Pavlis et al., 2012](#)). We processed Bureau Gravimetrique International (BGI) data, applying topographic correction with FA2BOUG ([Fullea et al., 2008](#)), employing a range of 167 km and a reduction density of 2.67 g/cm³. The data was separated into regional and residual components using a Gaussian filter with a standard deviation of 0.005 rad/km. The depth of source tops was estimated using the [Spector and Grant \(1970\)](#) method and processed through Oasis Montaj software (Figure 2A).

We aimed to detect gravimetric sources and assess their lateral extent. To increase visibility, we applied the tilt angle method ([Miller and Singh, 1994](#)), which calculates the tangent angle of the relationship between the vertical and horizontal derivatives. This technique helps distinguish anomalies of varying amplitudes and identify potential field directions associated with regional geological structures ([Godin and Harris, 2014](#)).

3.2. Bouguer anomaly

Figure 2B shows the Bouguer anomaly map from the EGM2008 model for the SFC NW and the BP SW boundary. Figure 2C shows the regional Bouguer anomaly, outlining the gravimetric domains corresponding to Tectonic Provinces. Low values characterize the SFC, with intermediate to high values along the W-NW edge. The Parnaíba Province has low values along the SE-NW direction, intermediate values in the NE-SW directions, and cores with high values. In the Borborema Province, gravimetric values are intermediate to high along the SE-NW direction in the Precambrian basement, while the Araripe basin corresponds to the lowest values. Figure 2D shows the residual Bouguer anomaly, highlighting high frequencies associated with shallow sources, particularly along the BP boundaries and propagating towards the centers of the basins. The values are consistent with data from [Oliveira and Medeiros \(2018\)](#) for gravimetric profiles of the boundaries between the Borborema Province and the São Francisco Craton along the Riacho do Pontal Orogen.

3.3. Tilt derivative applied to deep and shallow gravity data

Tilt derivative (TDR) analysis of regional Bouguer anomaly data identified deep lineaments, revealing two sigmoidal-shaped features: one extending from the Cristalândia block to São Raimundo Nonato and the other from the Riacho do Pontal Belt to the Pernambuco Lineament (Figure 2E). In the São Pedro Terrane, two regional lineaments were observed, one along the Pernambuco Shear Zone and another northeast-southwest oriented. TDR of residual data mapped "gravimetric worms" (Hornby et al., 1999) (Figure 2F), indicating shallow anomalies, with one group suggesting shear zones parallel to deep lineaments and another perpendicular to them. Figure 2G illustrates interpreted lineaments, outlining crustal blocks and "gravimetric worms."

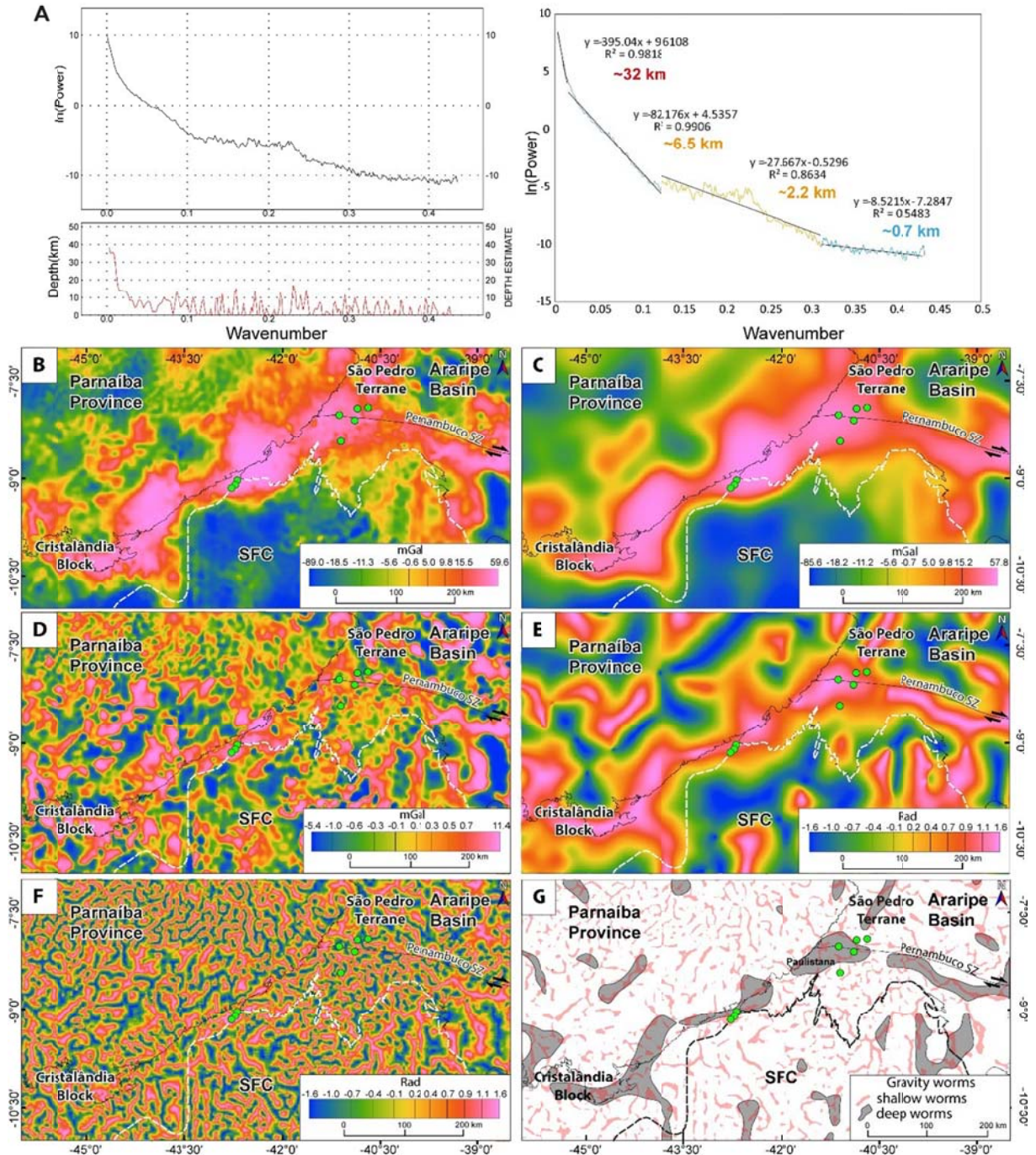


Figure 2. (A) Radial spectrum of the study area and the estimated depths of anomalies. We calculated depths from the slope of the power spectrum. (B) Map of the total Bouguer anomaly computed by the *Bureau Gravimetrique International* (BGI) from the gravitational model EGM2008. (C) Regional component extracted from the Bouguer anomaly of the EGM2008 model. (D) Residual component extracted from the Bouguer anomaly of the EGM2008 model. (E) Enhancement of the regional component using TDR. (F) Enhancement of the residual component through TDR. (G) Map of interpreted gravimetric lineaments.

4. Geochronology

The samples for geochronology were processed at the UNICAMP Isotopic Geology Laboratory. The extracted zircons were mounted on epoxy resin supports and analyzed using a Zeiss scanning electron microscope (model LEO 430i). U-Pb isotopic data were collected on 25 μm spots using a Photon Machines Excite 193 system coupled to a Thermo Scientific Element XR ICP-MS, operating at 10 Hz with a fluence of 4.74 J/cm $^{-2}$. Isotopes 204Pb, 206Pb, 207Pb, 232Th, 235U, and 238U were quantified, and data processing utilized Iolite software version 2.5 Visual Age ([Paton et al., 2010](#); [Petrus and Kamber, 2012](#)), with isochrons plotted using IsoplotR ([Vermeesch, 2018](#)). We investigated nine samples by geochronology, including two from the São Pedro Terrane, two from the Riacho do Pontal Belt basement, one along the Pernambuco Lineament, three from the Sobradinho-Remanso Complex, and one from the São Raimundo Nonato (Figure 1C). The results are in the supplementary material.



Figure 3. Field aspects of the studied rocks from the São Pedro Terrane and Sobradinho Complex. São Pedro Terrane: (A) SMD011 - Tonalitic gneisses; lightly banded syenogranite orthogneiss (RPE27; **B**) migmatitic banded syenogranite orthogneiss (RPW04; **C**; **D**) RPB25 - Rhyolitic dike, outcropping along the Transnortheast Railway, cutting through the Paleoproterozoic supracrustal rocks of the Itainzinho Complex; (E) RPB22 - Basement paragneiss of the Riacho do Pontal Belt. Sobradinho Complex: (**F**) SRND05A - Migmatitic granitic gneiss dome; (**G**) SRND05C - Sample of restite and granitic neosome present in the migmatitic part of the gneiss dome; (**H**) SRND04 - Granodioritic orthogneiss outcropping; (**I**) SRND16 - Metavolcano-sedimentary sequences cut by granitic aplite dikes, with a detailed location where the sample for dating was collected.

4.1.1. *SMD11 sample*

Tonalitic orthogneiss is gray and fine—to medium-grained (Figure 3A), with metamorphic banding alternating felsic and mafic minerals. Zircon grains are prismatic and light brown, ranging from 100-300 μm , with oscillatory zoning. Seventeen zircon cores provided a crystallization age of 3404 ± 4 (MSWD = 1.6).

4.1.2. *RPE-27 and RPW-04 Samples*

Syenogranite orthogneiss, pink, medium to coarse granulation. Zircon grains, prismatic to rounded, 100-150 μm , light to dark brown, some with oscillatory zoning. RPE-27: thirty-three grains, seven with an age of 2703 ± 4 (MSWD = 0.91). RPW-04: twenty-nine grains, twelve aged 2672 ± 5 (MSWD = 1.5).

4.1.3. *RPB-22 Sample*

Paragneiss with mafic and felsic bands. Sixty-four zircon grains were analyzed, with ages ranging from Mesoarchean to early Mesoproterozoic. The most significant population yields ages within 2050 – 1850 Ma, peaking at 1997 Ma. Younger grains provide ages of 1597 ± 38 Ma, 1580 ± 35 Ma, and 1404 ± 36 Ma.

4.1.4. *RPB-25 Sample*

Rhyolite intruding the Itainzinho Complex. Zircon grains are euhedral to rounded, with textures including oscillatory zoning. Six concordant grains yield a crystallization age of 1614 ± 8 Ma (MSWD = 2.5).

4.1.5. *SRND05A and SRND05C Samples*

Migmatitic gneiss dome. The grains suberic to euhedral, 100-300 μm , with oscillatory zoning. Ten core analyses yield an age of 3032 ± 14 Ma (MSWD = 1). SRND05C: melanosome and leucosome parts, yielding ages of 3106 ± 7 Ma, 3024 ± 9 Ma, and 2863 ± 15 Ma for melanosome grains, and 2631 ± 16 Ma for zircon rims analyses.

4.1.6. SRND04 Sample

Granitic to granodioritic orthogneiss. Subhedral to euhedral prismatic grains, 50- 300 μm , with oscillatory zoning. Six analyses yield a crystallization age of 2881 ± 12 Ma (MSWD = 3.3), like group III zircons from SRND05C.

4.1.7. SRND16 Sample

Muscovite schist crosscut by granitic aplites. Forty-four zircon grains were analyzed, with dominant populations centered around 2935 Ma, 2550 Ma, and 2035 Ma. The youngest concordant grain yields a $207\text{Pb}/206\text{Pb}$ age of 1625 ± 34 Ma (2σ).

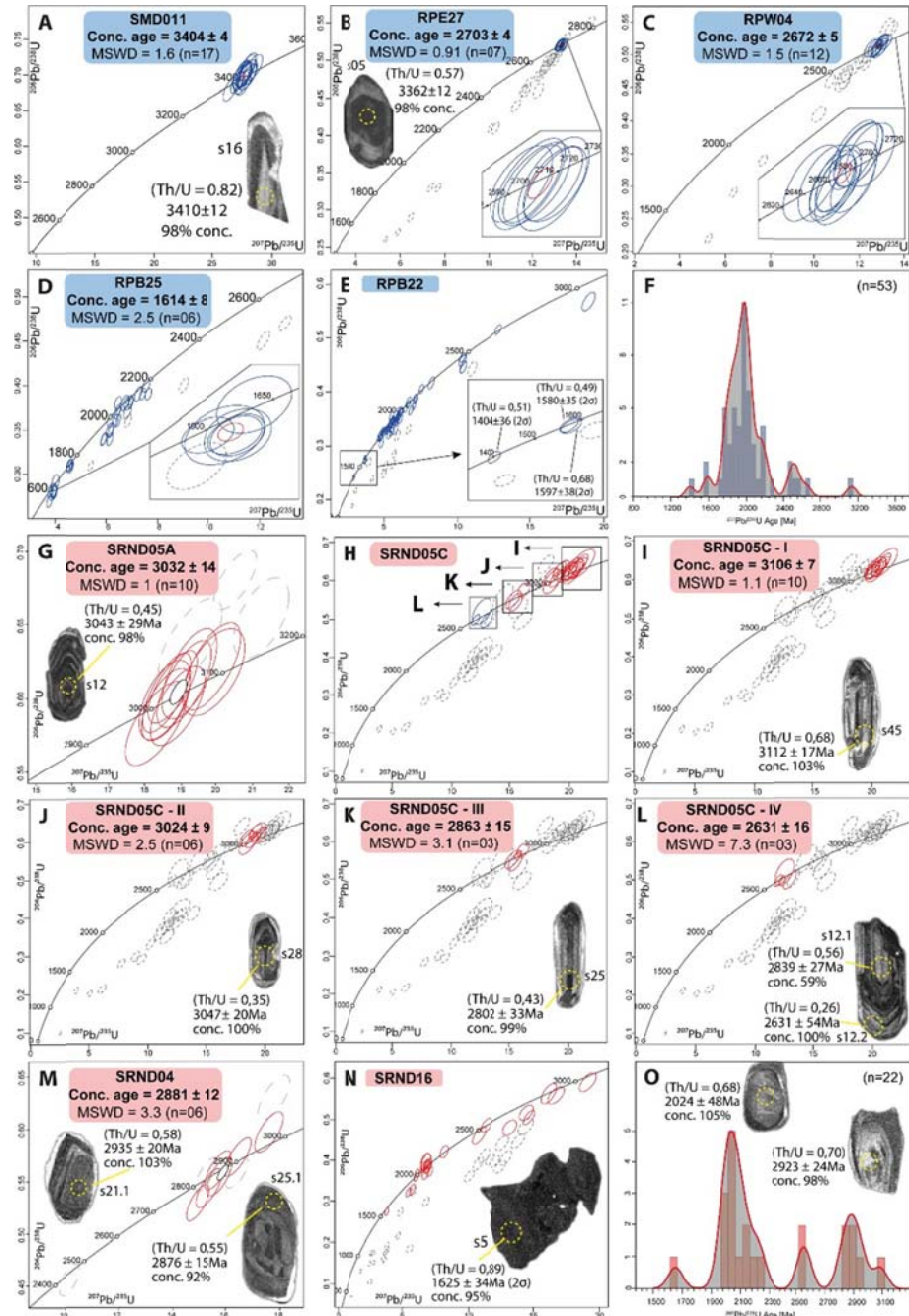


Figure 4. (A) SMD011 - Tonalitic gneisses. (B) RPE27 and (C) RPW04 - Sienitic orthogneisses. (D) RPB25 - Rhyolitic dike. (E - F) RPB22 - Basement paragneisses of the Riacho do Pontal Belt, concordant zircons grains > 90% (N) and probability plots (O). (G) SRND05A - Migmatitic gneiss dome. (H - L) SRND05C - Migmatite with distinguishable neosome and restite. (M) SRND04 - Granodioritic orthogneiss. (N - O) SRND16 - Interbedded schist within metavolcano-sedimentary sequences and iron formations, concordant detrital zircons grains > 90% (N), and probability plots (O).

5. Discussions

5.1. Gravimetric Lineaments

Deep gravimetric lineaments northwest of the São Francisco Craton (SFC), identified from the EGM2008 model Bouguer anomaly vertical derivative slope map, spatially align with Archean and Paleoproterozoic terranes. Shallow lineaments, termed "gravity worms," possibly indicate shear deformation or lateral fault movement bounding crustal ([Godin and Harris, 2014](#)). These lineaments, in Figure 5A alongside Paleoproterozoic crustal blocks and their transport directions, suggest the geometry and movement of these fragments, resembling exotic terranes as they migrate away from the SFC. Deep lineaments parallel major shear corridors like the Transbrasiliano Lineament, corresponding to Sobradinho, Cristalândia do Piauí, and São Pedro blocks ([Brito Neves et al., 2023](#)) blocks. Along the Pernambuco Lineament in the Transversal Zone, these lineaments shift orientation and behave as splays linked to the Transbrasiliano Lineament. Satellite gravimetric data effectively map crustal fragments, indicating mafic-rich rocks in the BP Archean-Paleoproterozoic terranes, likely remnants of the collision between the BP and São Francisco block. [Ganade et al. \(2021\)](#) proposes two stages of decratonization deformation, involving an oblique collision between SFC and West African Craton and subsequent dextral movement of the Transbrasiliano-Kandi Fault, leading to transpressional orogeny of the BP (Figure 5B). Paleoproterozoic blocks were transported via east-west shear zones, acting as corridors, from fragments of the São Francisco Paleocontinent located in the Transversal Zone of the BP, exemplified by the Alto Moxotó Terrane ([Lira Santos et al., 2022](#)).

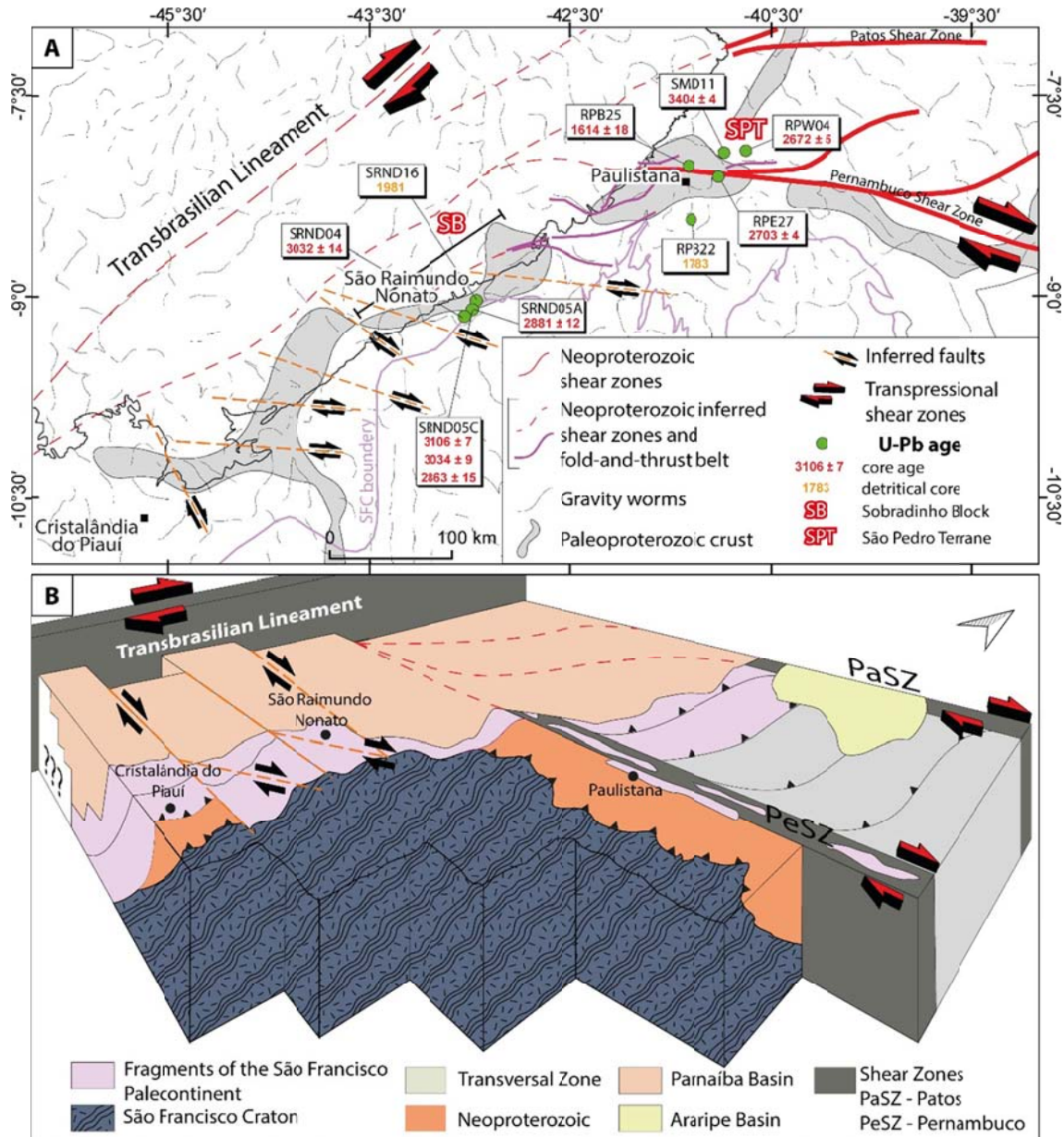


Figure 5. Results of interpreting gravity lineaments from the EGM2008 model for the study area. (A) Map showing the boundaries of anomalies interpreted as fragments of the Archean-Paleoproterozoic basement. (B) The geometric configuration of the transported crustal fragments during decratonization.

5.2. Geochronology, Fragmentation, and Transport of the Archean-Paleoproterozoic Crust

Our data strongly link the blocks in the northwest region of the São Francisco Craton (SFC) and the São Pedro Terrane (SPT), particularly concerning magmatic activity between 2.8 Ga and 2.6 Ga, aligning with the formation periods of the SFC ([Gordilho](#)

[Barbosa et al., 2023](#)). Ages obtained for the SPT range from 3404 ± 4 Ma to 2672 ± 5 Ma, while a paragneiss from the Riacho do Ponral Orogen exhibits a maximum age of 1625 ± 34 Ma, consistent with 1614 ± 8 Ma rhyolitic dikes in the Itainzinho Complex north of the study area.

In the Sobradinho Complex within the Sobradinho Block, ages of 3024 ± 9 Ma (SRND05C) and 3032 ± 14 Ma in leucosome from a gneissic dome were obtained. The residue yielded an age of 3106 ± 7 Ma. Additionally, ages of 2863 ± 15 Ma from zircon cores and 2631 ± 15 Ma at their edges suggest an earlier thermal event, followed by granitic magmatism around 2.8 Ga, the crystallization date of granodioritic orthogneiss. Muscovite schist crosscut by granitic aplitic showed an age of 1625 ± 34 Ma ([Fig. 4N](#)).

The similarities between the SFC and the Borborema Province support the hypothesis of a genetic relationship originating from the decratonization process ([Neves, 2021](#)). Based on the concept of a metacraton (Abdelsalam *et al.*, 2002; Liégeois *et al.*, 2013; Liégeois *et al.*, 2003), this process suggests that the BP resulted from reworking the weakened cratonic crust of the São Francisco Paleocontinent. Our results corroborate this hypothesis, especially for fragments northwest of the SFC and southwest of the BP.

Rocha *et al.* ([2019](#)) suggest that high P-wave velocities beneath the BP's Southern Subprovince indicate the SFC's extension beneath this region. This implies a northern location of the lithospheric boundary between the SFC and the BP than evident on the surface, suggesting the possible presence of another small block separated from the São Francisco Paleocontinent.

The age differences imply a continuous continental margin arc formation process between 3.0 - 2.8 Ga, with possible intraplate magmatism around 2.6 - 2.5 Ga ([Barros *et al.*, 2020](#); [Vale *et al.*, 2023](#)). Volcanism around 1.6 - 1.5 Ga in the eastern Borborema Province and the SCF Curaçá dike systems suggest a shared weakened crust between the two blocks ([Neves, 2021](#)).

We propose a scenario in which the Sobradinho Block, São Pedro Terrane, and Cristalândia Block originated during the Neoarchean collision, were later reworked during the Riacian orogeny, and remained stable until the end of the Orosirian. By the Statherian, this crust fragmented, possibly indicated by the intrusion of rhyolitic dikes in the Riacho do Pontal Orogen ([Amaral *et al.*, 2023](#)), with shear zones dispersing and transporting these crustal fragments by the end of the Neoproterozoic.

6. Conclusions

- Deep gravimetric lineaments represent fragments of Archean-Paleoproterozoic crust extending from the São Francisco Craton's northwest margin to the Pernambuco Shear Zone.
- Shallow gravimetric lineaments, or "gravimetric worms," indicate lateral displacement of shallow crustal fragments, offering insights into kinematic processes.
- Geochronological analyses reveal similarities between the Sobradinho Block and São Pedro Terrane, with intense magmatic activity between 3.4 – 3.1 Ga and 2.8 – 2.6 Ga.
- The alignment of zircon peaks in metasedimentary rocks with magmatic events supports the connection between magmatism and metasedimentary rock formation.
- Evidence in the Borborema Province and São Francisco Craton links the breakup of the Sobradinho-São Pedro Block to a taphrogenetic event around 1.7 - 1.5 Ga.
- Neoproterozoic shear zones transported the Archean-Paleoproterozoic fragments.

References

- Abdelsalam, M.G., Liégeois, J.-P. and Stern, R.J., 2002. The Saharan Metacraton: *Journal of African Earth Sciences*, **34**, p. 119–136, doi: 10.1016/S0899- 5362(02)00013-1.
- Almeida, F.F.M.D., Hasui, Y., De Brito Neves, B.B. and Fuck, R.A., 1981. Brazilian structural provinces: An introduction: *Earth-Science Reviews*, **17**, p. 1–29, doi: 10.1016/0012-8252(81)90003-9.
- Amaral, W.D.S., Santos, F.H.D., Martins De Sousa, D.F., Perpétuo, M.P., Brito Neves, B.B.D., Pitombeira, J.P.A. and Martins, D.T., 2023. A complex history of extension, subduction and collision in west Gondwana: Clues from the Riacho do Pontal orogen, Borborema Province (NE Brazil): *Journal of South American Earth Sciences*, **125**, p. 104297, doi: 10.1016/j.jsames.2023.104297.
- Archanjo, C.J., Hollanda, M.H.B.M.D. and Viegas, L.G.F., 2021. Late Ediacaran lateral-escape tectonics as recorded by the Patos shear zone (Borborema Province, NE Brazil): *Brazilian Journal of Geology*, **51**, p. e20200132, doi: 10.1590/2317- 4889202120200132.
- Arthaud, M.H., Caby, R., Fuck, R.A., Dantas, E.L. and Parente, C.V., 2008. Geology of the northern Borborema Province, NE Brazil and its correlation with Nigeria, NW Africa: *Geological Society, London, Special Publications*, **294**, p. 49–67, doi: 10.1144/SP294.4.
- Barbosa, J.S.F. and Sabaté, P., 2004. Archean and Paleoproterozoic crust of the São Francisco Craton, Bahia, Brazil: geodynamic features: *Precambrian Research*, **133**, p. 1–27, doi: 10.1016/j.precamres.2004.03.001.
- Barros, R.D.A., Caxito, F.D.A., Egydio-Silva, M., Dantas, E.L., Pinheiro, M.A.P., Rodrigues, J.B., Basei, M.A.S., Virgens-Neto, J.D. and Freitas, M.D.S., 2020. Archean and Paleoproterozoic crustal evolution and evidence for cryptic Paleoarchean-Hadean sources of the NW São Francisco Craton, Brazil: Lithochemistry, geochronology, and isotope systematics of the Cristalândia do Piauí Block: *Gondwana Research*, **88**, p. 268–295, doi: 10.1016/j.gr.2020.07.004.
- Bizzi, L.A., Schobbenhaus, C., Vidotti, R.M. and GONÇALVES, J.H.H. (Eds.), 2003. *Geologia, tectônica e recursos minerais do Brasil: texto, mapas e SIG*: CPRM, Brasilia.
- Brito Neves, B.B. de, 2011. The Paleoproterozoic in the South-American continent: Diversity in the geologic time: *Journal of South American Earth Sciences*, **32**, p. 270–286, doi: 10.1016/j.jsames.2011.02.004.

- Brito Neves, B.B.D., Santos, T.J.S.D. and Dantas, E.L., 2023. O Terreno Tectonoestratigráfico São Pedro: Oeste da Zona Transversal – Província Borborema: *Geologia USP. Série Científica*, **22**, p. 45–69, doi: 10.11606/issn.2316-9095.v22-197489.
- Brito Neves, B.B. de, Santos, E.J. and Van Schmus, W.R., 2000. Tectonic history of the Borborema province, northeastern Brazil. In: *Tectonic evolution of South America*.
- Caxito, F.D.A., Santos, L.C.M.D.L., Ganade, C.E., Bendaoud, A., Fettous, E.-H. and Bouyo, M.H., 2020. Toward an integrated model of geological evolution for NE Brazil-NW Africa: The Borborema Province and its connections to the Trans- Saharan (Benino-Nigerian and Tuareg shields) and Central African orogens: *Brazilian Journal of Geology*, **50**, p. e20190122, doi: 10.1590/2317-4889202020190122.
- Caxito, F.A., Uhlein, A., Dantas, E., Stevenson, R., Egydio-Silva, M. and Salgado, S.S., 2017. The Rio Preto and Riacho do Pontal Belts. In: *São Francisco Craton, Eastern Brazil, Regional Geology Reviews* (Heilbron, M., Cordani, U.G., and Alkmim, F.F., eds.) Springer International Publishing, Cham, p. 221–239.
- Caxito, F.A., Uhlein, A., Dantas, E.L., Stevenson, R., Salgado, S.S., Dussin, I.A. and Sial, A.D.N., 2016. A complete Wilson Cycle recorded within the Riacho do Pontal Orogen, NE Brazil: Implications for the Neoproterozoic evolution of the Borborema Province at the heart of West Gondwana: *Precambrian Research*, **282**, p. 97–120, doi: 10.1016/j.precamres.2016.07.001.
- Foley, S.F., 2008. Rejuvenation and erosion of the cratonic lithosphere: *Nature Geoscience*, **1**, p. 503–510, doi: 10.1038/ngeo261.
- Fullea, J., Fernàndez, M. and Zeyen, H., 2008. FA2BOUG—A FORTRAN 90 code to compute Bouguer gravity anomalies from gridded free-air anomalies: Application to the Atlantic-Mediterranean transition zone: *Computers & Geosciences*, **34**, p. 1665–1681, doi: 10.1016/j.cageo.2008.02.018.
- Ganade, C.E., Weinberg, R.F., Caxito, F.A., Lopes, L.B.L., Tesser, L.R. and Costa, I.S., 2021. Decratonization by rifting enables orogenic reworking and transcurrent dispersal of old terranes in NE Brazil: *Scientific Reports*, **11**, p. 5719, doi: 10.1038/s41598-021-84703-x.
- Godin, L. and Harris, L.B., 2014. Tracking basement cross-strike discontinuities in the Indian crust beneath the Himalayan orogen using gravity data – relationship to upper crustal faults: *Geophysical Journal International*, **198**, p. 198–215, doi: 10.1093/gji/ggu131.

- Gordilho Barbosa, R., Ferreira, A., Leitzke, F.P., Dos Santos, T.N., Conceição, R.V. and Martin, H., 2023. A review of 3.66 to 2.77 Ga crustal differentiation in the northern São Francisco Craton, Brazil: *International Geology Review*, **65**, p. 1541–1557, doi: 10.1080/00206814.2022.2098542.
- Heilbron, M., Cordani, U.G. and Alkmim, F.F. (Eds.), 2017. *São Francisco Craton, Eastern Brazil: Tectonic Genealogy of a Miniature Continent*: Springer International Publishing, Cham.
- Holdsworth, R.E., Handa, M., Miller, J.A. and Buick, I.S., 2001. Continental reactivation and reworking: an introduction: *Geological Society, London, Special Publications*, **184**, p. 1–12, doi: 10.1144/GSL.SP.2001.184.01.01.
- Hornby, P., Boschetti, F. and Horowitz, F.G., 1999. Analysis of potential field data in the wavelet domain: *Geophysical Journal International*, **137**, p. 175–196, doi: 10.1046/j.1365-246x.1999.00788.x.
- Lee, C.-T.A., Luffi, P. and Chin, E.J., 2011. Building and Destroying Continental Mantle: *Annual Review of Earth and Planetary Sciences*, **39**, p. 59–90, doi: 10.1146/annurev-earth-040610-133505.
- Liégeois, J.-P., Abdelsalam, M.G., Ennih, N. and Ouabadi, A., 2013. Metacraton: Nature, genesis and behavior: *Gondwana Research*, **23**, p. 220–237, doi: <https://doi.org/10.1146/annurev.ea.16.050188.002551>.
- Liégeois, J.P., Latouche, L., Bougrara, M., Navez, J. and Guiraud, M., 2003. The LATEA metacraton (Central Hoggar, Tuareg shield, Algeria): behaviour of an old passive margin during the Pan-African orogeny: *Journal of African Earth Sciences*, **37**, p. 161–190, doi: 10.1016/j.jafrearsci.2003.05.004.
- Lira Santos, L.C.M.D., Lages, G.A., Caxito, F.A., Dantas, E.L., Cawood, P.A., Lima, H.M. and Da Cruz Lima, F.J., 2022. Isotopic and geochemical constraints for a Paleoproterozoic accretionary orogen in the Borborema Province, NE Brazil: Implications for reconstructing Nuna/Columbia: *Geoscience Frontiers*, **13**, p. 101167, doi: 10.1016/j.gsf.2021.101167.
- Liu, S., Zhang, A., Lin, C., Zhang, B., Yuan, H., Huang, D., Steel, R.J. and Horton, B.K., 2021. Thrust duplexing and transpression in the Yanshan Mountains: Implications for early Mesozoic orogenesis and decratonization of the North China Craton: *Basin Research*, **33**, p. 2303–2327, doi: 10.1111/bre.12558.

- Miller, H.G. and Singh, V., 1994. Potential field tilt—a new concept for location of potential field sources: *Journal of Applied Geophysics*, **32**, p. 213–217, doi: 10.1016/0926-9851(94)90022-1.
- Neves, S.P., 2021. Comparative geological evolution of the Borborema Province and São Francisco Craton (eastern Brazil): Decratonization and crustal reworking during West Gondwana assembly and implications for paleogeographic reconstructions: *Precambrian Research*, **355**, p. 106119, doi: 10.1016/j.precamres.2021.106119.
- Oliveira, R.G. and Medeiros, W.E., 2018. Deep crustal framework of the Borborema Province, NE Brazil, derived from gravity and magnetic data: *Precambrian Research*, **315**, p. 45–65, doi: 10.1016/j.precamres.2018.07.004.
- Paton, C., Woodhead, J.D., Hellstrom, J.C., Hergt, J.M., Greig, A. and Maas, R., 2010. Improved Laser Ablation U-Pb Zircon Geochronology through Robust Downhole Fractionation Correction: *Geochemistry, Geophysics, Geosystems*, **11**, p. n/a-n/a, doi: 10.1029/2009gc002618.
- Pavlis, N.K., Holmes, S.A., Kenyon, S.C. and Factor, J.K., 2012. The development and evaluation of the Earth Gravitational Model 2008 (EGM2008): *Journal of Geophysical Research: Solid Earth*, **117**, p. n/a-n/a, doi: 10.1029/2011jb008916.
- Petrus, J.A. and Kamber, B.S., 2012. VizualAge: A Novel Approach to Laser Ablation ICP-MS u-Pb Geochronology Data Reduction: *Geostandards and Geoanalytical Research*, **36**, p. 247–270, doi: 10.1111/j.1751-908x.2012.00158.x.
- Rocha, M.P., Azevedo, P.A.D., Assumpção, M., Pedrosa-Soares, A.C., Fuck, R. and Von Huelsen, M.G., 2019. Delimiting the Neoproterozoic São Francisco Paleocontinental Block with P-wave traveltimes tomography: *Geophysical Journal International*, **219**, p. 633–644, doi: 10.1093/gji/ggz323.
- Santos, E.J. and Brito Neves, B.B., 1984. Província Borborema. In: *O Pré-Cambriano do Brasil* (Almeida, F.F.M.D., and Hasui, Y., eds.) Edgard Blucher, São Paulo, p. 123–186.
- Spector, A. and Grant, F.S., 1970. STATISTICAL MODELS FOR INTERPRETING AEROMAGNETIC DATA: *GEOPHYSICS*, **35**, p. 293–302, doi: 10.1190/1.1440092.
- Teixeira, W., Oliveira, E.P. and Marques, L.S., 2017. Nature and Evolution of the Archean Crust of the São Francisco Craton. In: *São Francisco Craton, Eastern Brazil, Regional Geology Reviews* (Heilbron, M., Cordani, U.G., and Alkmim, F.F., eds.) Springer International Publishing, Cham, p. 29–56.
- Trompette, R., 1994. *Geology of Western Gondwana (2000 - 500 Ma): Pan-African-Brasiliano Aggregation of South America and Africa*: CRC Press.

- Trompette, R.R., Uhlein, A., Silva, M.E. and Karmann, I., 1992. O CRÁTON BRASILIANO DO SÃO FRANCISCO - UMA REVISÃO: *Revista Brasileira de Geociências*, **22**, p. 481–486, doi: 10.25249/0375-7536.1991481486.
- Vale, J.A., Monteiro, L., Basto, C., Medeiros, V., Silveira, D., Uchôa Filho, E., Pedrosa Junior, N., Rodrigues, J. and Santos, T., 2023. Lithogeochemistry and zircon U-Pb geochronology of the Granjeiro Complex and associated units, Curral Novo do Piauí, NW-Borborema Province, Brazil: implications for Archean to Paleoproterozoic crustal evolution: *Journal of the Geological Survey of Brazil*, **6**, p. 239–262, doi: 10.29396/jgsb.2023.v6.n3.2.
- Van Schmus, W.R., De Brito Neves, B.B., Hackspacher, P. and Babinski, M., 1995. and geochronologic studies of the eastern Borborema Province, Northeastern Brazil: initial conclusions: *Journal of South American Earth Sciences*, **8**, p. 267–288, doi: 10.1016/0895-9811(95)00013-6.
- Van Schmus, W.R., Kozuch, M. and De Brito Neves, B.B., 2011. Precambrian history of the Zona Transversal of the Borborema Province, NE Brazil: Insights from Sm-Nd and U-Pb geochronology: *Journal of South American Earth Sciences*, **31**, p. 227–252, doi: 10.1016/j.jsames.2011.02.010.
- Van Schmus, W.R., Oliveira, E.P., Da Silva Filho, A.F., Toteu, S.F., Penaye, J. and Guimarães, I.P., 2008. Proterozoic links between the Borborema Province, NE Brazil, and the Central African Fold Belt: *Geological Society, London, Special Publications*, **294**, p. 69–99, doi: 10.1144/SP294.5.
- Vauchez, A., Neves, S., Caby, R., Corsini, M., Egydio-Silva, M., Arthaud, M. and Amaro, V., 1995. The Borborema shear zone system, NE Brazil: *Journal of South American Earth Sciences*, **8**, p. 247–266, doi: 10.1016/0895-9811(95)00012-5.
- Vermeesch, P., 2018. IsoplotR: A Free and Open Toolbox for Geochronology: *Geoscience Frontiers*, **9**, p. 1479–1493, doi: 10.1016/j.gsf.2018.04.001.
- Wu, F.-Y., Yang, J.-H., Xu, Y.-G., Wilde, S.A. and Walker, R.J., 2019. Destruction of the North China Craton in the Mesozoic: *Annual Review of Earth and Planetary Sciences*, **47**, p. 173–195, doi: 10.1146/annurev-earth-053018-060342.

4.2. São Francisco Paleocontinent Construction, Fragmentation, and Reworking in the Mineral System Evolution of the Curral Novo Iron District São Francisco Paleocontinent Construction, Fragmentation, and Reworking in the Mineral System Evolution of the Curral Novo Iron District

1. Introduction

Banded Iron Formations (BIF) are chemical sedimentary rocks containing layers with 20 to 30% iron interspersed with SiO₂ (James, 1954, 1983). These rocks have a broad spatial-temporal distribution, extending from the Archean to the Phanerozoic (Gross, 1983; Klein, 2005; Beukes and Gutzmer, 2008; Konhauser et al., 2017), and their deposition results from the intricate interplay of mantle, tectonic, oceanic, and biospheric processes (Bekker et al., 2010, 2014; Konhauser et al., 2017). Precambrian BIF are categorized into Algoma and Superior types based on their depositional characteristics and lithological associations (Gross, 1965, 1980). Algoma-type formations are linked to volcano-sedimentary sequences in granite-greenstone belts, deposited from the Eoarchean to the Paleoproterozoic, with their genesis tied to exhalative hydrothermal processes (Gross, 1980; James, 1983; Beukes and Gutzmer, 2008; Bekker et al., 2010, 2014). On the other hand, Superior-type BIF is found in cratonic platform sequences deposited during the Neoarchean and Paleoproterozoic, often interbedded with carbonates, quartz arenites, black shales, and restricted volcanic rocks (Gross, 1965, 1980).

The world's significant iron ore reserves, with grades > 60%, are mainly enriched Precambrian BIF (Beukes and Gutzmer, 2008; de Kock et al., 2008). These reserves are predominantly hosted in Superior-type BIF, such as the Iron Quadrangle, characterized by hematitic/goethitic ores with lower production costs (Rosière and Chemale Jr, 2000). In contrast, deposits hosted in Archean Algoma-type BIF, with magnetite as the dominant ore mineral, are smaller (Duuring and Hagemann, 2013a, 2013b). Ore generation in both cases is associated with syn-depositional processes, including the abundance of iron in host rocks, and post-depositional processes like fluid percolation, silica remobilization, and mineralized body preservation (Angerer et al., 2015; Hensler et al., 2015; Hagemann et al., 2016). Metamorphism also influences this system, as increasing metamorphic grade enhances the growth of iron oxide and quartz grains, aiding their separation during beneficiation (Maynard, 1991).

The mineralizing system enriching BIF involves syn- and post-depositional processes (Angerer and Hagemann, 2010; Angerer et al., 2015; Hagemann et al., 2016). Syn-

depositional processes, linked to the stratigraphy and geodynamic features of depositional environments, dictate iron fertility in BIF. Post-depositional processes dissolve silica and entail hypogene and supergene fluid percolation, facilitated by permeability at various scales. Geological structures play critical roles in the exhumation, geometry, preservation, and modification of mineralized bodies (Thorne et al., 2014).

Enrichment occurs via percolation of hydrothermal and meteoric fluids along faults and fractures (Morris, 1980; Beukes et al., 2003; Dalstra and Rosière, 2008; Lobato et al., 2008; Hagemann et al., 2016; Keyser et al., 2018, 2019a). These fluids dissolve silica, transforming primary iron-bearing minerals like siderite, ankerite, and iron silicates into hematite and magnetite microplates (Morris, 1980; Beukes et al., 2003; Dalstra and Rosière, 2008; Hensler et al., 2015; Hagemann et al., 2016). Trace element concentrations in iron oxides and exhibited textures provide insights into physicochemical conditions during enrichment (Rosière et al., 2001; Keyser et al., 2018, 2019b). In polydeformed Archean greenstone belt terranes, reconstructing depositional environments and the general geological structure of Algoma-type BIF is challenging due to metamorphism and deformation (Klein, 2005; Bekker et al., 2010). Understanding syn- and post-depositional processes at regional and deposit scales is critical for discovering new exploration areas.

Cratons and their margins are known for high mineral deposit concentrations (Groves and Santosh, 2021). While some studies explore the relationship between decratonization processes (Yang et al., 2008) and mineral deposit genesis, they often focus on gold deposits (Li and Santosh, 2014; Yang and Santosh, 2020; Yang et al., 2021, 2022; Li et al., 2022). The SFC and BP share pre-Brazilian similarities, such as older platform rocks, Siderian rocks, and diachronic taphrogenic events (Neves, 2021). Due to these similarities, some researchers suggest the possibility that the old terranes from BP are a product of São Francisco Paleocontinent (SFP) fragmentation in a decratonization process (Ganade et al., 2021; Neves, 2021). Here, we investigate how the construction and fragmentation of the SFP influenced iron ore deposit formation associated with BIF on the northwest margin of the CSF and in the southwest of the Borborema Province (BP) (Figure 1C). We demonstrate that BIF deposition and initial enrichment occurred during SFP construction, with its destruction possibly preserving proto-ore and ore. Transport and reworking of SFP fragments may have enhanced the mineral fertility of the Borborema Province basement, not only in iron but also in other metals.

2. Geological settings

The São Francisco Craton (SFC) and Borborema Province (BP) share pre-Brazilian similarities. Some researchers suggest that the old terrains of the BP might have originated from the fragmentation of the SFC during a decratonization process (Ganade et al., 2021; Neves, 2021). In this study, we investigated the iron formations of the Curral Novo Iron District (CND) (Sato, 2011; Vale et al., 2023), located in the Granjeiro Complex (Caxito et al., 2020; Brito Neves et al., 2023; Vale et al., 2023). This complex corresponds to the basement bounded to the south by the Pernambuco Lineament, which borders the Riacho do Pontal orogen to the north of the SFC and south of the BP (Caxito et al., 2016, 2017, 2020; dos Santos, 2017; Amaral et al., 2023).

The São Francisco Craton (SFC) basement comprises Archean nuclei recording magmatic events between 2.8-2.7 Ga (Teixeira et al., 2017). During the Rhyacian-Orosirian orogeny, these nuclei amalgamated (Trompette et al., 1992; Barbosa and Sabaté, 2004; Brito Neves, 2011; Teixeira et al., 2017). Subsequently, intraplate basin formation and magmatism episodes occurred, overlain by the Espinhaço and São Francisco supergroups, along with Neoproterozoic sedimentary rocks (Danderfer et al., 2009; Guadagnin, 2015; Paula-Santos et al., 2015; Costa et al., 2018). The Archean nuclei of Sobradinho, Gavião, Serrinha, Jequié, and Cristalândia constitute the North-Northwest basement of the SFC. The collision between Gavião, Serrinha, and Jequié blocks in the Paleoproterozoic led to the formation of the Itabuna-Curaçá-Salvador orogenic belt (ICS) (Barbosa and Sabaté, 2002, 2004; Martins De Sousa et al., 2020).

Neoproterozoic orogenic belts developed along the SFC margins due to collision between the São Francisco-Congo paleocontinent, Amazonian cratons, and São Luiz-West Africa, forming the western sector of the Gondwana Supercontinent (Figure 1A) (Trompette, 1994; Arthaud et al., 2008; Van Schmus et al., 2008; Caxito et al., 2020). The Borborema Province (BP) is one of the orogenic systems resulting from this collision (Almeida et al., 1981). The BP comprises Archean nuclei reworked in the Paleoproterozoic, intruded by Neoproterozoic granites, and covered by Neoproterozoic basins (Figure 1B) (Caxito et al., 2020). Regional shear zones mark the end of this collision, dividing the province into three segments: North, Transversal, and South sub-provinces, further subdivided into domains (Brito Neves, 1975; Brito Neves and Cordani, 1991; Trompette, 1997). Extensive ductile shear zones formed due to this convergence, characterized by a preferred NNE-SSW and E-W direction, as evidenced by well-developed mylonitic belts (Figure 1B) (Corsini et al., 1991; Vauchez et al.,

1995).

The Granjeiro Complex is bordered to the west by the Rio Piranhas-Seridó Domain, to the north by the Orós-Jaguaribe Belt, limited by the Malta shear zone, and to the south by the Paulistana-Monte Orebe and Itaizinho domains, delineated by the Patos Lineament (Caxito et al., 2020). This complex is divided into two main exposure areas: one in the central-eastern portion, near Granjeiro in Ceará state, and the other in the southwest of the Patos Shear Zone, spanning Piauí and Pernambuco states. The connection between these two sections is covered by the Araripe Basin (Vasconcelos and Gomes, 1998). These sections are referred to as the Northern Granjeiro Complex (NGC), corresponding to the exposure area in Ceará, and the Southern Granjeiro Terrane (SGC), occurring between Piauí and Pernambuco states.

The oldest unit within the Granjeiro Complex consists of paraderived and orthoderived gneisses and an exhalative metavolcano-sedimentary association, initially interpreted as remnants of oceanic crust, intruded by Archean tonalitic to granodioritic metaplutonic rocks (Gomes and Vasconcelos, 2000). The Tonalitic and granodioritic orthogneisses in the GC exhibit calcic to alkali-calcic characteristics with low mafic mineral content. They show low lithophile element concentrations, significant fractionation of light rare earth elements, and slightly negative Eu anomalies (Vale et al., 2023). U-Pb geochronology indicates a Paleoarchean protolith age of 3.5 – 3.4 Ga for tonalitic orthogneiss zircon (Martins, 2017; Pitarello et al., 2019; Brito Neves et al., 2023; Vale et al., 2023).

The metavolcano-sedimentary unit consists of felsic and mafic metatuffs, amphibolites, magnesian schists, serpentinites, originating from mafic and ultramafic protoliths with a komatiitic and basaltic composition and banded iron formations (Gomes and Vasconcelos, 2000; Costa, 2010; Ancelmi, 2016; Pitarello et al., 2019; Vale et al., 2023). These rocks are linked to oceanic plate subduction, displaying geochemical affinities like modern island arc rocks (Costa, 2010; Pitarello et al., 2019; Vale et al., 2023). Intrusive syenogranitic plutons, dated to 2.651 Ga, intrude these units (Martins, 2017; Pitarello et al., 2019; Brito Neves et al., 2023; Vale et al., 2023). These granites are metaluminous to peraluminous, alkali-calcic, and ferrous, with a slight enrichment of light rare earth elements over heavy rare earth elements and high lithophile and high field potential element contents (Vale et al., 2023).

The GC underwent significant crustal reworking during the Paleoproterozoic, starting from the Rhyacian, with a metamorphic peak in metavolcanosedimentary rocks indicated by U- Pb dating of amphibolite zircon at 2.2 Ga (Vale et al., 2023). A significant

magmatic event related to global continental extension during the Statherian period, dated to 1.75 – 1.6 Ga (Amaral et al., 2023; Vale et al., 2023), led to hydrothermal alteration in surrounding amphibolites and iron formations, resulting in silicification, albitization, potassification, carbonatization, sulfidation, and iron reconcentration. $\delta^{34}\text{S}$ values ranging from -3.11 to +2.3 per mil in hydrothermal sulfides suggest magmatic sources for sulfur associated with the hydrothermal system (Vale, 2018; Vale et al., 2023).

Based on mineralogical and geochemical analyses, the BIF of the CND were categorized into three groups by Pitarello et al.(2019): i) Magnetite Meta-BIF, interpreted as a product of Oxide Facies metamorphism, with contributions from high-temperature hydrothermal fluids indicated by positive Eu anomalies and minor Ce anomalies typical of Archean BIF; ii) Grunerite Meta-BIF, corresponding to Silicate and Carbonate Facies metamorphism. Although its geochemical signature did not exhibit characteristics of chemical sediments, its REE pattern suggested that hydrothermal processes, interaction with adjacent rocks, and supergene enrichment processes altered these rocks; iii) Garnet Meta-BIF, this group would correspond to Silicate and Carbonate Facies metamorphism contaminated by clastic debris, possibly deposited in areas close to the continent. Costa (2010) identified two types of ore at the Manga Velha locality: i) Magnetite BIF, metamorphosed in the amphibolite facies with amphiboles of the cummingtonite-grunerite series; ii) Hydrothermal IronStone corresponding to magnetite injected into structural planes, interpreted as percolation and remobilization of ore into the host rock by hydrothermal fluids. The geochemical signatures of the host rocks suggested that these chemical sediments were deposited in a back-arc basin (Costa, 2010; Ancelmi, 2016; Pitarello et al., 2019).

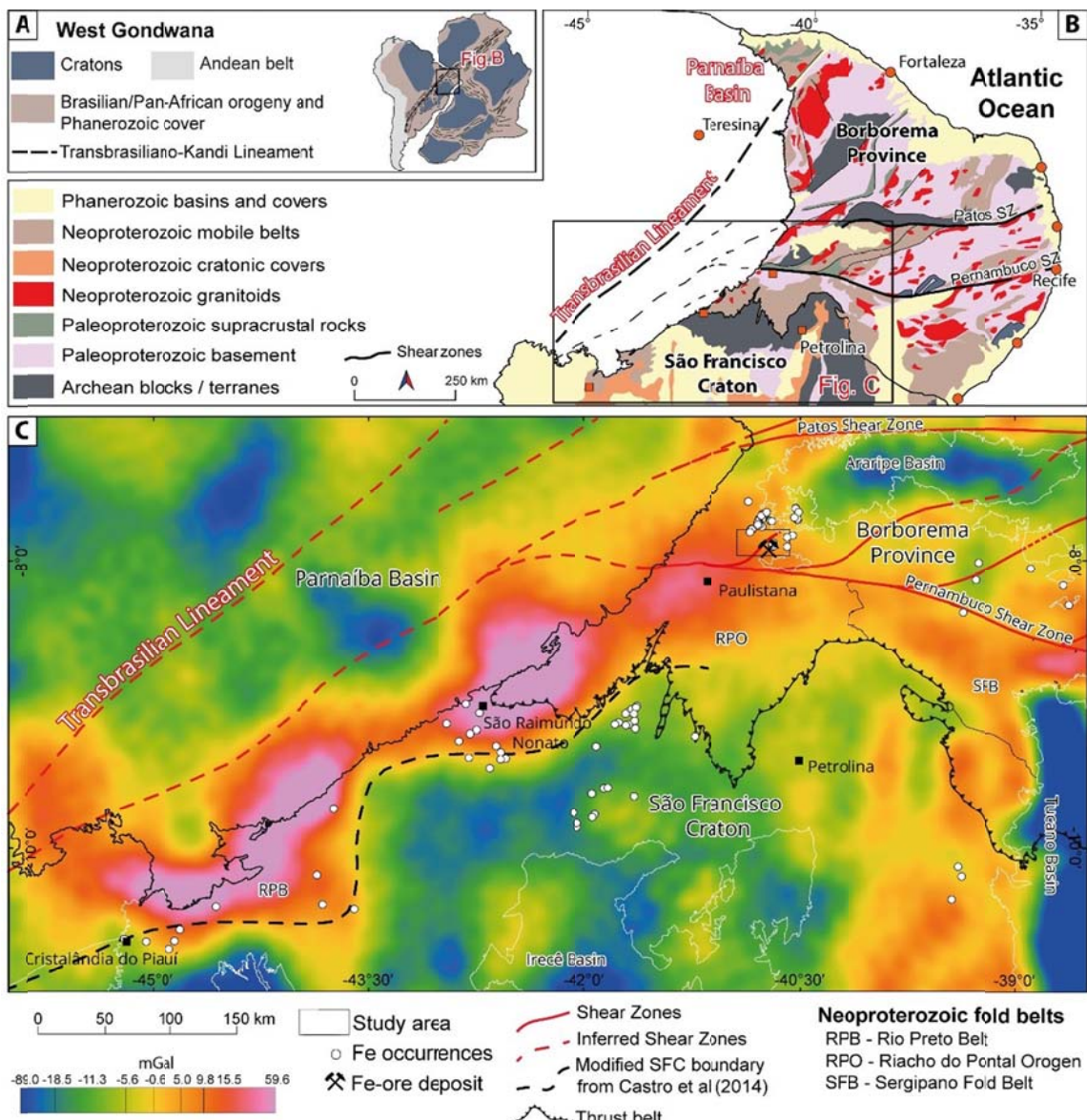


Figure 1 - Simplified tectonic map of the BP and location of the study area: (A) Location of the BP in the context of West Gondwana. (B) BP highlighting the main tectonic units comprising the study area. (C) Map of the Total Bouguer Anomaly from the EGM2008 Model (Pavlis et al., 2012), showing the main regional structures (Modified from Buzzi et al., (2003) and the location of the CND and iron ore occurrences. The iron ore occurrences were collected from the GSB available at <https://geosgb.sgb.gov.br/>).

3. Remote sensing

3.1. Structural lineaments

Geological structures are critical in thickening and enriching the proto-ore, potentially doubling its thickness and facilitating the percolation of hypogenic and supergene fluids (Dalstra and Rosière, 2008; Dalstra, 2014; Thorne et al., 2014; Hagemann et al., 2016). We used remote sensing to visualize the spatial distribution of these regional structures and their relationship with the ore, aiming to understand their contribution to forming the mineral system responsible for enriching the proto-ore. To map shear zones and structural lineaments, we employed satellite imagery and the Copernicus DSM GLO-30 Digital Surface Model (ESA, 2022), with a resolution of 30 meters. Through processing and interpreting these images, we identified and delineated structural lineaments, predominantly characterized by regional transpressional shear zones with dextral kinematics and inferred the presence of faults (Figure 2A and 2B). To understand the relationship between high-grade ore occurrences and geological structures, we investigated the proximity between the ore and fault zones and how they interact with the density of structural lineaments in the region.

Figure 2C shows the distance between fault zones and high-grade ore. This map reveals that the high-grade ore is located near regions of more significant ductile deformation, with mineral occurrences, albeit less enriched, occurring at slightly greater distances, except for samples northwest of the study area. The closer proximity to these ductile deformation zones may have facilitated the percolation of supergene fluids, inferred by a stronger association with hydrothermal minerals, as discussed in the next section. Figure 2D depicts the density of structural lineaments derived from the Copernicus DEM. Here, high-grade ore is associated with higher structural lineament density regions. We can attribute the higher density of fractures to greater structural permeability, which contributed to increased circulation of supergene fluids and late-stage ore enrichment.

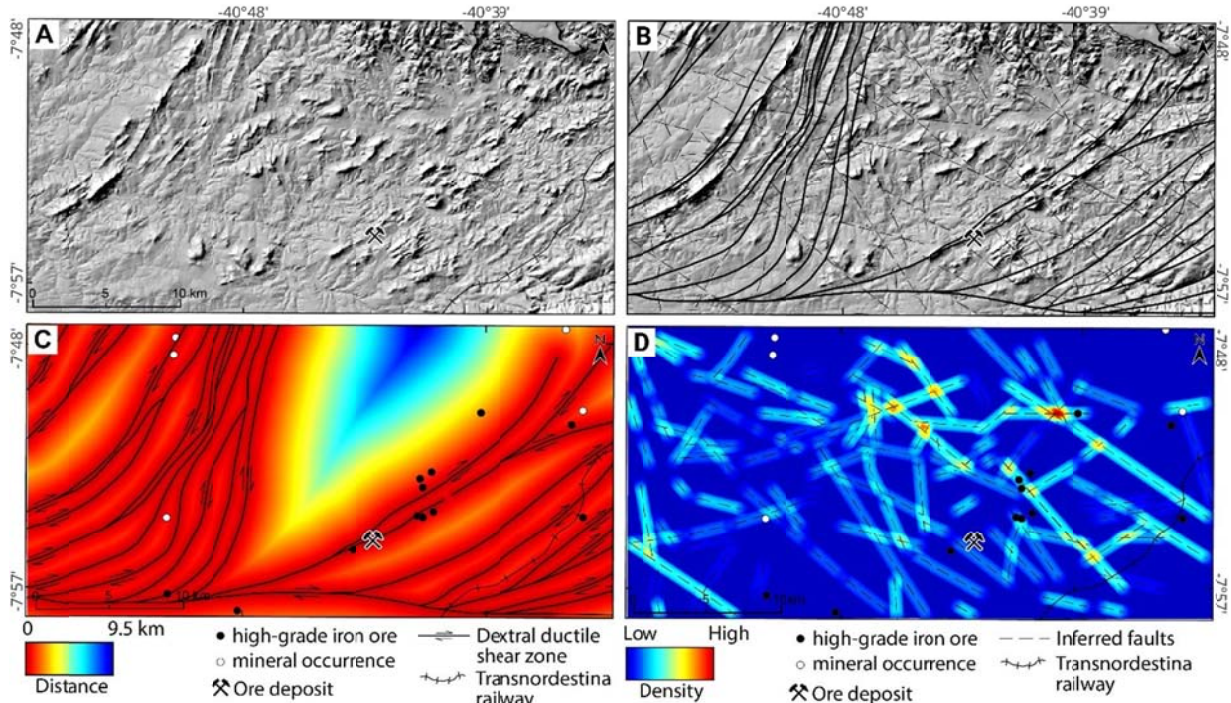


Figure 2 – Extraction of structural information from the Copernicus DSM GLO-30 Digital Surface Model: (A) Digital model with lighting from 315N and a 45° inclination. (B) Interpretation of shear zones and structural lineaments. (C) Distance map in kilometers from the shear zones. (D) Density map of structural lineaments extracted from the interpretation of the Copernicus DSM GLO-30 image.

3.2. Principal Component Analysis

We utilized Landsat 8 OLI satellite imagery to visualize the spatial distribution of iron oxide and hydrated minerals in the study area. To extract these insights, we applied Principal Component Analysis (PCA) following the methodology proposed by Loughlin (1991) adapted from Feature-Oriented Principal Components Selection (FPCS) (Crosta and McMoore, 1989). In this technique, we utilized the loadings of the eigenvectors from the Principal Components (PCs) to indicate which component images are related to the spectral signatures of specific targets. By generating the PCs using fewer bands, we aimed to avoid spectral contrast and increase the likelihood that a single PC summarizes a specific mineral class.

We applied Principal Component Analysis (PCA) to bands 2, 4, 5, and 6 of Landsat 8 to enhance regions rich in iron oxides. Bands 4 and 6 correspond to Red and SWIR wavelengths, exhibiting maximum reflectance for iron oxide minerals. Bands 2 and 5, Blue

and NIR, show low reflectance. Table 1 displays the eigenvector matrix for the PCs for iron oxide in the study area. We selected PC4 to map these materials as it demonstrates higher corresponding eigenvector values. However, PC4 was negated to ensure maximum reflectance values appear in bright pixels (Figure 3C).

Table 1 - Eigenvectors of the PCs of bands 2, 4, 5, and 6 of Landsat 8 for detecting iron oxide minerals.

	Band 2	Band 4	Band 5	Band 6
PC1	0.149	0.404	0.555	0.711
PC2	-0.060	0.025	0.786	-0.615
PC3	-0.386	-0.816	0.262	0.340
PC4	0.908	-0.412	0.072	-0.013

We used PCA to map minerals containing hydroxyl on bands 2, 5, 6, and 7 of Landsat 8 imagery. Minerals containing hydroxyl and carbonates exhibit absorption in the Visible and Near-Infrared (VNIR) and Short-Wave Infrared (SWIR) regions ([Rowan and Mars, 2003](#); [Huntington, 2007](#)), as represented by bands 5 and 7. Higher reflectance is observed in bands 2 and 6. We selected PC3 to map minerals related to hydrothermal alteration because it is the component that shows the best contrast between the targets' absorption and reflectance. The values of the Eigenvectors generated in the PCA are presented in Table 2. The image corresponding to PC3 is shown in Figure 3D.

Table 2 - Eigenvectors of the PCs of bands 2, 5, 6, and 7 of Landsat 8 for detecting hydroxyl and carbonate-bearing minerals.

	Band 2	Band 4	Band 5	Band 6
PC1	0.139	-0.495	-0.675	-0.530
PC2	0.006	-0.828	0.192	0.527
PC3	-0.148	-0.244	0.713	-0.641
PC4	-0.979	0.102	-0.011	0.175

According to Loughlin (1991), a ternary image can be generated using the PCs obtained for the enhancement of iron oxide minerals (F) and hydroxyl minerals (H), the third image is the sum between F and H (Figure 3E). The resulting ternary image is presented in

Figure 3F. Finally, in Figure 3G we integrate all the structural information extracted from the Copernicus DEM with the PCs for Fe oxides and hydrated minerals using QGIS 3.34 software. We use a spatial intersection function to define regions where both iron oxide values and hydrated minerals occur (regions in yellow in Figure 3G).

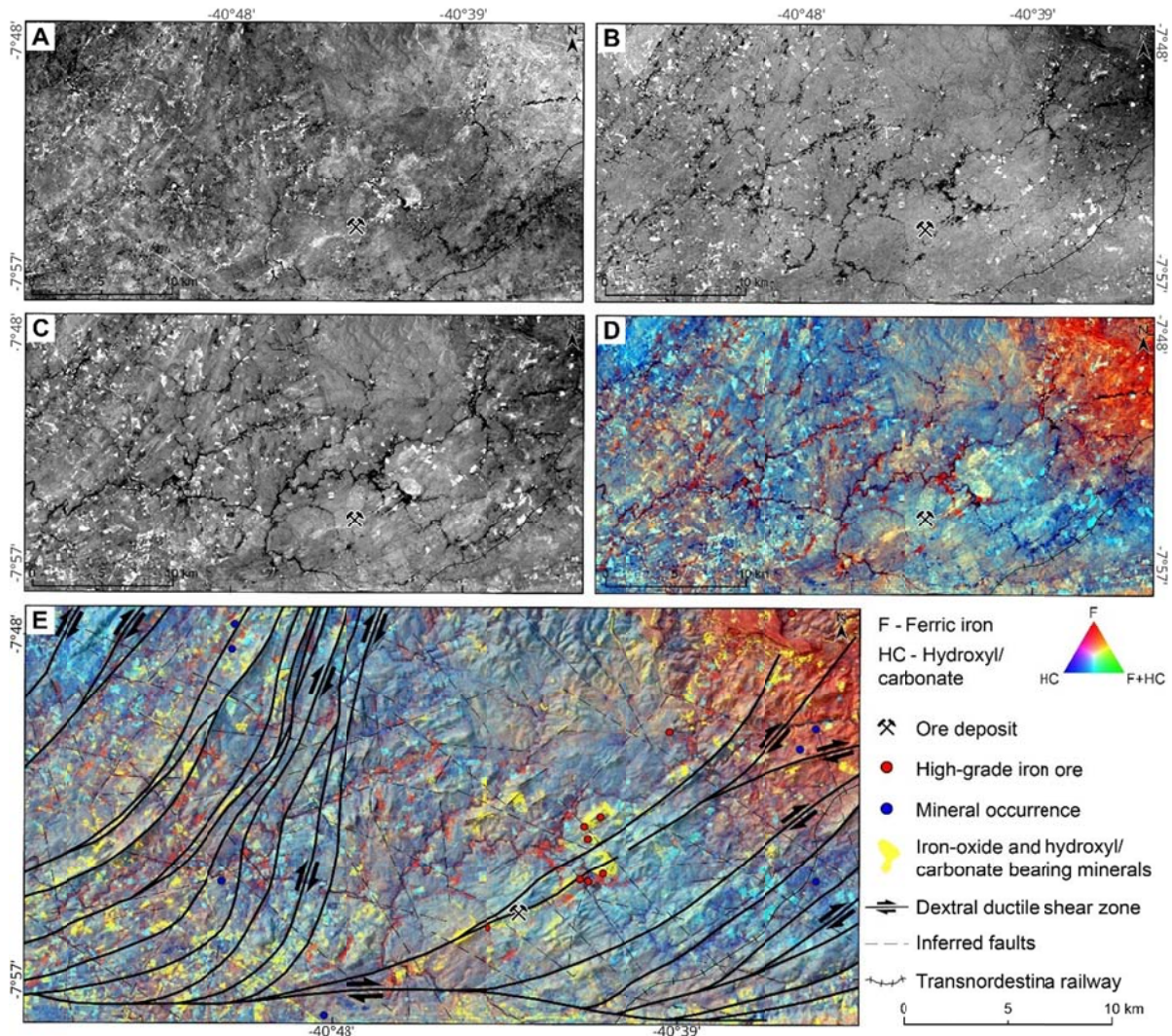


Figure 3 – PCs for spectral target enhancement. (A) PC4 image of Landsat 8 bands 2, 4, 5, and 6 for iron oxide enhancement - F (bright pixels). (B) PC4 image of Landsat 8 bands 2, 5, 6, and 7 for regions rich in hydroxyl minerals and carbonates - H (bright pixels). (C) The sum of F and H highlights regions where these two pieces of information predominate. (D) Ternary image the PCs F, F+H, and H in red, green, and blue channels. (E) Integration of structural information with the distribution of regions where the intersection of iron oxide and hydroxyl/carbonate-bearing minerals occurs.

4. Structural settings

The geometric and kinematic analysis of the present geological structures allowed us to identify five deformation events (D1, D2, D3, D4 and D5). We divided the structures based on their morphological and spatial characteristics using the definition of deformational facies described by [Tikoff and Fossen \(1999\)](#), which involved classifying the orientation of L-type tectonics (such as stretching lineations and fold axes) and S-type tectonics (such as foliation planes) within homologous deformation zones. Planar features were labeled according to their chronological order, while linear features were classified as Lx when related to fold axes, Lb for mineral stretching, and Lx for stretching.

During field surveys, we identified two deposition sequences. The first is interleaved with fragments of the TTG basement and intruded by granitoids, predominantly in the eastern sector of the study area. The second sedimentary sequence is found west of the area and consists of metasediments of arkosic composition, with basic and acidic dikes parallel to foliation. Below, we describe each deformation event and the associated geometric features.

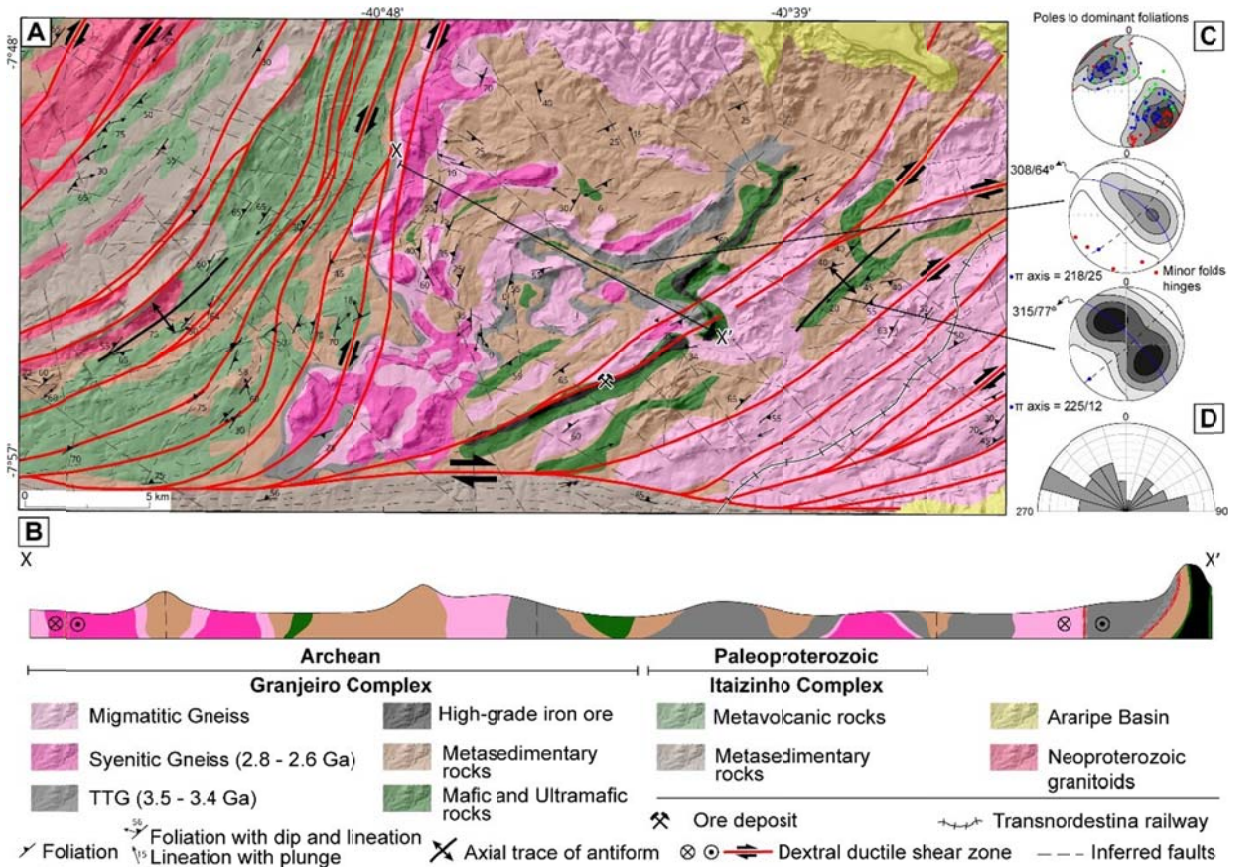


Figure 4 – (A) Structural map of the study area within the Granjeiro Complex. (B) Cross-section X-X' depicted in Figure 4A illustrates structural features. (C) Stereonet diagrams displaying D1 and D2 deformational fabric orientations were generated using the Orient software by Vollmer (2023). (D) Histogram illustrating the spatial distribution of structural lineaments extracted from the Copernicus DSM GLO-30 Digital Surface Model.

4.1. D1 Event

Event D1 is characterized by extensional deformation in the greenstone belt strata, which deposited the proto-ore (S01). Although transpressional deformation zones surround the entire area, some regions show low deformation interference, preserving pre-transcurrent structural markers. Regionally, these features are observed in the center of the study area, following an irregular foliation pattern. In the central area, metavolcanic-sedimentary rocks predominate. They display an irregular foliation pattern and minimal deformation preserved through deformation partitioning, suggesting a lozenge-bearing tectonic concept. This circular pattern resembles dome and keel structures observed in other Archean records.

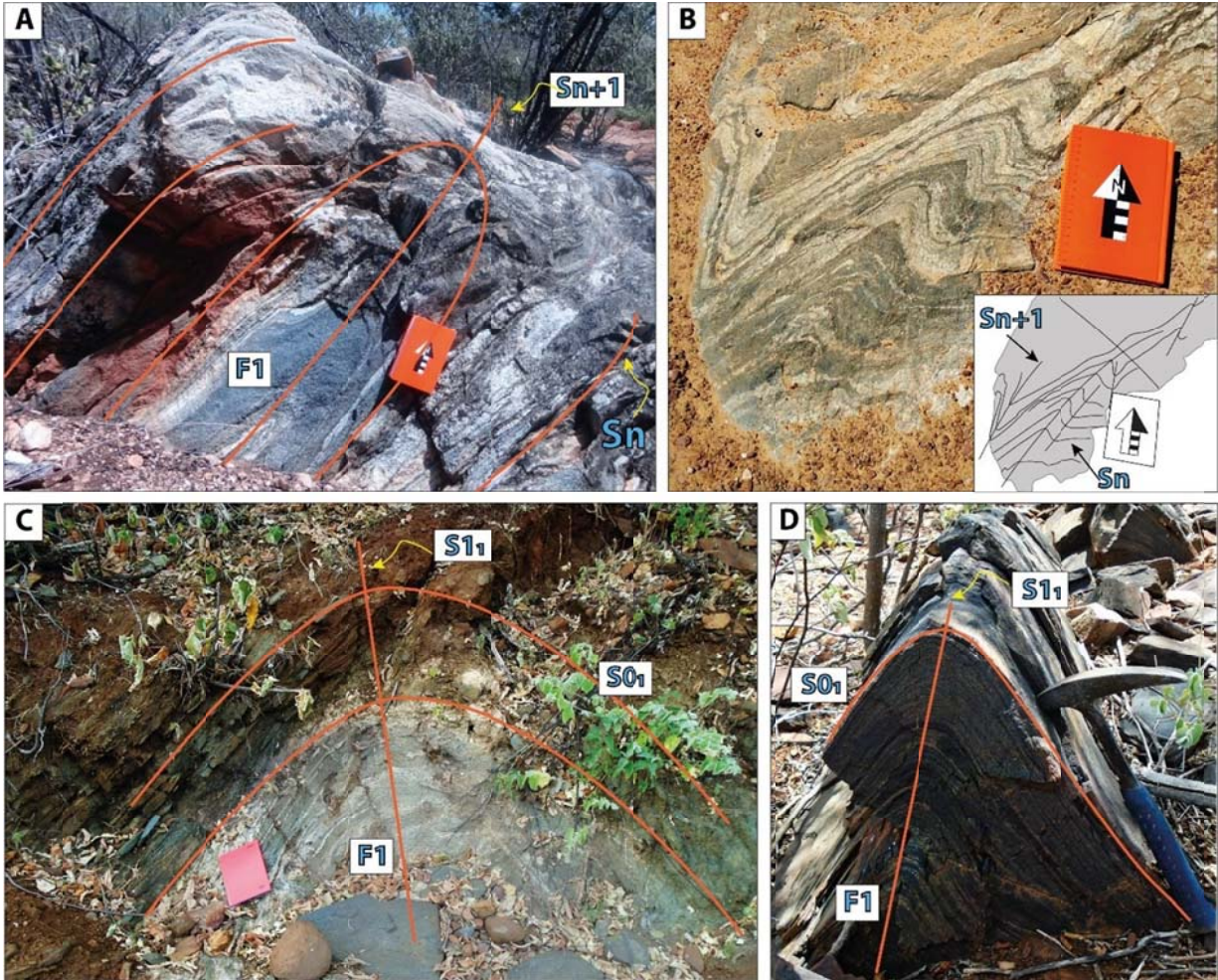


Figure 5 – Geometric patterns, at outcrop scale, of structures developed during Events D1 and D2: (A) F1 close folds in TTG basement rocks with axial plane corresponding to Sn+1 foliation, trending NE-SW and dipping towards NW. (B) F1 folds in TTG gneiss rock formed from Sn. (C) Symmetrical open F1 folds in metavolcanic rocks formed from S01, forming axial plane S1₁ dipping NE-SW towards SE. (D) Symmetrical, isoclinal to tight F1 folds formed from the shortening of S0₁ in BIF deposition, forming axial plane S1₁ dipping NE-SW towards NW.

4.2. D2 Event

Figure X illustrates the main features of deformation D2. In the TTGs, the oldest rocks of the basement, whose banded gneisses (Sn), this deformation generates F1 folds (Fig. 5A). The F1 folds are tight, with a moderately inclined axial plane and a gentle plunge axis (Lb1) (Fig. 5B). The axial plane of the F1 folds forms the Sn+1 foliation trending NE-SW with dip angles varying from moderate to high, migrating to zones of higher deformation and forming mylonitic bands. Parallel to Sn+1, there is a stretching mineral lineation Lx+1

trending NNE. In the central area of the study, where deformation was less intense, the F1 folds formed in the metasediments ([Fig. 5C](#)) and meta-ultramafic rocks ([Fig. 5D](#)) of the iron formations deposition sequence (S01) are cylindrical, closed with vertical axial planes (S11) and horizontal axes.

We interpret the deformation that originated the F1 folds as progressive and developed during the closure of the iron formations deposition basin, the high-grade ore proto-ore. The age for the development of this event was interpreted as earlier than 2.6 Ga and related to the amalgamation of paleo- and mesoarchean blocks in the Neoarchean.

4.3. D3 and D4 Event

Events D3 and D4 correspond, respectively, to the deposition of sediments in a rift environment and the closure of this basin. Event D3 is marked by the deposition of layer S02, composed of immature sediments such as meta-quartzitic sandstones and arkosic (meta-) sandstone ([Fig. 6A](#)). These rocks are interbedded with mafic and felsic dikes, characterizing bimodal volcanism ([Fig. 6B](#)). The compressional deformation associated with the closure of this basin formed F2 folds with axial plane S1₂ ([Fig. 6D](#)). In the basement, deformation event D4 resulted in isoclinal folds with axial plane S2₁ over foliation S1₁ ([Fig. 6E, 6F and 6G](#)).

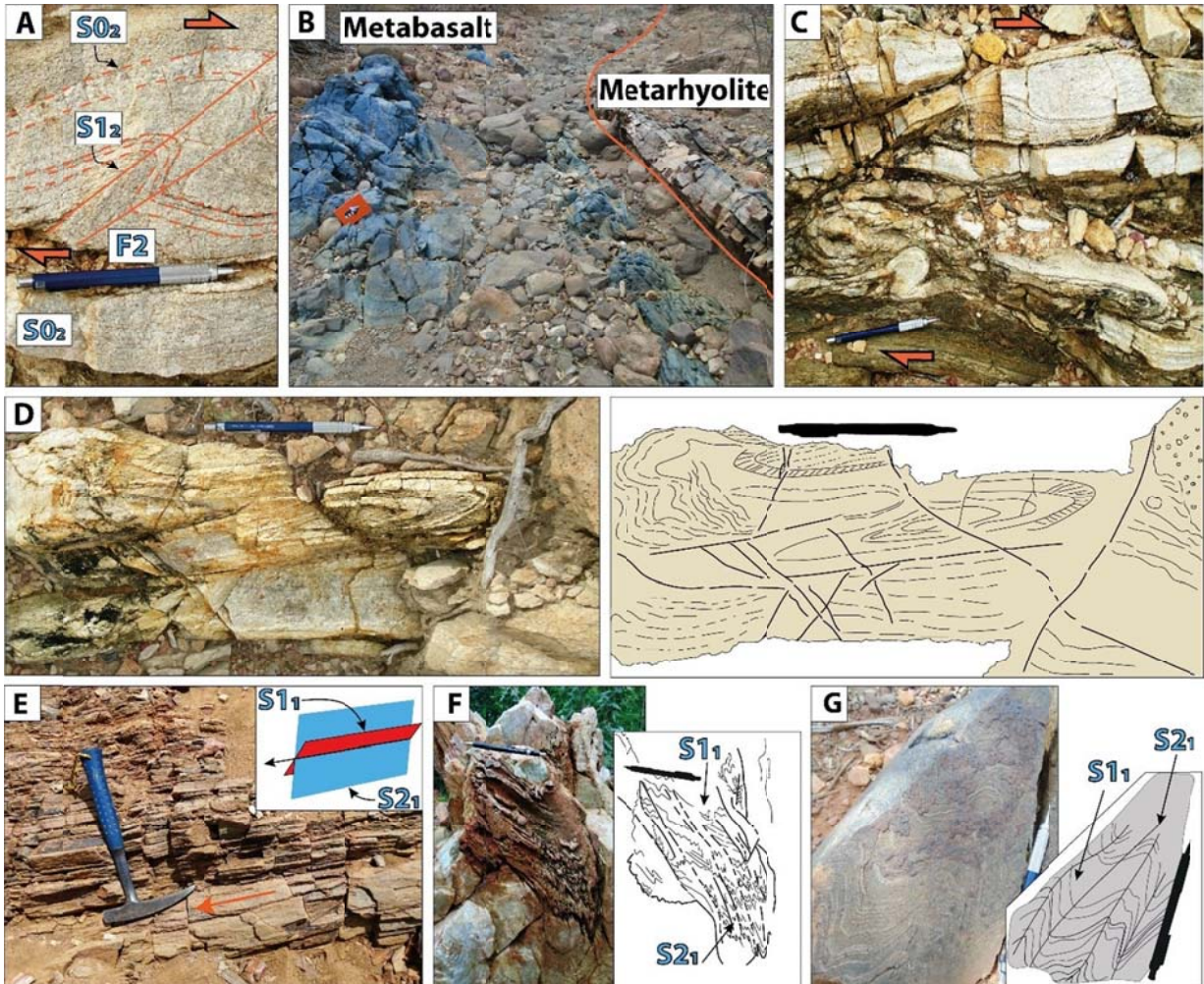


Figure 6 – Structural characteristics of Events D3 and D4: (A) Shear fault-bend folding (F2) in arkosic metasandstone formed due to the deformation of S0₂. (B) Outcrop showing the contact between metabasalt and metarhyolite. (C) Drag folds (F2) formed in layer S0₂, generating the axial plane. The progression of these structures results in overturned folds and fault-propagation folding. (D) Interpretation of an outcrop displaying tight/symmetrical isoclinal folds and sheath folds. (E - G) Outcrops illustrating the relationship between deformation (S1₁) over (S2₁), producing intersection lineation.

4.4. D5 Event

Deformation event D5 is characterized by a subvertical mylonitic foliation, labeled Sn+3, oriented NE-SW and E-W, and an obliquely dipping stretching lineation, denoted as Lx+3. This deformation event is the most significant in the area, impacting all lithotypes, generating mylonites and ultramylonites, and forming drag folds and sheath folds (Fig. 6C and 6D).

This deformation phase is associated with forming the Pernambuco Shear Zone,

which originated during the Neoproterozoic Brasiliano/Pan-African Orogeny and demonstrates dextral transcurrent-transpressive movement (Fig. 7A). In the study area, these occur as second- order shear zones associated with forming the Pernambuco Shear Zone. The foliation is vertical, oriented NNE-SSW, with significant rotation (Fig. 7B) and grain fragmentation. The stretching lineation plunges steeply towards ESE (Fig. 7C) near the shear zone, but at distances greater than 200m from the shear zone, it dips at a shallower angle. This resulted in bands ranging from milonitic to ultramylonitic, with several hundred-meter widths. After the D5 event, brittle structures developed, characterized by synthetic and antithetic Riedel faults (17 A) (Fig. 7D – 7G).

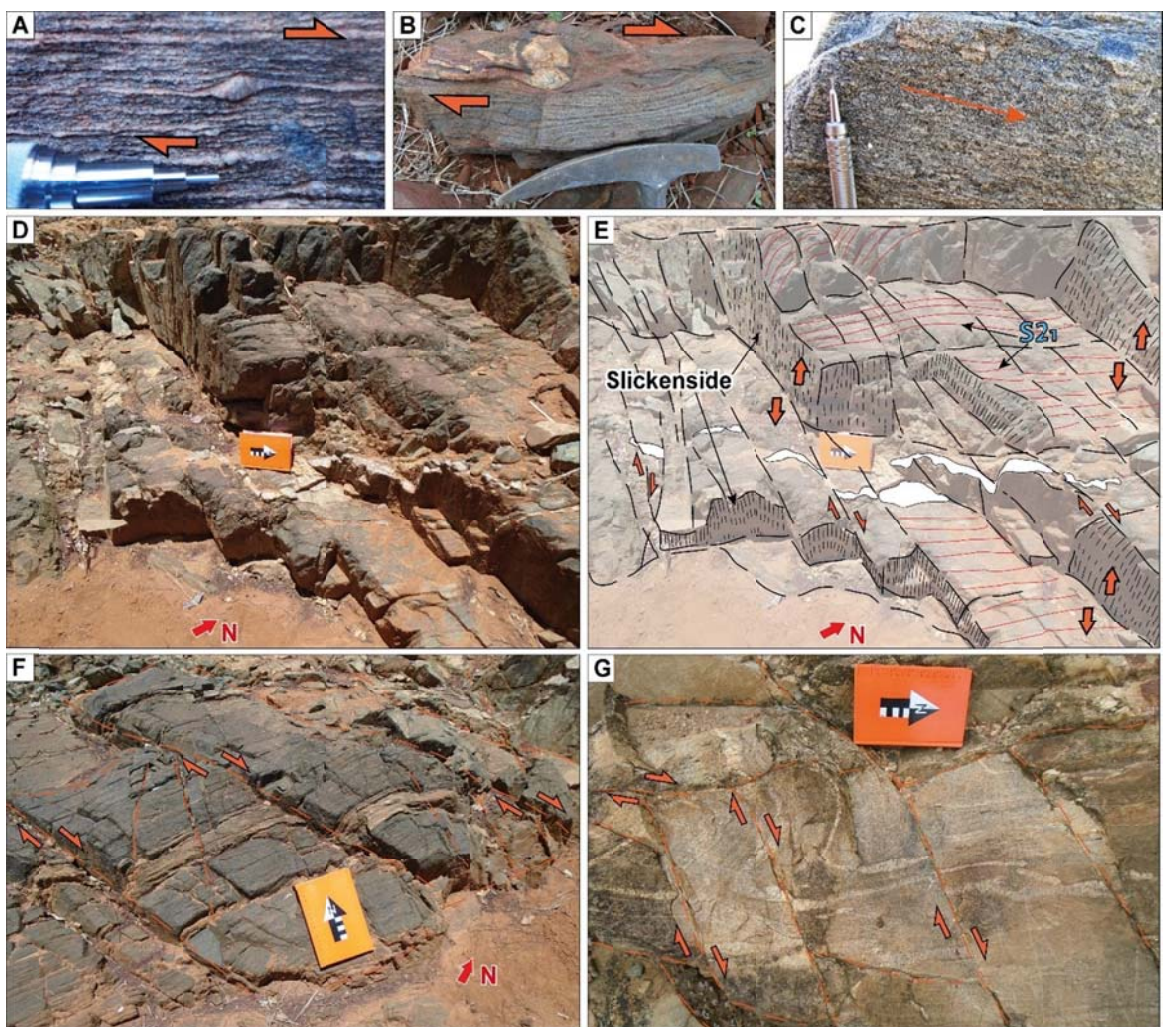


Figure 7 – Structural characteristics of Events D5 and faults. (A) Kinematic indicator of dextral shear motion in simple shear. (B) Porphyroblast rotation observed in BIF iron ore. (C) Stretching lineation on the SN foliation plane in gneiss. (D) Outcrop displaying the pattern of normal faults in ultramafic rocks. (E) Sketch of fault planes and kinematic markers indicating dextral motion. (F) Outcrop of ultramafic rock exhibiting Riedel fault deformation pattern. (G) Normal faults are cutting through an arkosic metasandstone layer.

5. Discussions

5.1. Tectonic controls on proto-ore deposition and preservation

There are three tectonic settings where BIFs are found (Hagemann et al., 2016): Algoma-type BIFs, Lake Superior-type BIFs, and Rapitan–Urucum-type BIFs. Algoma-type banded iron formations are commonly associated with submarine-emplaced volcanic rocks in convergent margin settings within Archean and Paleoproterozoic granite-greenstone belts (Gross, 1980, 1983; Beukes and Gutzmer, 2008; Konhauser et al., 2017). Lake Superior-type BIFs are present in Proterozoic sedimentary rock sequences along passive margins and are associated with some of the most significant known accumulations of iron hosted by BIFs (Gross, 1980, 1983; Beukes and Gutzmer, 2008). Rapitan–Urucum-type BIFs are found in Neoproterozoic sedimentary successions, dating from 715 to 580 Ma (Hoffman et al., 1998; Klein, 2005; Beukes and Gutzmer, 2008; Bekker et al., 2010; Konhauser et al., 2017).

Ancelmi (2016) proposed a tectonic model for the GC, suggesting that the metavolcanic-sedimentary sequence represents a greenstone belt formed in a back-arc basin within a subduction system, with the formation of a magmatic arc around 2.7-2.6 Ga. In their study, Pitarello et al. (2019) reported a sedimentation age of 2.654 ± 26 Ga, linked to the basaltic volcanism of the GC. They categorized the BIF based on their predominant metamorphic minerals as follows: Magnetite BIF, characterized by the prevalence of magnetite or hematite; Grunerite BIF, primarily composed of grunerite and magnetite; and Garnet BIF, distinguished by the presence of garnet and magnetite. These mineralogical associations suggest significant levels of high-grade metamorphism (Klein, 1983, 2005; Pitarello et al., 2019). These characteristics categorize the BIFs in the CND as Algoma-type (Santos et al., 2014).

We have identified a second depositional environment in the CND, associated with an intracontinental rift system formed around 1.75 - 1.6 Ga (Amaral et al., 2023; Vale et al., 2023), evidenced in the field by bimodal magmatism and arkosic (meta-) sandstone (see Figure 6 A - D). The normal faults are critical in preserving the ore bodies from erosion, acting as containment mechanisms, and supplying basinal fluids (Dalstra and Rosière, 2008; Hagemann et al., 2016). We hypothesize that these structures preserved the ore bodies within the CND. Changes in the tectonic regime are necessary to preserve iron ore mineralization in high-grade terrains (Müller et al., 2005; Courtney-Davies et al., 2022). Examples where normal faults have preserved mineralizations can be seen in Australian deposits such as Paraburadoo (Dalstra, 2006), Mount Tom Price (Taylor et al., 2001), and Mount Wall (Thorne et al., 2014),

as well as in Thabazimbi Mine (Basson and Koegelenberg, 2017), Sishen Mine (Basson et al., 2017), and Jwaneng Mine (Creus et al., 2018) in South Africa.

5.2. Structural Architecture: Impacts on Proto-ore Enrichment and Ore Body Geometry

High-grade iron ore is the result of the enrichment of iron formations, a process driven by the leaching of silica. Geological structures are critical in this process, facilitating fluid percolation and protecting mineral deposits from erosion (Dalstra and Rosière, 2008). According to Hagemann et al. (2016), geological structures that form high-grade iron ore deposits can be categorized as pre-, syn-, and post-mineralization structures. Pre-mineralization structures form before mineralization and play a continuous role in ore formation, either passively acting as conduits for fluids or actively being reactivated during mineralization. Syn-mineralization structures arise simultaneously with ore deposition. They can be active, like normal faults, or passive, like collapse breccias. Post-mineralization structures, including foliations, ductile shear zones, faults, and fractures, influence fluid flow, altering the texture and mineralogy of the deposit and shaping and preserving existing ore bodies (Maynard, 1991; Rosière and Rios, 2004; Dalstra and Rosière, 2008; Hensler et al., 2015).

Despite deformation having obscured information about pre-mineralization structures, indicators of the primary deposition layer (S01) can still be identified. In the central area of the study site, we can observe traces of F1 folds formed by the shortening of metavolcano-sedimentary sequences during the closure of the deposition basin. These folds are open in regions further from the shear zones and have southeastward vergence.

We have discovered, ductile shear zones played a dual and critical role in forming the CND ore. Firstly, they acted as conduits for hydrothermal fluid flow, a fact substantiated by the proximity between hydrothermal alteration zones mapped using PCs and occurrences of high-grade ore. Secondly, these structures exerted control over the geometry of ore bodies, with a distinct northeast-southwest direction parallel to these structures (see Map). The reactivation of these shear zones, as demonstrated by Archanjo et al. (2021) may have significantly contributed to the influx of hydrothermal fluids. This structural control along shear zones is a recurring pattern observed in deposits such as Carajás (Pinheiro and Holdsworth, 1997; Holdsworth and Pinheiro, 2000; Rosière et al., 2006; Dalstra and Rosière, 2008; Figueiredo e Silva et al., 2008; Teixeira et al., 2021) and QF (Rosière and Chemale Jr, 2000; Rosière et al., 2001; Rosière and Rios, 2004; Dalstra and Rosière, 2008).

The findings of this study also indicate a correlation between regions with higher density of structural lineaments and ore localization. These structures are associated with areas exhibiting a higher density of lineaments, suggesting that brittle tectonics played a significant role in the percolation of supergene fluids. Structural lineaments related to faults displaced ore bodies. Normal faults formed during intense crustal extension in a Statherian rift environment were responsible for preserving the ore bodies (Dalstra, 2006, 2014; Dalstra and Rosière, 2008; Hagemann et al., 2016). The GC is between two significant basins and has undergone two additional major extensional events. This region forms the basement of both the Parnaíba Basin and the Araripe Basin (Castro et al., 2014; Porto et al., 2022; Souza Filho and Seoane, 2024). The synthetic faults structurally control the iron formations in the study area, whereas the antithetic faults may have served as potential fluid migration zones affecting the BIFs (Costa, 2010; Vale et al., 2023). In future studies, it is critical to understand how Paleozoic and

Mesozoic extensions have influenced these mineralizations. Normal faults play a role in block movement, often concealing ore bodies, leading to what are known as blind deposits. According to Dalstra and Rosière (2008), in the Hamersley province, over the last three decades, Hamersley Iron Pty. Ltd. identified over 80% of concealed targets using structural criteria, typically by locating potential fault zones or areas with complex folding patterns.

5.3. Mineral System and a Approach for discovering regional scale targets

The Mineral System concept addresses mineral deposits as small-scale expressions of geodynamic processes occurring over varying temporal and spatial scales (Wyborn et al., 1994). This concept is inspired by the successful Petroleum System concept used in oil exploration (Wyborn et al., 1994). Mineral systems comprise four critical elements: lithospheric architecture, favorable geodynamics, fertility, and preservation of the primary deposition zone (McCuaig et al., 2010; Groves et al., 2022).

In mineral exploration, the Mineral System concept aids in identifying the essential factors needed to form a mineral deposit (McCuaig et al., 2010). In practice, the aim is to systematically analyze the components of the studied system and translate them into information that can be mapped. This information is then used to identify targets and increase the efficiency of mineral exploration projects (Ford and McCuaig, 2010; McCuaig et al., 2010; McCuaig and Hronsky, 2014; Yousefi et al., 2019).

According to Angerer et al.(2015), five critical elements are essential for forming and preserving iron ore deposits in BIFs: (i) Iron fertility within BIFs; (ii) Fluid flows capable of dissolving silica; (iii) High permeability across various scales; (iv) Exhumation and supergene modification of ore bodies; (v) Preservation of iron ore bodies. These elements can be understood as factors related to the tectonic deposition setting, fluid pathways, and mineral alterations ([Hagemann et al., 2016](#)).

We present the mineral system that formed the CND. This system is embedded in the geodynamic framework of the stabilization and eventual disintegration of the São Francisco Paleocontinent ([Brito Neves, 2011](#); [Caxito et al., 2020](#); [Ganade et al., 2021](#); [Neves, 2021](#)). Figure 8 provides an overview of CND mineralization evolution and enrichment process.

Our study reveals that the initial enrichment stage occurred in back-arc basins, coinciding with iron fertility in the GC, and was linked to BIF deposition. The subsequent closure of these basins during the late Archean triggered metamorphism of these sequences, accompanied by intense magmatic activity, which ultimately led to the formation of granite-greenstone belt sequences ([Fig. 8A](#)). These rocks underwent deformation, resulting in the thickening of proto-ore layers. During the Rhyacian orogeny between 2.2 and 1.9 Ga, the second enrichment stage involved the circulation of endogenous fluids ([Fig. 8B](#)). In the third stage of enrichment, we link the interaction of magmatic/metamorphic fluids with the circulation of basin fluids to a tectonic shift from a collisional environment, forming the São Francisco Paleocontinent, to its fragmentation into an extensional regime in the Statherian ([Fig. 8C](#)). Normal faults played a role in preserving ore bodies from erosion during this stage.

The fourth stage, associated with the Brasiliano-Pan-African orogeny in this region, gave rise to a system of dextral shear zones that controlled the geometry of ore bodies. These zones increased the structural permeability of the ore, facilitating the percolation of hypogene fluids ([Fig. 8D](#)). This relationship is evident in Landsat 8 PC images of bands 2, 5, 6, and 7, showcasing the proximity of these structures to zones rich in hydrated minerals. Subsequently, fault development associated with the opening of the Parnaíba and Araripe basins further increased structural permeability, favoring the circulation of supergene fluids. With this configuration, our model aligns with the End-Member Granite-Greenstone Belt Hosted Carajás- Type Model proposed by [Hagemann et al. \(2016\)](#).

Cratons and their margins are renowned for harboring high concentrations of mineral deposits ([Groves and Santosh, 2021, 2021](#)). Many studies have explored the relationship between decratonization processes and the genesis of mineral deposits. For

instance, [Li & Santosh \(2014\)](#), [Yang et al. \(2021\)](#), [Yang & Santosh \(2020\)](#), and [Li et al. \(2022\)](#) primarily focus on gold deposits. [Courtney-Davies et al. \(2022\)](#) demonstrated that the fragmentation of Nuna, indicated by geochronology in hematite, led to iron ore formation during the Nuna supercontinent breakup at 1.26-1.22 Ga. We propose that the fragmentation event of the São Francisco Paleocontinent during the Statherian, as discussed in [Neves \(2021\)](#) and [Ganade et al. \(2021\)](#), was pivotal in the formation of iron deposits associated with BIFs on the northwest margin of the CSF and in the southwest of the BP. Moreover, the dispersal of crustal fragments from this Paleocontinent may have "fertilized" the basement of the BP not only with iron but also with other elements.

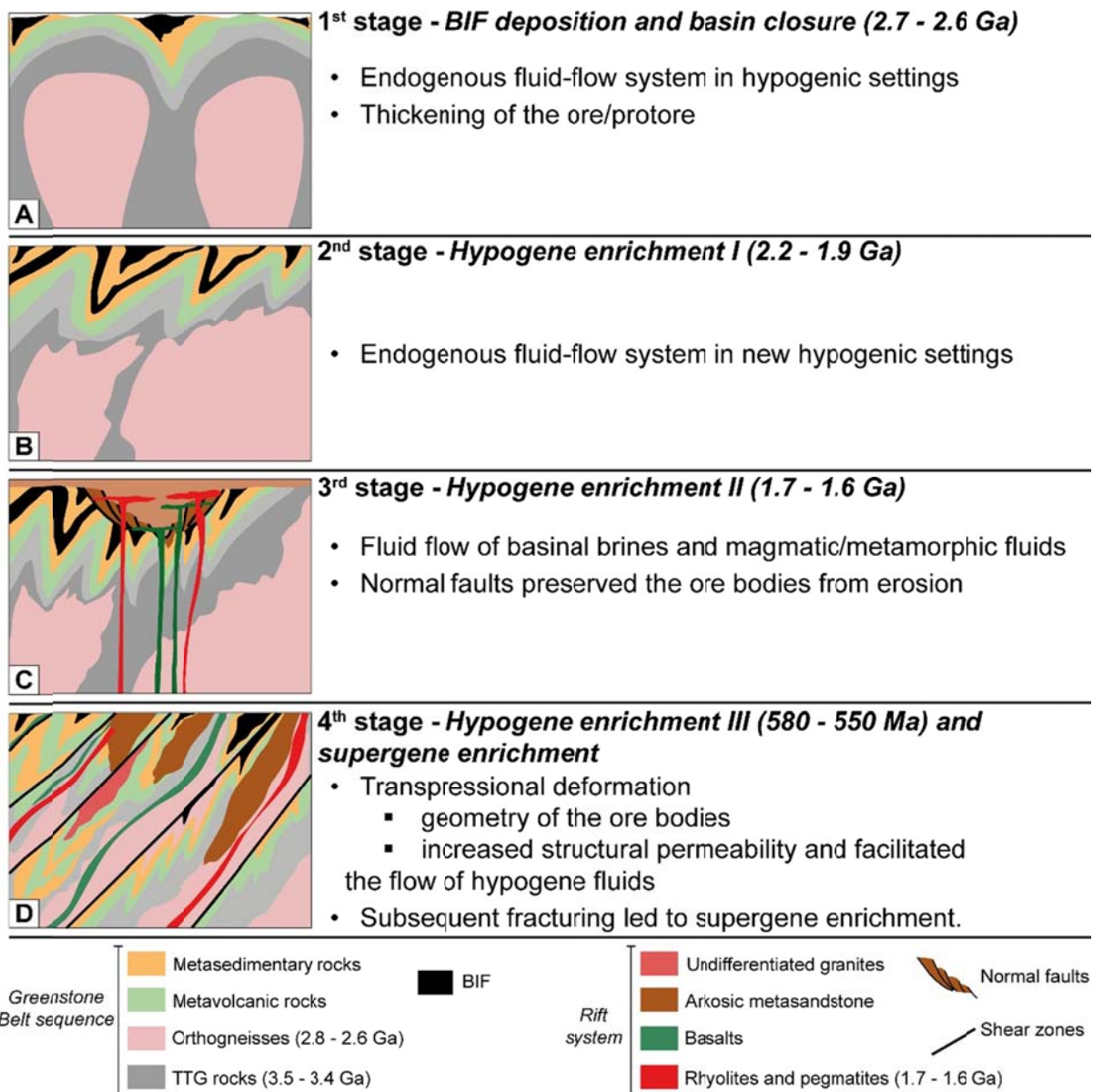


Figure 8 - Enrichment stages of BIF-hosted iron in the CND: (A) First stage: Deposition of BIFs and mineral fertility. (B) Second stage: Hypogene enrichment associated with fluid circulation during the Rhyacian orogeny. (C) Third stage: Enrichment linked to crustal extension, leading to the fragmentation of the São Francisco Paleocontinent (Neves, 2021). The formation of normal faults in this new tectonic configuration also preserved the mineralization. (D) Fourth stage: Enrichment phase marked by the emplacement of shear zones during the Brasiliano-Pan-African orogeny, controlling the geometry of ore bodies and favoring the circulation of hypogene fluids, resulting in the final stage of hypogene enrichment. Subsequently, normal faults formed due to the development of the Parnaíba and Araripe basins, increasing the structural permeability of these rocks and leading to supergene enrichment.

6. Conclusions

The proposed mineral system for the CND is well-aligned with the End-Member Granite-Greenstone Belt Hosted Carajás-Type Model proposed by [Hagemann et al. \(2016\)](#). This system is contextualized within the formation and subsequent weakening of the São Francisco Paleocontinent. Originating from the amalgamation of Archean blocks during the Paleoproterozoic, the Paleocontinent underwent decratonization during the Statherian period.

We demonstrate the presence of two distinct depositional environments in the CND. The first is associated with the deposition of BIF, acting as a geodynamic counterbalance to iron fertility associated with Archean blocks, while the second is linked to a Statherian extensional event marked by normal faults that preserved the ore and facilitated the circulation of hypogene and basinal fluids.

Additionally, the dispersal of São Francisco Paleocontinent fragments, facilitated by shear zones developed during the Brasiliano-Pan-African orogeny, may have enriched the basement of the Borborema Province with various elements beyond iron. Second-order shear zones within the CND, associated with the Pernambuco and Patos Lineaments, play a critical role in controlling ore bodies, enhancing structural permeability, and facilitating the circulation of hypogene fluids during their development and reactivations.

References

- Almeida, F.F.M.D., Hasui, Y., De Brito Neves, B.B., Fuck, R.A., 1981. Brazilian structural provinces: An introduction. *Earth-Science Reviews* 17, 1–29. [https://doi.org/10.1016/0012-8252\(81\)90003-9](https://doi.org/10.1016/0012-8252(81)90003-9)
- Amaral, W.D.S., Santos, F.H.D., Martins De Sousa, D.F., Perpétuo, M.P., Brito Neves, B.B.D., Pitombeira, J.P.A., Martins, D.T., 2023. A complex history of extension, subduction and collision in west Gondwana: Clues from the Riacho do Pontal orogen, Borborema Province (NE Brazil). *Journal of South American Earth Sciences* 125, 104297. <https://doi.org/10.1016/j.jsames.2023.104297>
- Ancelmi, M.F., 2016. Geocronologia e geoquímica das rochas arqueanas do Complexo Granjeiro, Província Borborema. Doutor em Ciências. Universidade Estadual de Campinas, Campinas, SP. <https://doi.org/10.47749/T/UNICAMP.2016.979098>
- Angerer, T., Duuring, P., Hagemann, S.G., Thorne, W., McCuaig, T.C., 2015. A mineral system approach to iron ore in Archaean and Palaeoproterozoic BIF of Western Australia. *Ore Deposits in an Evolving Earth*. Geological Society of London. <https://doi.org/10.1144/SP393.11>
- Angerer, T., Hagemann, S.G., 2010. The BIF-Hosted High-Grade Iron Ore Deposits in the Archean Koolyanobbing Greenstone Belt, Western Australia: Structural Control on Synorogenic- and Weathering-Related Magnetite-, Hematite-, and Goethite-rich Iron Ore. *Economic Geology* 105, 917–945. <https://doi.org/10.2113/econgeo.105.5.917>
- Archanjo, C.J., Hollanda, M.H.B.M.D., Viegas, L.G.F., 2021. Late Ediacaran lateral-escape tectonics as recorded by the Patos shear zone (Borborema Province, NE Brazil). *Brazilian Journal of Geology* 51, e20200132. <https://doi.org/10.1590/2317-4889202120200132>
- Arthaud, M.H., Caby, R., Fuck, R.A., Dantas, E.L., Parente, C.V., 2008. Geology of the northern Borborema Province, NE Brazil and its correlation with Nigeria, NW Africa. *Geological Society, London, Special Publications* 294, 49–67. <https://doi.org/10.1144/SP294.4>
- Barbosa, J.S.F., Sabaté, P., 2004. Archean and Paleoproterozoic crust of the São Francisco Craton, Bahia, Brazil: geodynamic features. *Precambrian Research* 133, 1–27. <https://doi.org/10.1016/j.precamres.2004.03.001>
- Barbosa, J.S.F., Sabaté, P., 2002. Geological features and the paleoproterozoic collision of four archean crustal segments of the São Francisco craton, Bahia, Brazil. A synthesis. *Anais Da Academia Brasileira de Ciencias* 74, 343–359. <https://doi.org/10.1590/S0001-37652002000200009>

- Basson, I.J., Anthonissen, C.J., McCall, M.J., Stoch, B., Britz, J., Deacon, J., Strydom, M., Cloete, E., Botha, J., Bester, M., Nel, D., 2017. Ore-structure relationships at Sishen Mine, Northern Cape, Republic of South Africa, based on fully-constrained implicit 3D modelling. *Ore Geology Reviews* 86, 825–838. <https://doi.org/10.1016/j.oregeorev.2017.04.007>
- Basson, I.J., Koegelenberg, C., 2017. Structural controls on Fe mineralization at Thabazimbi Mine, South Africa. *Ore Geology Reviews* 80, 1056–1071. <https://doi.org/10.1016/j.oregeorev.2016.08.022>
- Bekker, A., Planavsky, N., Rasmussen, B., Krapez, B., Hofmann, A., Slack, J., Rouxel, O., Konhauser, K., 2014. Iron formations: Their origins and implications for ancient seawater chemistry. *Treatise on Geochemistry*. Elsevier, 561–628.
- Bekker, A., Slack, J.F., Planavsky, N., Krapez, B., Hofmann, A., Konhauser, K.O., Rouxel, O.J., 2010. Iron Formation: The Sedimentary Product of a Complex Interplay among Mantle, Tectonic, Oceanic, and Biospheric Processes. *Economic Geology* 105, 467–508. <https://doi.org/10.2113/gsecongeo.105.3.467>
- Beukes, N., Gutzmer, J., 2008. Origin and Paleoenvironmental Significance of Major Iron Formations at the Archean-Paleoproterozoic Boundary. *Banded Iron Formation-Related High-Grade Iron Ore, Reviews in Economic Geology*. NA-NA. <https://doi.org/10.5382/rev.15.01>
- Beukes, N.J., Gutzmer, J., Mukhopadhyay, J., 2003. The geology and genesis of high-grade hematite iron ore deposits. *Applied Earth Science* 112, 18–25. <https://doi.org/10.1179/037174503225011243>
- Bizzi, L.A., Schobbenhaus, C., Vidotti, R.M., GONÇALVES, J.H.H. (Eds.), 2003. *Geologia, tectônica e recursos minerais do Brasil: texto, mapas e SIG*. CPRM, Brasilia.
- Brito Neves, B.B., Cordani, U.G., 1991. Tectonic evolution of South America during the late Proterozoic. *Precambrian Research* 53, 23–40.
- Brito Neves, B.B.D., Santos, T.J.S.D., Dantas, E.L., 2023. O Terreno Tectonoestratigráfico São Pedro: Oeste da Zona Transversal – Província Borborema. *Geologia USP. Série Científica* 22, 45–69. <https://doi.org/10.11606/issn.2316-9095.v22-197489>
- Brito Neves, B.B. de, 2011. The Paleoproterozoic in the South-American continent: Diversity in the geologic time. *Journal of South American Earth Sciences* 32, 270–286. <https://doi.org/10.1016/j.jsames.2011.02.004>
- Brito Neves, B.B. de, 1975. Regionalização geotectônica do Precambriano nordestino. phd. Universidade de São Paulo.

- Castro, D.L. de, Fuck, R.A., Phillips, J.D., Vidotti, R.M., Bezerra, F.H.R., Dantas, E.L., 2014. Crustal structure beneath the Paleozoic Parnaíba Basin revealed by airborne gravity and magnetic data, Brazil. *Tectonophysics* 614, 128–145. <https://doi.org/10.1016/j.tecto.2013.12.009>
- Caxito, F.A., Uhlein, A., Dantas, E., Stevenson, R., Egydio-Silva, M., Salgado, S.S., 2017. The Rio Preto and Riacho do Pontal Belts. In: Heilbron, M., Cordani, U.G., Alkmim, F.F. (Eds.), São Francisco Craton, Eastern Brazil, Regional Geology Reviews. Springer International Publishing, Cham, 221–239. https://doi.org/10.1007/978-3-319-01715-0_12
- Caxito, F.A., Uhlein, A., Dantas, E.L., Stevenson, R., Salgado, S.S., Dussin, I.A., Sial, A.D.N., 2016. A complete Wilson Cycle recorded within the Riacho do Pontal Orogen, NE Brazil: Implications for the Neoproterozoic evolution of the Borborema Province at the heart of West Gondwana. *Precambrian Research* 282, 97–120. <https://doi.org/10.1016/j.precamres.2016.07.001>
- Caxito, F.D.A., Santos, L.C.M.D.L., Ganade, C.E., Bendaoud, A., Fettous, E.-H., Bouyo, M.H., 2020. Toward an integrated model of geological evolution for NE Brazil-NW Africa: The Borborema Province and its connections to the Trans-Saharan (Benino-Nigerian and Tuareg shields) and Central African orogens. *Brazilian Journal of Geology* 50, e20190122. <https://doi.org/10.1590/2317-4889202020190122>
- Corsini, M., Vauchez, A., Archanjo, C., De Sá, E.F.J., 1991. Strain transfer at continental scale from a transcurrent shear zone to a transpressional fold belt: The Patos-Seridó system, northeastern Brazil. *Geology* 19, 586. [https://doi.org/10.1130/0091-7613\(1991\)019<0586:STACSF>2.3.CO;2](https://doi.org/10.1130/0091-7613(1991)019<0586:STACSF>2.3.CO;2)
- Costa, Á.F., 2010. Litogeоquímica das rochas encaixantes E do minériode ferro da região de Curral Novo. Trabalho de Conclusão de Curso, UFBA, Salvador.
- Costa, A.F.D.O., Danderfer, A., Bersan, S.M., 2018. Record of a Statherian rift-sag basin in the Central Espinhaço Range: Facies characterization and geochronology. *Journal of South American Earth Sciences* 82, 311–328. <https://doi.org/10.1016/j.jsames.2017.10.014>
- Courtney-Davies, L., Danišik, M., Ramanaidou, E.R., Kirkland, C.L., Evans, N.J., Piechocka, A.M., McInnes, B.I.A., 2022. Hematite geochronology reveals a tectonic trigger for iron ore mineralization during Nuna breakup. *Geology* 50, 1318–1323. <https://doi.org/10.1130/G50374.1>

- Creus, P.K., Basson, I.J., Stoch, B., Mogorosi, O., Gabanakgosi, K., Ramsden, F., Gaegopolwe, P., 2018. Structural analysis and implicit 3D modelling of Jwaneng Mine: Insights into deformation of the Transvaal Supergroup in SE Botswana. *Journal of African Earth Sciences* 137, 9–21. <https://doi.org/10.1016/j.jafrearsci.2017.09.010>
- Crosta, A.P., McMoore, J., 1989. Enhancement of Landsat Thematic Mapper imagery for residual soil mapping in SW Minas Gerais State Brazil, a prospecting case history in greenstone belt terrain. Presented at the Seventh Thematic Conference on Remote Sensing for Exploration Geology (Erim), Calgary, Alberta, Canada.
- Dalstra, H.J., 2014. Structural evolution of the Mount Wall region in the Hamersley province, Western Australia and its control on hydrothermal alteration and formation of high-grade iron deposits. *Journal of Structural Geology* 67, 268–292. <https://doi.org/10.1016/j.jsg.2014.03.005>
- Dalstra, H.J., 2006. Structural controls of bedded iron ore in the Hamersley Province, Western Australia – an example from the Paraburadoo Ranges. *Applied Earth Science* 115, 139–145. <https://doi.org/10.1179/174327506x138959>
- Dalstra, H.J., Rosière, C.A., 2008. Structural Controls on High-Grade Iron Ores Hosted by Banded Iron Formation: A Global Perspective. *Banded Iron Formation-Related High-Grade Iron Ore*. Society of Economic Geologists. <https://doi.org/10.5382/Rev.15.03>
- Danderfer, A., De Waele, B., Pedreira, A.J., Nalini, H.A., 2009. New geochronological constraints on the geological evolution of Espinhaço basin within the São Francisco Craton—Brazil. *Precambrian Research* 170, 116–128. <https://doi.org/10.1016/j.precamres.2009.01.002>
- de Kock, M.O., Evans, D.A.D., Gutzmer, J., Beukes, N.J., Dorland, H.C., 2008. Origin and Timing of Banded Iron Formation-Hosted High-Grade Hard Hematite Deposits—A Paleomagnetic Approach. *Banded Iron Formation-Related High-Grade Iron Ore*. Society of Economic Geologists. <https://doi.org/10.5382/Rev.15.02>
- dos Santos, F.H. da S.A., Wagner; Filho, Evilarde Carvalho Uchôa; Martins, Douglas T., 2017. Detrital zircon U-Pb ages and whole-rock geochemistry of the Neoproterozoic Paulistana and Santa Filomena complexes, Borborema Province, northeastern Brazil: implications for source area composition, provenance, and tectonic setting. *International Geology Review* 59, 1861–1884. <https://doi.org/10.1080/00206814.2017.1300074>
- Duuring, P., Hagemann, S., 2013a. Leaching of silica bands and concentration of magnetite in Archean BIF by hypogene fluids: Beebyn Fe ore deposit, Yilgarn Craton, Western Australia. *Mineralium Deposita* 48, 341–370. <https://doi.org/10.1007/s00126-012-0428-1>

- Duuring, P., Hagemann, S., 2013b. Genesis of superimposed hypogene and supergene Fe orebodies in BIF at the Madoonga deposit, Yilgarn Craton, Western Australia. *Mineralium Deposita* 48, 371–395. <https://doi.org/10.1007/s00126-012-0429-0>
- ESA, 2022. Copernicus DEM. <https://doi.org/10.5270/ESA-c5d3d65>
- Figueiredo e Silva, R.C., Lobato, L.M., Rosière, C.A., Hagemann, S., Zucchetti, M., Baars, F.J., Morais, R., Andrade, I., 2008. A Hydrothermal Origin for the Jaspilite-Hosted, Giant Serra Norte Iron Ore Deposits in the Carajás Mineral Province, Pará State, Brazil. *Banded Iron Formation-Related High-Grade Iron Ore*. Society of Economic Geologists. <https://doi.org/10.5382/Rev.15.10>
- Ford, A., McCuaig, T.C., 2010. The effect of map scale on geological complexity for computer-aided exploration targeting. *Ore Geology Reviews* 38, 156–167. <https://doi.org/10.1016/j.oregeorev.2010.03.008>
- Ganade, C.E., Weinberg, R.F., Caxito, F.A., Lopes, L.B.L., Tesser, L.R., Costa, I.S., 2021. Decratonization by rifting enables orogenic reworking and transcurrent dispersal of old terranes in NE Brazil. *Scientific Reports* 11, 5719. <https://doi.org/10.1038/s41598-021-84703-x>
- Gomes, J.R. de C., Vasconcelos, A.M., 2000. Jaguaribe-SW, folha SB.24-Y. Programa levantamentos geológicos básicos do brasil. CPRM - Serviço Geológico do Brasil.
- Gross, G., 1965. Geology of iron deposits in Canada, Vol. 1 general geology and evaluation of ore deposits: Geological Survey of Canada. *Economic Geology Report* 22, 81.
- Gross, G.A., 1983. Tectonic systems and the deposition of iron-formation. *Precambrian Research* 20, 171–187. [https://doi.org/10.1016/0301-9268\(83\)90072-4](https://doi.org/10.1016/0301-9268(83)90072-4)
- Gross, G.A., 1980. A classification of iron formations based on depositional environments. *The Canadian Mineralogist* 18, 215–222.
- Groves, D.I., Santosh, M., 2021. Craton and thick lithosphere margins: The sites of giant mineral deposits and mineral provinces. *Gondwana Research* 100, 195–222. <https://doi.org/10.1016/j.gr.2020.06.008>
- Groves, D.I., Santosh, M., Müller, D., Zhang, L., Deng, J., Yang, L.-Q., Wang, Q.-F., 2022. Mineral systems: Their advantages in terms of developing holistic genetic models and for target generation in global mineral exploration. *Geosystems and Geoenvironment* 1, 100001. <https://doi.org/10.1016/j.geogeo.2021.09.001>
- Guadagnin, F., 2015. 26, 227–245.

- Hagemann, S.G., Angerer, T., Duuring, P., Rosière, C.A., Silva, R.C.F. e, Lobato, L., Hensler, A.S., Walde, D.H.G., 2016. BIF-hosted iron mineral system: A review. *Ore Geology Reviews* 76, 317–359. <https://doi.org/10.1016/j.oregeorev.2015.11.004>
- Hensler, A.-S., Hagemann, S.G., Rosière, C.A., Angerer, T., Gilbert, S., 2015. Hydrothermal and metamorphic fluid-rock interaction associated with hypogene “hard” iron ore mineralisation in the Quadrilátero Ferrífero, Brazil: Implications from in-situ laser ablation ICP-MS iron oxide chemistry. *Ore Geology Reviews* 69, 325–351. <https://doi.org/10.1016/j.oregeorev.2015.02.023>
- Hoffman, P.F., Kaufman, A.J., Halverson, G.P., Schrag, D.P., 1998. A neoproterozoic snowball earth. *Science (New York, N.Y.)* 281, 1342–1346. <https://doi.org/10.1126/science.281.5381.1342>
- Holdsworth, R.E., Pinheiro, R.V.L., 2000. The anatomy of shallow-crustal transpressional structures: insights from the Archaean Carajás fault zone, Amazon, Brazil. *Journal of Structural Geology* 22, 1105–1123. [https://doi.org/10.1016/S0191-8141\(00\)00036-5](https://doi.org/10.1016/S0191-8141(00)00036-5)
- Huntington, J.F., 2007. The Role of Remote Sensing in Finding Hydrothermal Mineral Deposits on Earth. In: Bock, G.R., Goode, J.A. (Eds.), *Novartis Foundation Symposia*. Wiley, 214–235. <https://doi.org/10.1002/9780470514986.ch12>
- James, H.L., 1983. Chapter 12 Distribution of Banded Iron-Formation in Space and Time. In: Trendall, A.F., Morris, R.C. (Eds.), *Iron-Formation Facts and Problems, Developments in Precambrian Geology*. Elsevier, 471–490. [https://doi.org/10.1016/S0166-2635\(08\)70053-7](https://doi.org/10.1016/S0166-2635(08)70053-7)
- James, H.L., 1954. Sedimentary facies of iron-formation. *Economic Geology* 49, 235–293.
- Keyser, W., Ciobanu, C.L., Cook, N.J., Courtney-Davies, L., Kennedy, A., Wade, B.P., Ehrig, K., Dmitrijeva, M., Kontonikas-Charos, A., Feltus, H., Johnson, G., 2019a. Petrographic and geochronological constraints on the granitic basement to the Middleback Ranges, South Australia. *Precambrian Research* 324, 170–193. <https://doi.org/10.1016/j.precamres.2019.01.024>
- Keyser, W., Ciobanu, C.L., Cook, N.J., Dmitrijeva, M., Courtney-Davies, L., Feltus, H., Gilbert, S., Johnson, G., Ehrig, K., 2019b. Iron-oxides constrain BIF evolution in terranes with protracted geological histories: The Iron Count prospect, Middleback Ranges, South Australia.
- Lithos 324–325, 20–38. <https://doi.org/10.1016/j.lithos.2018.10.035>
- Keyser, W., Ciobanu, C.L., Cook, N.J., Johnson, G., Feltus, H., Johnson, S., Dmitrijeva, M., Ehrig, K., Nguyen, P.T., 2018. Petrography and trace element signatures of iron-oxides in deposits from the Middleback Ranges, South Australia: From banded iron formation to ore. *Ore Geology Reviews* 93, 337–360. <https://doi.org/10.1016/j.oregeorev.2018.01.006>

- Klein, C., 2005. Some Precambrian banded iron-formations (BIFs) from around the world: Their age, geologic setting, mineralogy, metamorphism, geochemistry, and origins. *American Mineralogist* 90, 1473–1499. <https://doi.org/10.2138/am.2005.1871>
- Klein, C., 1983. Diagenesis and metamorphism of Precambrian banded iron-formations. *Developments in Precambrian Geology*. Elsevier, 417–469.
- Konhauser, K.O., Planavsky, N.J., Hardisty, D.S., Robbins, L.J., Warchola, T.J., Haugaard, R., Lalonde, S.V., Partin, C.A., Oonk, P.B.H., Tsikos, H., Lyons, T.W., Bekker, A., Johnson, C.M., 2017. Iron formations: A global record of Neoarchaean to Palaeoproterozoic environmental history. *Earth-Science Reviews* 172, 140–177. <https://doi.org/10.1016/j.earscirev.2017.06.012>
- Li, L., Li, C., Li, Q., Yuan, M.-W., Zhang, J.-Q., Li, S.-R., Santosh, M., Shen, J.-F., Zhang, H.-F., 2022. Indicators of decratonic gold mineralization in the North China Craton. *Earth-Science Reviews* 228, 103995. <https://doi.org/10.1016/j.earscirev.2022.103995>
- Li, S.-R., Santosh, M., 2014. Metallogeny and craton destruction: Records from the North China Craton. *Ore Geology Reviews* 56, 376–414. <https://doi.org/10.1016/j.oregeorev.2013.03.002>
- Lobato, L.M., Figueiredo Rosaline Cristina, E.S., Hagemann, S., Thorne, W., Zucchetti, M., 2008. Hypogene Alteration Associated with High-Grade Banded Iron Formation-Related Iron Ore. *Banded Iron Formation-Related High-Grade Iron Ore*. Society of Economic Geologists. <https://doi.org/10.5382/Rev.15.04>
- Loughlin, W.P., 1991. Principal Component Analysis for Alteration Mapping. *Photogrammetric Engineering and Remote Sensing* 57, 1163–1169.
- Martins De Sousa, D.F., Oliveira, E.P., Amaral, W.S., Baldim, M.R., 2020. The Itabuna-Salvador-Curaçá Orogen revisited, São Francisco Craton, Brazil: New zircon U–Pb ages and Hf data support evolution from archean continental arc to paleoproterozoic crustal reworking during block collision. *Journal of South American Earth Sciences* 104, 102826. <https://doi.org/10.1016/j.jsames.2020.102826>
- Martins, D.T., 2017. GEOLOGIA DO TERRENO ARQUEANO GRANJEIRO (3.4 a 2.6 Ga), PROVÍNCIA BORBOREMA. master. Universidade Federal do Ceará.
- Maynard, J.B., 1991. Iron: Syngenetic deposition controlled by the evolving ocean-atmosphere system. *Sedimentary and Diagenetic Mineral Deposits: A Basin Analysis Approach to Exploration*. Society of Economic Geologists. <https://doi.org/10.5382/Rev.05.10>

- McCuaig, T.C., Beresford, S., Hronsky, J., 2010. Translating the mineral systems approach into an effective exploration targeting system. *Ore Geology Reviews* 38, 128–138. <https://doi.org/10.1016/j.oregeorev.2010.05.008>
- McCuaig, T.C., Hronsky, J.M.A., 2014. The Mineral System Concept<\mathsemicolon>The Key to Exploration Targeting<\mathsemicolon>. Building Exploration Capability for the 21st Century. Society of Economic Geologists. <https://doi.org/10.5382/sp.18.08>
- Morris, R., 1980. A textural and mineralogical study of the relationship of iron ore to banded iron-formation in the Hamersley iron province of Western Australia. *Economic Geology* 75, 184–209.
- Müller, S.G., Krape, B., Barley, M.E., Fletcher, I.R., 2005. Giant iron-ore deposits of the Hamersley province related to the breakup of Paleoproterozoic Australia: New insights from in situ SHRIMP dating of baddeleyite from mafic intrusions. *Geology* 33, 577. <https://doi.org/10.1130/G21482.1>
- Neves, S.P., 2021. Comparative geological evolution of the Borborema Province and São Francisco Craton (eastern Brazil): Decratonization and crustal reworking during West Gondwana assembly and implications for paleogeographic reconstructions. *Precambrian Research* 355, 106119. <https://doi.org/10.1016/j.precamres.2021.106119>
- Paula-Santos, G.M., Babinski, M., Kuchenbecker, M., Caetano-Filho, S., Trindade, R.I., Pedrosa-Soares, A.C., 2015. New evidence of an Ediacaran age for the Bambuí Group in southern São Francisco craton (eastern Brazil) from zircon U–Pb data and isotope chemostratigraphy. *Gondwana Research* 28, 702–720. <https://doi.org/10.1016/j.gr.2014.07.012>
- Pavlis, N.K., Holmes, S.A., Kenyon, S.C., Factor, J.K., 2012. The development and evaluation of the Earth Gravitational Model 2008 (EGM2008). *Journal of Geophysical Research: Solid Earth* 117, n/a-n/a. <https://doi.org/10.1029/2011jb008916>
- Pinheiro, R.V.L., Holdsworth, R.E., 1997. The structure of the Carajás N-4 ironstone deposit and associated rocks: relationship to Archaean strike-slip tectonics and basement reactivation in the Amazon region, Brazil. *Journal of South American Earth Sciences* 10, 305–319. [https://doi.org/10.1016/S0895-9811\(97\)00018-7](https://doi.org/10.1016/S0895-9811(97)00018-7)
- Pitarello, M.Z., Santos, T.J.S. dos, Ancelmi, M.F., 2019. Syn-to post-depositional processes related to high grade metamorphic BIFs: Geochemical and geochronological evidences from a Paleo to Neoarchean (3.5–2.6 Ga) terrane in NE Brazil. *Journal of South American Earth Sciences* 96, 102312. <https://doi.org/10.1016/j.jsames.2019.102312>
- Porto, A., Carvalho, C., Lima, C., Heilbron, M., Caxito, F., La Terra, E., Fontes, S.L., 2022.

- The Neoproterozoic basement of the Parnaíba Basin (NE Brazil) from combined geophysical-geological analysis: A missing piece of the western Gondwana puzzle. *Precambrian Research* 379, 106784. <https://doi.org/10.1016/j.precamres.2022.106784>
- Rosière, C.A., Baars, F.J., Seoane, J.C.S., Lobato, L.M., da Silva, L.L., de Souza, S.R.C., Mendes, G., 2006. Structure and iron mineralisation of the Carajás Province. *Applied Earth Science* 115, 126–133. <https://doi.org/10.1179/174327506x138986>
- Rosière, C.A., Chemale Jr, F., 2000. Brazilian iron formations and their geological setting. *Revista Brasileira de Geociências* 30, 274–278.
- Rosière, C.A., Rios, F.J., 2004. THE ORIGIN OF HEMATITE IN HIGH-GRADE IRON ORES BASED ON INFRARED MICROSCOPY AND FLUID INCLUSION STUDIES: THE EXAMPLE OF THE CONCEIÇÃO MINE, QUADRILÁTERO FERRÍFERO, BRAZIL. *Economic Geology* 99, 611–624. <https://doi.org/10.2113/gsecongeo.99.3.611>
- Rosière, C.A., Siemes, H., Quade, H., Brokmeier, H.-G., Jansen, E.M., 2001. Microstructures, textures and deformation mechanisms in hematite. *Journal of Structural Geology* 23, 1429–1440. [https://doi.org/10.1016/S0191-8141\(01\)00009-8](https://doi.org/10.1016/S0191-8141(01)00009-8)
- Rowan, L.C., Mars, J.C., 2003. Lithologic mapping in the Mountain Pass, California area using Advanced Spaceborne Thermal Emission and Reflection Radiometer (ASTER) data. *Remote Sensing of Environment* 84, 350–366. [https://doi.org/10.1016/S0034-4257\(02\)00127-X](https://doi.org/10.1016/S0034-4257(02)00127-X)
- Santos, E.J., Souza Neto, J.A., Silva, M.M.R., Beurlen, H., Cavalcanti, J.A.D., Silva, M.G., Costa, A.F., Santos, L.C.M.L., Santos, R.B., 2014. Metalogênese das porções norte e central da Província Borborema. *Metalogênese Das Províncias Tectônicas Brasileiras*. Silva M.G., Rocha Neto M.B., Jost H., Kuyumijan R.M., CPRM, Belo Horizonte, 343–388.
- Sato, E.N., 2011. Proposta metodológica sobre dados de geofísica aeroportada na prospecção de minério de Fe: indicação de ambientes geológicos propícios e geração de mapas de probabilidade na região de Curral Novo do Piauí (PI). master. Universidade de São Paulo.
- Souza Filho, R.G.D., Seoane, J.C.S., 2024. Neoproterozoic lithospheric structures at the Borborema Province: Integration of magnetotelluric resistivity sections and their relations to neighboring lithospheric blocks of the Parnaíba Basin and São Francisco Craton. *Journal of South American Earth Sciences* 138, 104879. <https://doi.org/10.1016/j.jsames.2024.104879>
- Taylor, D., Dalstra, H., Harding, A., Broadbent, G., Barley, M., 2001. Genesis of high-grade hematite orebodies of the Hamersley Province, Western Australia. *Economic Geology* 96, 837–873.

- Teixeira, N.A., Campos, L.D., Paula, R.R.D., Lacasse, C.M., Ganade, C.E., Monteiro, C.F., Lopes, L.B.L., Oliveira, C.G.D., 2021. Carajás Mineral Province - Example of metallogeny of a rift above a cratonic lithospheric keel. *Journal of South American Earth Sciences* 108, 103091. <https://doi.org/10.1016/j.jsames.2020.103091>
- Teixeira, W., Oliveira, E.P., Marques, L.S., 2017. Nature and Evolution of the Archean Crust of the São Francisco Craton. In: Heilbron, M., Cordani, U.G., Alkmim, F.F. (Eds.), *São Francisco Craton, Eastern Brazil, Regional Geology Reviews*. Springer International Publishing, Cham, 29–56. https://doi.org/10.1007/978-3-319-01715-0_3
- Thorne, W.S., Hagemann, S.G., Sepe, D., Dalstra, H.J., Banks, D.A., 2014. Structural Control, Hydrothermal Alteration Zonation, and Fluid Chemistry of the Concealed, High-Grade 4EE Iron Orebody at the Paraburadoo 4E Deposit, Hamersley Province, Western Australia. *Economic Geology* 109, 1529–1562. <https://doi.org/10.2113/econgeo.109.6.1529>
- Tikoff, B., Fossen, H., 1999. Three-dimensional reference deformations and strain facies. *Journal of Structural Geology* 21, 1497–1512.
- Trompette, R., 1997. Neoproterozoic (600 ma) aggregation of western gondwana: a tentative scenario. *Precambrian Research* 82, 101–112.
- Trompette, R., 1994. *Geology of Western Gondwana (2000 - 500 Ma): Pan-African-Brasiliano Aggregation of South America and Africa*, 1st ed. CRC Press. <https://doi.org/10.1201/9781003077664>
- Trompette, R.R., Uhlein, A., Silva, M.E., Karmann, I., 1992. O cráton brasileiro - uma revisão. *Rev Bras Geoc* 22, 481–486.
- Vale, J.A.R. do, 2018. Caracterização geoquímica e geocronológica do Complexo Granjeiro Sul, Província Borborema, NE Brasil: implicações para a evolução crustal paleoarqueana do distrito ferrífero de Curral Novo do Piauí. phd. INSTITUTO DE GEOCIÊNCIAS.
- Vale, J.A., Monteiro, L., Basto, C., Medeiros, V., Silveira, D., Uchôa Filho, E., Pedrosa Junior, N., Rodrigues, J., Santos, T., 2023. Lithogeochemistry and zircon U-Pb geochronology of the Granjeiro Complex and associated units, Curral Novo do Piauí, NW-Borborema Province, Brazil: implications for Archean to Paleoproterozoic crustal evolution. *Journal of the Geological Survey of Brazil* 6, 239–262. <https://doi.org/10.29396/jgsb.2023.v6.n3.2>
- Van Schmus, W.R., Oliveira, E.P., Da Silva Filho, A.F., Toteu, S.F., Penaye, J., Guimarães, I.P., 2008. Proterozoic links between the Borborema Province, NE Brazil, and the Central African Fold Belt. *Geological Society, London, Special Publications* 294, 69–99. <https://doi.org/10.1144/SP294.5>

- Vasconcelos, A.M., Gomes, F.E.M., 1998. Geologia e metalogênese - folha Iguatu SB.24-Y-B, programa levantamentos geológicos básicos do Brasil. Estado do Ceará, escala 1:250.000. CPRM - Serviço Geológico do Brasil.
- Vauchez, A., Neves, S., Caby, R., Corsini, M., Egydio-Silva, M., Arthaud, M., Amaro, V., 1995. The Borborema shear zone system, NE Brazil. *Journal of South American Earth Sciences* 8, 247–266. [https://doi.org/10.1016/0895-9811\(95\)00012-5](https://doi.org/10.1016/0895-9811(95)00012-5)
- Yang, C.-X., Santosh, M., 2020. Ancient deep roots for Mesozoic world-class gold deposits in the north China craton: An integrated genetic perspective. *Geoscience Frontiers* 11, 203–214. <https://doi.org/10.1016/j.gsf.2019.03.002>
- Yang, J.-H., Wu, F.-Y., Wilde, S.A., Belousova, E., Griffin, W.L., 2008. Mesozoic decratonization of the North China block. *Geology* 36, 467. <https://doi.org/10.1130/g24518a.1>
- Yang, J.-H., Xu, L., Sun, J.-F., Zeng, Q., Zhao, Y.-N., Wang, H., Zhu, Y.-S., 2021. Geodynamics of decratonization and related magmatism and mineralization in the North China Craton. *Science China Earth Sciences* 64, 1409–1427. <https://doi.org/10.1007/s11430-020-9732-6>
- Yang, L.-Q., Deng, J., Groves, D.I., Santosh, M., He, W.-Y., Li, N., Zhang, L., Zhang, R.-R., Zhang, H.-R., 2022. Metallogenic ‘factories’ and resultant highly anomalous mineral endowment on the craton margins of China. *Geoscience Frontiers* 13, 101339. <https://doi.org/10.1016/j.gsf.2021.101339>
- Yousefi, M., Kreuzer, O.P., Nykänen, V., Hronsky, J.M.A., 2019. Exploration information systems – A proposal for the future use of GIS in mineral exploration targeting. *Ore Geology Reviews* 111, 103005. <https://doi.org/10.1016/j.oregeorev.2019.103005>

5. Discussão e Conclusões

Neste trabalho, abordamos a formação dos depósitos de ferro na margem noroeste do cráton São Francisco e sudoeste da Província Borborema sob a perspectiva da hipótese da fragmentação do Paleocontinente São Francisco ([Neves 2021](#)), um processo conhecido como decratonização, que ocorreu entre 1.8 e 1.6 Ga ([Ganade et al. 2021](#); [Neves 2021](#)). Buscamos entender como a decratonização influenciou a formação desses depósitos, analisando um depósito ao norte do Lineamento Pernambuco no Terreno São Pedro, Província Borborema Transversal, e ocorrências de formações ferríferas do Complexo Sobradinho, no sudeste do Piauí, no município de São Raimundo Nonato. Com base nos dados obtidos até agora, chegamos às seguintes conclusões:

- Análises gravimétricas usando a inclinação da derivada vertical do modelo EGM2008 revelam a presença de fragmentos crustais arqueano-paleoproterozoicos nas margens. Os lineamentos profundos extraídos deste processamento, nos permitiram mapear a geometria e limites dos fragmentos estudados, enquanto lineamentos residuais, relacionados às zonas de deformação cisalhante regional, nos ajudaram a entender a cinemática de transporte dos blocos, predominantemente destral.
- A análise geocronológica U-Pb de zircões permitiu identificar eventos magmáticos ocorridos em torno de 3.0 e 2.8-2.7 Ga, tanto no Terreno São Pedro quanto no Complexo Sobradinho. Uma idade de 2.6 Ga, observada nas bordas dos zircões, pode estar relacionada ao metamorfismo desse evento principal. Com base nessas informações, inferimos que ambas as áreas estudadas podem ter pertencido ao mesmo bloco continental, que constituiu a base do Paleocontinente São Francisco e que foram unidas durante a orogênese Riaciana para formar a estrutura do Paleocontinente São Francisco. A presença de zircões detritícios em intervalos similares e a ocorrência de magmatismo riolítico do Complexo Itainzinho e aplitos graníticos do Complexo Sobradinho, reforçam esta ideia.
- Com base na hipótese de decratonização do Paleocontinente São Francisco, proposta por [Neves \(2021\)](#), identificamos quatro eventos importantes de deformação que desempenham um papel significativo na arquitetura regional do depósito de ferro de Curral Novo. Definimos estes eventos usando dados estratigráficos disponíveis na literatura, levantamentos estruturais e por meio de interpretações aerogeofísicas. No evento D1, observamos o primeiro enriquecimento das formações ferríferas relacionado ao evento colisional e à circulação de fluidos hipogênicos, resultantes de intensa atividade magmática em torno de 2.8-2.7 Ga e possíveis eventos anorogênicos em 2.6 Ga ([Barros et al. 2020](#); [Vale 2018](#)). O evento D2 envolveu as rochas arqueanas do embasamento durante a colisão riaciana Tran-samazonica, conforme indicado pelas idades das bordas

dos zircões e dados geoquímicos. Durante o evento D3, que ocorreu por volta de 1.8-1.6 Ga em um contexto extensional re-lacionado ao sistema de rifts Epinhaço-Orós/Jaguaribe, houve a preservação dos depósitos minerais e a circulação de fluidos hidrotermais. O evento D4 envolveu a reativação das zonas de cisalhamento neoproterozoicas ([Archanjo et al. 2021](#)), influenciando a geometria dos corpos de minério.

Dentro da perspectiva de investigar a formação das mineralizações de ferro à luz do processo de decratonização, é importante ressaltar, conforme destacado por [Teixeira et al. \(2019\)](#) em relação aos depósitos de ouro na Bahia, que o período da orogênese Riaciana e da subsequente destruição do Paleocontinente São Francisco durante o Estateriano foi uma época significativa em termos de metalogenia. Além disso, durante o período Neoproterozoico, quando o Cráton São Francisco assumiu sua configuração atual e a Província Borborema se desenvolveu em um contexto metacratônico, esses depósitos foram novamente retrabalhados.

BIBLIOGRAFIA

- Abbott, D. H. & Isley, A. E. 2002. "The Intensity, Occurrence, and Duration of Superplume Events and Eras over Geological Time". Em: *Journal of Geodynamics* **34**.2, pp. 265–307. ISSN: 0264-3707. DOI: [10.1016/S0264-3707\(02\)00024-8](https://doi.org/10.1016/S0264-3707(02)00024-8). URL: <http://www.sciencedirect.com/science/article/pii/S0264370702000248>.
- Almeida, F., Hasui, Y., De Brito Neves, B. & Fuck, R. 1981. "Brazilian Structural Provinces: An Introduction". Em: *Earth-Science Reviews* **17**.1-2, pp. 1–29. ISSN: 00128252. DOI: [10.1016/0012-8252\(81\)90003-9](https://doi.org/10.1016/0012-8252(81)90003-9). URL: <https://linkinghub.elsevier.com/retrieve/pii/0012825281900039>(acesso em 05/08/2023).
- Ancelmi, M. F. 2016. "Geocronologia e Geoquímica Das Rochas Arqueanas Do Complexo Granjeiro, Província Borborema". Tese PhD. Universidade Estadual de Campinas. DOI: [10.47749/t.unicamp.2016.979098](https://doi.org/10.47749/t.unicamp.2016.979098).
- Angelim, L. A. d. A., Moraes, J. F. S., Santos, E. J. d. & Silva, M. A. d. 1997. *Petrolina, folha SC.24-V-C, Estados da Bahia, Pernambuco e Piauí*. Brasília: CPRM, 1997. 102 p., il. 2 mapas. Escala 1:250.000. Programa Levantamentos Geológicos Básicos do Brasil.
- Angerer, T., Duuring, P., Hagemann, S. G., Thorne, W. & McCuaig, T. C. 2015. "A Mineral System Approach to Iron Ore in Archaean and Palaeoproterozoic BIF of Western Australia". Em: *Ore Deposits in an Evolving Earth*. Geological Society of London. ISBN: 978-1-86239-626-5. DOI: [10.1144/SP393.11](https://doi.org/10.1144/SP393.11). URL: <https://doi.org/10.1144/SP393.11>.
- Angerer, T. & Hagemann, S. G. 2010. "The BIF-hosted High-Grade Iron Ore Deposits in the Archean Koolyanobbing Greenstone Belt, Western Australia: Structural Control on Synorogenic-and Weathering-Related Magnetite-, Hematite-, and Goethite-Rich Iron Ore". Em: *Economic Geology* **105**.5, pp. 917–945.
- Angerer, T., Hagemann, S. G. & Danyushevsky, L. V. 2012. "Geochemical Evolution of the Banded Iron Formation-Hosted High-Grade Iron Ore System in the Koolyanobbing Greenstone Belt, Western Australia**". Em: *Economic Geology* **107**.4, pp. 599–644. ISSN: 0361-0128. DOI: [10.2113/econgeo.107.4.599](https://doi.org/10.2113/econgeo.107.4.599). URL: <https://doi.org/10.2113/econgeo.107.4.599>.
- Archangelo, C. J., Hollanda, M. H. B. M. D. & Viegas, L. G. F. 2021. "Late Ediacaran Lateral-Escape Tectonics as Recorded by the Patos Shear Zone (Borborema Province, NE Brazil)". Em: *Brazilian Journal of Geology* **51**.2, e20200132. ISSN: 2317-4692, 2317-4889. DOI: [10.1590/2317-4889202120200132](https://doi.org/10.1590/2317-4889202120200132). URL: http://www.scielo.br/scielo.php?script=sci_arttext&pid=S2317-48892021000200309&tlang=en(acesso em 23/08/2023).

- Arndt, N., Coltice, N., Helmstaedt, H. & Gregoire, M. 2009. "Origin of Archean Subcontinental Lithospheric Mantle: Some Petrological Constraints". Em: *Lithos* **109**.1-2, pp. 61–71. DOI: [10.1016/j.lithos.2008.10.019](https://doi.org/10.1016/j.lithos.2008.10.019).
- Augusto, G. G. d. S., Basto, C. F., UchÔa Filho, E. C. & Barros, R. d. A. 2017. *Geologia e Recursos Minerais Da Folha São Raimundo Nonato SC. 23-XD-II: Estado Do Piauí*. CPRM.
- Aulbach, S. 2012. "Craton Nucleation and Formation of Thick Lithospheric Roots". Em: *Lithos* **149**, pp. 16–30. DOI: [10.1016/j.lithos.2012.02.011](https://doi.org/10.1016/j.lithos.2012.02.011).
- Aulbach, S., Griffin, W. L., Pearson, N. J., O'Reilly, S. Y. & Doyle, B. J. 2007. "Lithosphere Formation in the Central Slave Craton (Canada): Plume Subcretion or Lithosphere Accretion?" Em: *Contributions to Mineralogy and Petrology* **154**.4, pp. 409–427. DOI: [10.1007/s00410-007-0200-1](https://doi.org/10.1007/s00410-007-0200-1).
- Barbosa, J. & Sabaté, P. 2004. "Archean and Paleoproterozoic Crust of the São Francisco Craton, Bahia, Brazil: Geodynamic Features". Em: *Precambrian Research* **133**.1-2, pp. 1–27. ISSN: 03019268. DOI: [10.1016/j.precamres.2004.03.001](https://doi.org/10.1016/j.precamres.2004.03.001). URL: <https://linkinghub.elsevier.com/retrieve/pii/S0301926804000658> (acesso em 07/08/2023).
- Barros, R. D. A., Caxito, F. D. A., Egydio-Silva, M., Dantas, E. L., Pinheiro, M. A. P., Rodrigues, J. B., Basei, M. A. S., Virgens-Neto, J. D. & Freitas, M. D. S. 2020. "Archean and Paleoproterozoic Crustal Evolution and Evidence for Cryptic Paleoarchean-Hadean Sources of the NW São Francisco Craton, Brazil: Lithochimistry, Geochronology, and Isotope Systematics of the Cristalândia Do Piauí Block". Em: *Gondwana Research* **88**, pp. 268–295. ISSN: 1342937X. DOI: [10.1016/j.gr.2020.07.004](https://doi.org/10.1016/j.gr.2020.07.004). URL: <https://linkinghub.elsevier.com/retrieve/pii/S1342937X20302239> (acesso em 08/08/2023).
- Bedini, R., Bodinier, J.-L., Dautria, J.-M. & Morten, L. 1997. "Evolution of LILE-enriched Small Melt Fractions in the Lithospheric Mantle: A Case Study from the East African Rift". Em: *Earth and Planetary Science Letters* **153**.1-2, pp. 67–83. DOI: [10.1016/s0012-821x\(97\)00167-2](https://doi.org/10.1016/s0012-821x(97)00167-2).
- Bekker, A., Slack, J. F., Planavsky, N., Krapez, B., Hofmann, A., Konhauser, K. O. & Rouxel, O. J. 2010. "Iron Formation: The Sedimentary Product of a Complex Interplay among Mantle, Tectonic, Oceanic, and Biospheric Processes". Em: *Economic Geology* **105**.3, pp. 467–508.
- Bekker, A., Planavsky, N., Rasmussen, B., Krapez, B., Hofmann, A., Slack, J., Rouxel, O. & Konhauser, K. 2014. "Iron Formations: Their Origins and Implications for Ancient Seawater Chemistry". Em: *Treatise on Geochemistry*. Vol. 12. Elsevier, pp. 561–628.

- Beukes, N. J., Gutzmer, J. & Mukhopadhyay, J. 2003. "The Geology and Genesis of High-Grade Hematite Iron Ore Deposits". Em: *Applied Earth Science* **112**.1, pp. 18–25. DOI: [10.1179/037174503225011243](https://doi.org/10.1179/037174503225011243). URL: <https://doi.org/10.1179/037174503225011243>.
- Beukes, N. J. & Gutzmer, J. E. N. S. 2008. "Origin and Paleoenvironmental Significance of Major Iron Formations at the Archean-Paleoproterozoic Boundary". Em: *Reviews in Economic Geology* **15**, pp. 5–47.
- Bird, P. 1978. "Initiation of Intracontinental Subduction in the Himalaya". Em: *Journal of Geophysical Research: Solid Earth* **83**.B10, pp. 4975–4987. DOI: [10.1029/jb083ib10p04975](https://doi.org/10.1029/jb083ib10p04975).
- 1979. "Continental Delamination and the Colorado Plateau". Em: *Journal of Geophysical Research: Solid Earth* **84**.B13, pp. 7561–7571. DOI: [10.1029/jb084ib13p07561](https://doi.org/10.1029/jb084ib13p07561).
- Bizzi, L., Schobbenhaus, C., Vidotti, R. & Gonçalves, J. 2003. "Geologia, Tectônica e Recursos Minerais Do Brasil". Em: *Geologia, Tectônica e Recursos Minerais do Brasil*.
- Boyd, F. 1989. "Compositional Distinction between Oceanic and Cratonic Lithosphere". Em: *Earth and Planetary Science Letters* **96**.1-2, pp. 15–26. DOI: [10.1016/0012-821x\(89\)90120-9](https://doi.org/10.1016/0012-821x(89)90120-9).
- Brito Neves, B. B., Santos, E. J. & Van Schmus, W. R. 2000. "Tectonic History of the Borborema Province, Northeastern Brazil". Em: *Tectonic Evolution of South America*.
- Brito Neves, B. B. 2011. "The Paleoproterozoic in the South-American Continent: Diversity in the Geologic Time". Em: *Journal of South American Earth Sciences* **32**.4, pp. 270–286. ISSN: 08959811. DOI: [10.1016/j.jsames.2011.02.004](https://doi.org/10.1016/j.jsames.2011.02.004). URL: <https://linkinghub.elsevier.com/retrieve/pii/S0895981111000125> (acesso em 07/08/2023).
- Brito Neves, B. B. D., Santos, T. J. S. D. & Dantas, E. L. 2023. "O Terreno Tectonoestratigráfico São Pedro: Oeste Da Zona Transversal – Província Borborema". Em: *Geologia USP. Série Científica* **22**.4, pp. 45–69. ISSN: 2316-9095. DOI: [10.11606/issn.2316-9095.v22-197489](https://doi.org/10.11606/issn.2316-9095.v22-197489). URL: <https://www.revistas.usp.br/guspse/article/view/207991> (acesso em 08/08/2023).
- Caxito, F. D. A., Santos, L. C. M. D. L., Ganade, C. E., Bendaoud, A., Fettous, E.-H. & Bouyo, M. H. 2020. "Toward an Integrated Model of Geological Evolution for NE Brazil-NW Africa: The Borborema Province and Its Connections to the Trans-Saharan (Benino-Nigerian and Tuareg Shields) and Central African Orogens". Em: *Brazilian Journal of Geology* **50**.2, e20190122. ISSN: 2317-4692, 2317-4889. DOI: [10.1590/2317-4889202020190122](https://doi.org/10.1590/2317-4889202020190122). URL: http://www.scielo.br/scielo.php?script=sci_arttext&pid=S2317-48892020000200605&tlang=en (acesso em 05/08/2023).

- Cloud, P. 1973. "Paleoecological Significance of the Banded Iron-Formation". Em: *Economic Geology* **68**.7, pp. 1135–1143. ISSN: 0361-0128. DOI: [10.2113/gsecongeo.68.7.1135](https://doi.org/10.2113/gsecongeo.68.7.1135). eprint: <https://pubs.geoscienceworld.org/economicgeology/article-pdf/68/7/1135/3484914/1135.pdf>. URL: <https://doi.org/10.2113/gsecongeo.68.7.1135>.
- Costa, Á. F. 2010. "Litogeоquímica Das Rochas Encaixantes E Do Minériode Ferro Da Região de Curral Novo". Em: *Trabalho de conclusão de curso, UFBA, Salvador*.
- Dalstra, H. J. 2014. "Structural Evolution of the Mount Wall Region in the Hamersley Province, Western Australia and Its Control on Hydrothermal Alteration and Formation of High-Grade Iron Deposits". Em: *Journal of Structural Geology* **67**, pp. 268–292. DOI: [10.1016/j.jsg.2014.03.005](https://doi.org/10.1016/j.jsg.2014.03.005).
- Dalstra, H. J. & Rosière, C. A. 2008. "Structural Controls on High-Grade Iron Ores Hosted by Banded Iron Formation: A Global Perspective". Em: *Banded Iron Formation-Related High-Grade Iron Ore*. Society of Economic Geologists. ISBN: 978-1-934969-07-6. DOI: [10.5382/Rev.15.03](https://doi.org/10.5382/Rev.15.03). URL: <https://doi.org/10.5382/Rev.15.03>.
- Davies, G. F. 1994. "Thermomechanical Erosion of the Lithosphere by Mantle Plumes". Em: *Journal of Geophysical Research: Solid Earth* **99**.B8, pp. 15709–15722. ISSN: 0148-0227. DOI: [10.1029/94JB00119](https://doi.org/10.1029/94JB00119). URL: <https://agupubs.onlinelibrary.wiley.com/doi/10.1029/94JB00119> (acesso em 22/10/2023).
- Delgado, I. d. M., Souza, J. D. de, Silva, L. C. da, Silveira Filho, N. C. da, Santos, R. A. dos, Pedreira, A. J., Guimarães, J. T., Angelim, L. d. A., Vasconcelos, A. M., Gomes, I. P. et al. 2003. "Geotectônica Do Escudo Atlântico". Em: *Geologia, Tectônica e Recursos Minerais do Brasil* **5**, pp. 227–334.
- Deng, J., Mo, X., Zhao, H., Wu, Z., Luo, Z. & Su, S. 2004. "A New Model for the Dynamic Evolution of Chinese Lithosphere: 'continental Roots–Plume Tectonics'". Em: *Earth-Science Reviews* **65**.3-4, pp. 223–275. DOI: [10.1016/j.earscirev.2003.08.001](https://doi.org/10.1016/j.earscirev.2003.08.001).
- Evans, K., McCuaig, T., Leach, D., Angerer, T. & Hagemann, S. 2013. "Banded Iron Formation to Iron Ore: A Record of the Evolution of Earth Environments?" Em: *Geology* **41**.2, pp. 99–102. DOI: [10.1130/g33244.1](https://doi.org/10.1130/g33244.1).
- Ewers, W. E. & Morris, R. C. 1981. "Studies of the Dales Gorge Member of the Brockman Iron Formation, Western Australia". Em: *Economic Geology* **76**.7, pp. 1929–1953. ISSN: 0361-0128. DOI: [10.2113/gsecongeo.76.7.1929](https://doi.org/10.2113/gsecongeo.76.7.1929). eprint: <https://pubs.geoscienceworld.org/economicgeology/article-pdf/76/7/1929/3487039/1929.pdf>. URL: <https://doi.org/10.2113/gsecongeo.76.7.1929>.

- Ford, A. & McCuaig, T. 2010. "The Effect of Map Scale on Geological Complexity for Computer-Aided Exploration Targeting". Em: *Ore Geology Reviews* **38**.3, pp. 156–167. DOI: [10.1016/j.oregeorev.2010.03.008](https://doi.org/10.1016/j.oregeorev.2010.03.008).
- Fullea, J., Fernàndez, M. & Zeyen, H. 2008. "FA2BOUG—A FORTRAN 90 Code to Compute Bouguer Gravity Anomalies from Gridded Free-Air Anomalies: Application to the Atlantic- Mediterranean Transition Zone". Em: *Computers & Geosciences* **34**.12, pp. 1665–1681. DOI: [10.1016/j.cageo.2008.02.018](https://doi.org/10.1016/j.cageo.2008.02.018).
- Ganade, C. E., Weinberg, R. F., Caxito, F. A., Lopes, L. B. L., Tesser, L. R. & Costa, I. S. 2021. "Decratonization by Rifting Enables Orogenic Reworking and Transcurrent Dispersal of Old Terranes in NE Brazil". Em: *Scientific Reports* **11**.1, p. 5719. ISSN: 2045-2322. DOI: [10.1038/s41598-021-84703-x](https://doi.org/10.1038/s41598-021-84703-x). URL: <https://www.nature.com/articles/s41598-021-84703-x>(acesso em 05/08/2023).
- Gao, S., Rudnick, R. L., Carlson, R. W., McDonough, W. F. & Liu, Y.-S. 2002. "Re-Os Evidence for Replacement of Ancient Mantle Lithosphere beneath the North China Craton". Em: *Earth and Planetary Science Letters* **198**.3-4, pp. 307–322. DOI: [10.1016/s0012-821x\(02\)00489-2](https://doi.org/10.1016/s0012-821x(02)00489-2).
- Gao, S., Rudnick, R. L., Yuan, H.-L., Liu, X.-M., Liu, Y.-S., Xu, W.-L., Ling, W.-L., Ayers, J., Wang, X.-C. & Wang, Q.-H. 2004. "Recycling Lower Continental Crust in the North China Craton". Em: *Nature* **432**.7019, pp. 892–897. ISSN: 0028-0836, 1476-4687. DOI: [10.1038/nature03162](https://doi.org/10.1038/nature03162). URL: <https://www.nature.com/articles/nature03162>(acesso em 25/08/2023).
- Godin, L. & Harris, L. B. 2014. "Tracking basement cross-strike discontinuities in the Indian crust beneath the Himalayan orogen using gravity data – relationship to upper crustal faults". Em: *Geophysical Journal International* **198**.1, pp. 198–215. ISSN: 1365-246X. DOI: [10.1093/gji/ggu131](https://doi.org/10.1093/gji/ggu131).
- Gole, M. J. & Klein, C. 1981. "Banded Iron-Formations through Much of Precambrian Time". Em: *The Journal of Geology* **89**.2, pp. 169–183. DOI: [10.1086/628578](https://doi.org/10.1086/628578). eprint: <https://doi.org/10.1086/628578>. URL: <https://doi.org/10.1086/628578>.
- Gomes, J. R. d. C. & Vasconcelos, A. M. 2000. *Jaguaribe-SW, Folha SB.24-Y. Programa Levantamentos Geológicos Básicos Do Brasil*. CPRM - Serviço Geológico do Brasil.

- Goodwin, A. M. 1973. "Archean Iron-Formations and Tectonic Basins of the Canadian Shield". Em: *Economic Geology* **68**.7, pp. 915–933. ISSN: 0361-0128. DOI: [10.2113/gsecongeo.68.7.915](https://doi.org/10.2113/gsecongeo.68.7.915). eprint: <https://pubs.geoscienceworld.org/economicgeology/article-pdf/68/7/915/3485035/915.pdf>. URL: <https://doi.org/10.2113/gsecongeo.68.7.915>.
- Gourcerol, B., Thurston, P., Kontak, D., Côté-Mantha, O. & Biczok, J. 2016. "Depositional Setting of Algoma-type Banded Iron Formation". Em: *Precambrian Research* **281**, pp. 47–79. ISSN: 0301-9268. DOI: [10.1016/j.precamres.2016.04.019](https://doi.org/10.1016/j.precamres.2016.04.019). URL: <http://www.sciencedirect.com/science/article/pii/S0301926816301085>.
- Griffin, W. L., Andi, Z., O'Reilly, S. Y. & Ryan, C. G. 1998. "Phanerozoic Evolution of the Lithosphere beneath the Sino-Korean Craton". Em: *Mantle Dynamics and Plate Interactions in East Asia*. American Geophysical Union, pp. 107–126. DOI: [10.1029/gd027p0107](https://doi.org/10.1029/gd027p0107).
- Griffin, W., O'Reilly, S., Abe, N., Aulbach, S., Davies, R., Pearson, N., Doyle, B. & Kivi, K. 2003. "The Origin and Evolution of Archean Lithospheric Mantle". Em: *Precambrian Research* **127**.1-3, pp. 19–41. DOI: [10.1016/s0301-9268\(03\)00180-3](https://doi.org/10.1016/s0301-9268(03)00180-3).
- Gross, G. 1965. "Geology of Iron Deposits in Canada, Vol. 1 General Geology and Evaluation of Ore Deposits: Geological Survey of Canada". Em: *Economic Geology Report* **22**, p. 81.
- Gross, G. A. 1980. "A Classification of Iron Formations Based on Depositional Environments". Em: *The Canadian Mineralogist* **18**.2, pp. 215–222.
- 1983. "Tectonic Systems and the Deposition of Iron-Formation". Em: *Precambrian Research* **20**.2, pp. 171–187. ISSN: 0301-9268. DOI: [10.1016/0301-9268\(83\)90072-4](https://doi.org/10.1016/0301-9268(83)90072-4). URL: <http://www.sciencedirect.com/science/article/pii/0301926883900724>.
- Groves, D. I. & Santosh, M. 2021. "Craton and Thick Lithosphere Margins: The Sites of Giant Mineral Deposits and Mineral Provinces". Em: *Gondwana Research* **100**, pp. 195–222. DOI: [10.1016/j.gr.2020.06.008](https://doi.org/10.1016/j.gr.2020.06.008).
- Groves, D. I., Phillips, G. N., Ho, S. E., Houstoun, S. M. & Standing, C. A. 1987. "Craton-Scale Distribution of Archean Greenstone Gold Deposits; Predictive Capacity of the Metamorphic Model". Em: *Economic Geology* **82**.8, pp. 2045–2058.
- Groves, D. I., Santosh, M., Müller, D., Zhang, L., Deng, J., Yang, L.-Q. & Wang, Q.-F. 2022. "Mineral Systems: Their Advantages in Terms of Developing Holistic Genetic Models and for Target Generation in Global Mineral Exploration". Em: *Geosystems and Geoenvironment* **1**.1, p. 100001. DOI: [10.1016/j.geogeo.2021.09.001](https://doi.org/10.1016/j.geogeo.2021.09.001).

- Gung, Y., Panning, M. & Romanowicz, B. 2003. "Global anisotropy and the thickness of continents". Em: *Nature* **422**.6933, pp. 707–711. ISSN: 1476-4687. DOI: [10.1038/nature01559](https://doi.org/10.1038/nature01559).
- Hagemann, S. G., Angerer, T., Duuring, P., Rosière, C. A., Silva, R. C. F. e, Lobato, L., Hens- ler, A. S. & Walde, D. H. G. 2016. "BIF-hosted Iron Mineral System: A Review". Em: *Ore Geology Reviews* **76**, pp. 317–359. ISSN: 0169-1368. DOI: [10.1016/j.oregeorev.2015.11.004](https://doi.org/10.1016/j.oregeorev.2015.11.004). URL: <http://www.sciencedirect.com/science/article/pii/S0169136815301815>.
- Heilbron, M., Cordani, U. & Alkmim, F. 2017. "The Paleomagnetic Record of the São Francisco-Congo Craton". Em: *São Francisco Craton, Eastern Brazil*, pp. 305–320.
- Hoffman, P. F. 1988. "United Plates of America, The Birth of a Craton: Early Proterozoic Assembly and Growth of Laurentia". Em: *Annual Review of Earth and Planetary Sciences* **16**.1, pp. 543–603. ISSN: 0084-6597, 1545-4495. DOI: [10.1146/annurev.ea.16.050188.002551](https://doi.org/10.1146/annurev.ea.16.050188.002551). URL:<https://www.annualreviews.org/doi/10.1146/annurev.ea.16.050188.002551> (acesso em 22/10/2023).
- Hoffman, P. F. 2014. "The Origin of Laurentia: Rae Craton as the Backstop for Proto-Laurentian Amalgamation by Slab Suction". Em: *Geoscience Canada* **41**.3, p. 313. ISSN: 1911-4850, 0315-0941. DOI: [10.12789/geocanj.2014.41.049](https://doi.org/10.12789/geocanj.2014.41.049). URL: <https://journals.lib.unb.ca/index.php/GC/article/view/21296> (acesso em 22/10/2023).
- Holdsworth, R. E., Handa, M., Miller, J. A. & Buick, I. S. 2001. "Continental Reactivation and Reworking: An Introduction". Em: *Geological Society, London, Special Publications* **184**.1, pp. 1–12. ISSN: 0305-8719, 2041-4927. DOI: [10.1144/GSL.SP.2001.184.01.01](https://doi.org/10.1144/GSL.SP.2001.184.01.01). URL: <https://www.lyellcollection.org/doi/10.1144/GSL.SP.2001.184.01.01> (acesso em 08/08/2023).
- Holland, H. D. 1978. "The Chemistry of the Atmosphere and Oceans-(v. 1)". Em. 1984. *The Chemical Evolution of the Atmosphere and Oceans*. Princeton University Press.
- 1973. "The Oceans; a Possible Source of Iron in Iron-Formations". Em: *Economic Geology* **68**.7, pp. 1169–1172. ISSN: 0361-0128. DOI: [10.2113/gsecongeo.68.7.1169](https://doi.org/10.2113/gsecongeo.68.7.1169). eprint: <https://pubs.geoscienceworld.org/economicgeology/article-pdf/68/7/1169/3484968/1169.pdf>. URL: <https://doi.org/10.2113/gsecongeo.68.7.1169>.
- Huston, D. L. & Logan, G. A. 2004. "Barite, BIFs and Bugs: Evidence for the Evolution of the Earth's Early Hydrosphere". Em: *Earth and Planetary Science Letters* **220**.1, pp. 41–55. ISSN: 0012-821X. DOI: [10.1016/S0012-821X\(04\)00034-2](https://doi.org/10.1016/S0012-821X(04)00034-2). URL: <http://www.sciencedirect.com/science/article/pii/S0012821X04000342>.

- Isley, A. E. 1995. "Hydrothermal Plumes and the Delivery of Iron to Banded Iron Formation". Em: *The Journal of Geology* **103**.2, pp. 169–185. ISSN: 00221376, 15375269. JSTOR: [30079749](https://www.jstor.org/stable/30079749). URL: <http://www.jstor.org/stable/30079749>.
- James, H. L. 1983. "Chapter 12 Distribution of Banded Iron-Formation in Space and Time". Em: *Iron-Formation Facts and Problems*. Ed. por A. F. Trendall & R. C. Morris. Vol. 6. Developments in Precambrian Geology. Elsevier, pp. 471–490. DOI: [10.1016/S0166-2635\(08\)70053-7](https://doi.org/10.1016/S0166-2635(08)70053-7). URL: <http://www.sciencedirect.com/science/article/pii/S0166263508700537>.
- James, H. L. 1954. "Sedimentary Facies of Iron-Formation". Em: *Economic Geology* **49**.3, pp. 235–293.
- Kappler, A., Pasquero, C., Konhauser, K. O. & Newman, D. K. 2005. "Deposition of Banded Iron Formations by Anoxygenic Phototrophic Fe(II)-Oxidizing Bacteria". Em: *Geology* **33**.11, pp. 865–868. ISSN: 0091-7613. DOI: [10.1130/G21658.1](https://doi.org/10.1130/G21658.1). eprint: <https://pubs.geoscienceworld.org/geology/article-pdf/33/11/865/3528264/i0091-7613-33-11-865.pdf>. URL: <https://doi.org/10.1130/G21658.1>.
- Kay, R. & Kay, S. M. 1993. "Delamination and Delamination Magmatism". Em: *Tectonophysics* **219**.1-3, pp. 177–189. DOI: [10.1016/0040-1951\(93\)90295-u](https://doi.org/10.1016/0040-1951(93)90295-u).
- Klein, C. 1983. "Diagenesis and Metamorphism of Precambrian Banded Iron-Formations". Em: *Developments in Precambrian Geology*. Vol. 6. Elsevier, pp. 417–469.
- 2005. "Some Precambrian Banded Iron-Formations (BIFs) from around the World: Their Age, Geologic Setting, Mineralogy, Metamorphism, Geochemistry, and Origins". Em: *American Mineralogist* **90**.10, pp. 1473–1499.
- Klein, C. & Beukes, N. J. 1993. "Sedimentology and Geochemistry of the Glaciogenic Late Proterozoic Rapitan Iron-Formation in Canada". Em: *Economic Geology* **88**.3, pp. 542–565. ISSN: 0361-0128. DOI: [10.2113/gsecongeo.88.3.542](https://doi.org/10.2113/gsecongeo.88.3.542). eprint: <https://pubs.geoscienceworld.org/economicgeology/article-pdf/88/3/542/3491160/542.pdf>. URL: <https://doi.org/10.2113/gsecongeo.88.3.542>.
- Kock, M. O., Evans, D. A. D., Gutzmer, J., Beukes, N. J. & Dorland, H. C. 2008. "Origin and Timing of Banded Iron Formation-Hosted High-Grade Hard Hematite Deposits—A Paleomagnetic Approach". Em: *Banded Iron Formation-Related High-Grade Iron Ore*. Society of Economic Geologists. ISBN: 978-1-934969-07-6. DOI: [10.5382/Rev.15.02](https://doi.org/10.5382/Rev.15.02). URL: <https://doi.org/10.5382/Rev.15.02>.

- Krapež, B., Barley, M. E. & Pickard, A. L. 2003. "Hydrothermal and Resedimented Origins of the Precursor Sediments to Banded Iron Formation: Sedimentological Evidence from the Early Palaeoproterozoic Brockman Supersequence of Western Australia". Em: *Sedimentology* **50**.5, pp. 979–1011. DOI: [10.1046/j.1365-3091.2003.00594.x](https://doi.org/10.1046/j.1365-3091.2003.00594.x). eprint: <https://onlinelibrary.wiley.com/doi/pdf/10.1046/j.1365-3091.2003.00594.x>. URL: <https://onlinelibrary.wiley.com/doi/abs/10.1046/j.1365-3091.2003.00594.x>.
- Kusky, T. M., Windley, B. F., Wang, L., Wang, Z., Li, X. & Zhu, P. 2014. "Flat Slab Subduction, Trench Suction, and Craton Destruction: Comparison of the North China, Wyoming, and Brazilian Cratons". Em: *Tectonophysics* **630**, pp. 208–221. DOI: [10.1016/j.tecto.2014.05.028](https://doi.org/10.1016/j.tecto.2014.05.028).
- Lascelles, D. F. 2013. "Plate Tectonics Caused the Demise of Banded Iron Formations". Em: *Applied Earth Science* **122**.4, pp. 230–241. DOI: [10.1179/1743275814Y.0000000043](https://doi.org/10.1179/1743275814Y.0000000043). eprint: <https://doi.org/10.1179/1743275814Y.0000000043>. URL: <https://doi.org/10.1179/1743275814Y.0000000043>.
- Lee, C.-T. A., Luffi, P. & Chin, E. J. 2011. "Building and Destroying Continental Mantle". Em: *Annual Review of Earth and Planetary Sciences* **39**.1, pp. 59–90. ISSN: 0084-6597, 1545-4495. DOI: [10.1146/annurev-earth-040610-133505](https://doi.org/10.1146/annurev-earth-040610-133505). URL: <https://www.annualreviews.org/doi/10.1146/annurev-earth-040610-133505> (acesso em 08/08/2023).
- Lee, C.-T. A. 2006. "Geochemical/Petrologic Constraints on the Origin of Cratonic Mantle". Em: *Archean Geodynamics and Environments*. American Geophysical Union, pp. 89–114. DOI: [10.1029/164gm08](https://doi.org/10.1029/164gm08).
- Li, Y.-L., Konhauser, K. O., Kappler, A. & Hao, X.-L. 2013. "Experimental Low-Grade Alteration of Biogenic Magnetite Indicates Microbial Involvement in Generation of Banded Iron Formations". Em: *Earth and Planetary Science Letters* **361**, pp. 229–237. ISSN: 0012-821X. DOI: [10.1016/j.epsl.2012.10.025](https://doi.org/10.1016/j.epsl.2012.10.025). URL: <http://www.sciencedirect.com/science/article/pii/S0012821X12005870>.
- Li, Y.-L., Konhauser, K. O. & Zhai, M. 2017. "The Formation of Magnetite in the Early Archean Oceans". Em: *Earth and Planetary Science Letters* **466**, pp. 103–114. ISSN: 0012-821X. DOI: [10.1016/j.epsl.2017.03.013](https://doi.org/10.1016/j.epsl.2017.03.013). URL: <http://www.sciencedirect.com/science/article/pii/S0012821X17301437>.

- Li, L., Li, C., Li, Q., Yuan, M.-W., Zhang, J.-Q., Li, S.-R., Santosh, M., Shen, J.-F. & Zhang, H.-F. 2022. "Indicators of Decratonic Gold Mineralization in the North China Craton". Em: *Earth- Science Reviews* **228**, p. 103995. ISSN: 00128252. DOI: [10.1016/j.earscirev.2022.103995](https://doi.org/10.1016/j.earscirev.2022.103995). URL: <https://linkinghub.elsevier.com/retrieve/pii/S0012825222000794> (acesso em 23/10/2023).
- Li, S.-R. & Santosh, M. 2014. "Metallogeny and Craton Destruction: Records from the North China Craton". Em: *Ore Geology Reviews* **56**, pp. 376–414. ISSN: 01691368. DOI: [10.1016/j.oregeorev.2013.03.002](https://doi.org/10.1016/j.oregeorev.2013.03.002). URL: <https://linkinghub.elsevier.com/retrieve/pii/S0169136813000863> (acesso em 23/10/2023).
- Martins, D. T. 2017. "GEOLOGIA DO TERRENO ARQUEANO GRANJEIRO (3.4 a 2.6 Ga), PROVÍNCIA BORBOREMA". Diss. de mestr. Universidade Federal do Ceará.
- McCuaig, T. C., Beresford, S. & Hronsky, J. 2010. "Translating the Mineral Systems Approach into an Effective Exploration Targeting System". Em: *Ore Geology Reviews* **38**, pp. 128–138. DOI: [10.1016/j.oregeorev.2010.05.008](https://doi.org/10.1016/j.oregeorev.2010.05.008).
- McCuaig, T. C. & Hronsky, J. M. A. 2014. "The Mineral System Concept<sub></sub>>The Key to Exploration Targeting</sub>>". Em: *Building Exploration Capability for the 21st Century*. Society of Economic Geologists. DOI: [10.5382/sp.18.08](https://doi.org/10.5382/sp.18.08).
- Menzies, M. A. & Xu, Y. 1998. "Geodynamics of the North China Craton". Em: *Mantle Dynamics and Plate Interactions in East Asia*. American Geophysical Union, pp. 155–165. DOI: [10.1029/gd027p0155](https://doi.org/10.1029/gd027p0155).
- Menzies, M., Xu, Y., Zhang, H. & Fan, W. 2007. "Integration of Geology, Geophysics and Geochemistry: A Key to Understanding the North China Craton". Em: *Lithos* **96**, pp. 1–21. DOI: [10.1016/j.lithos.2006.09.008](https://doi.org/10.1016/j.lithos.2006.09.008).
- Miller, H. G. & Singh, V. 1994. "Potential Field Tilt—a New Concept for Location of Potential Field Sources". Em: *Journal of Applied Geophysics* **32**, pp. 213–217. DOI: [10.1016/0926-9851\(94\)90022-1](https://doi.org/10.1016/0926-9851(94)90022-1).
- Miyano, T. & Klein, C. 1983. "Conditions of Riebeckite Formation in the Iron-Formation of the Dales Gorge Member, Hamersley Group, Western Australia". Em: *American Mineralogist* **68**, pp. 517–529. ISSN: 0003-004X. eprint: https://pubs.geoscienceworld.org/ammin/article-pdf/68/5-6/517/4212505/am68_517.pdf.
- Navarro, M. S., Tonetto, E. M. & Oliveira, E. P. 2017. "Peixe Zircon: New Brazilian Reference Material for U-Pb Geochronology by LA-SF-ICP-MS". Em: *Goldschmidt Conference*, <https://goldschmidtabstracts.info/2017/3815.Pdf>.

- Neves, S. P. 2021. "Comparative Geological Evolution of the Borborema Province and São Francisco Craton (Eastern Brazil): Decratonization and Crustal Reworking during West Gondwana Assembly and Implications for Paleogeographic Reconstructions". Em: *Precambrian Research* **355**, p. 106119. ISSN: 03019268. DOI: [10.1016/j.precamres.2021.106119](https://doi.org/10.1016/j.precamres.2021.106119). URL: <https://linkinghub.elsevier.com/retrieve/pii/S0301926821000292> (acesso em 05/08/2023).
- Ohmoto, H., Watanabe, Y., Yamaguchi, K. E., Naraoka, H., Haruna, M., Kakegawa, T., Hayashi, K.-i. & Kato, Y. 2006. "Chemical and Biological Evolution of Early Earth: Constraints from Banded Iron Formations". Em: *Evolution of Early Earth's Atmosphere, Hydrosphere, and Biosphere - Constraints from Ore Deposits*. Geological Society of America. ISBN: 978-0-8137-1198-0. DOI: [10.1130/2006.1198\(17\)](https://doi.org/10.1130/2006.1198(17)). URL: [https://doi.org/10.1130/2006.1198\(17\)](https://doi.org/10.1130/2006.1198(17)).
- Paton, C., Woodhead, J. D., Hellstrom, J. C., Herdt, J. M., Greig, A. & Maas, R. 2010. "Improved Laser Ablation U-Pb Zircon Geochronology through Robust Downhole Fractionation Correction". Em: *Geochemistry, Geophysics, Geosystems* **11**.3, n/a–n/a. DOI: [10.1029/2009gc002618](https://doi.org/10.1029/2009gc002618).
- Pavlis, N. K., Holmes, S. A., Kenyon, S. C. & Factor, J. K. 2012. "The Development and Evaluation of the Earth Gravitational Model 2008 (EGM2008)". Em: *Journal of Geophysical Research: Solid Earth* **117**.B4, n/a–n/a. DOI: [10.1029/2011jb008916](https://doi.org/10.1029/2011jb008916).
- Pearson, D. & Wittig, N. 2008. "Formation of Archaean Continental Lithosphere and Its Diamonds: The Root of the Problem". Em: *Journal of the Geological Society* **165**.5, pp. 895–914. ISSN: 0016-7649, 2041-479X. DOI: [10.1144/0016-76492008-003](https://doi.org/10.1144/0016-76492008-003). URL: <https://www.lyellcollection.org/doi/10.1144/0016-76492008-003> (acesso em 22/10/2023).
- Peslier, A. H., Woodland, A. B., Bell, D. R. & Lazarov, M. 2010. "Olivine Water Contents in the Continental Lithosphere and the Longevity of Cratons". Em: *Nature* **467**.7311, pp. 78–81. DOI: [10.1038/nature09317](https://doi.org/10.1038/nature09317).
- Petrus, J. A. & Kamber, B. S. 2012. "VizualAge: A Novel Approach to Laser Ablation ICP-MS u-Pb Geochronology Data Reduction". Em: *Geostandards and Geoanalytical Research* **36**.3, pp. 247–270. DOI: [10.1111/j.1751-908x.2012.00158.x](https://doi.org/10.1111/j.1751-908x.2012.00158.x).
- Pitarello, M. Z., Santos, T. J. S. dos & Ancelmi, M. F. 2019. "Syn-to Post-Depositional Processes Related to High Grade Metamorphic BIFs: Geochemical and Geochronological Evidences from a Paleo to Neoarchean (3.5-2.6 Ga) Terrane in NE Brazil". Em: *Journal of South American Earth Sciences* **96**, p. 102312. ISSN: 0895-9811. DOI: [10.1016/j.jsames.2019.102312](https://doi.org/10.1016/j.jsames.2019.102312). URL: <http://www.sciencedirect.com/science/article/pii/S089598111830289X>.

- Planavsky, N. J., Asael, D., Hofmann, A., Reinhard, C. T., Lalonde, S. V., Knudsen, A., Wang, X., Ossa, F. O., Pecoits, E., Smith, A. J. et al. 2014. "Evidence for Oxygenic Photosynthesis Half a Billion Years before the Great Oxidation Event". Em: *Nature Geoscience* 7.4, pp. 283–286.
- Rosière, C. A., Siemes, H., Quade, H., Brokmeier, H.-G. & Jansen, E. M. 2001. "Microstructures, Textures and Deformation Mechanisms in Hematite". Em: *Journal of Structural Geology* 23.9, pp. 1429–1440. ISSN: 0191-8141. DOI: 10.1016/S0191-8141(01)00009-8. URL: <http://www.sciencedirect.com/science/article/pii/S0191814101000098>.
- Ruppel, C. 1995. "Extensional Processes in Continental Lithosphere". Em: *Journal of Geophysical Research: Solid Earth* 100.B12, pp. 24187–24215. DOI: 10.1029/95jb02955.
- Sato, E. N. 2011. "Proposta Metodológica Sobre Dados de Geofísica Aeroportada Na Prospecção de Minério de Fe: Indicação de Ambientes Geológicos Propícios e Geração de Mapas de Probabilidade Na Região de Curral Novo Do Piauí (PI)". Diss. de mestr. Universidade de São Paulo.
- Şengör, A. C., Lom, N. & Polat, A. 2021. "The Nature and Origin of Cratons Constrained by Their Surface Geology". Em: *GSA Bulletin* 134.5-6, pp. 1485–1505. DOI: 10.1130/b36079.1.
- Silva, L., McNaughton, N., Melo, R. & Fletcher, I. 1997. "U-Pb SHRIMP Ages in the Itabuna- Caraíba TTG High-Grade Complex: The First Window beyond the Paleoproterozoic Over-printing of the Eastern Jequié Craton, NE Brazil". Em: *Proceedings 2nd International Symposium on Granites and Associated Mineralizations*, pp. 282–283.
- Simonson, B. M. 1985. "Sedimentological Constraints on the Origins of Precambrian Iron-Formations". Em: *GSA Bulletin* 96.2, pp. 244–252. ISSN: 0016-7606. DOI: 10.1130/0016-7606(1985) 96<244 : SCOTOO> 2 . 0 . CO; 2. eprint: <https://pubs.geoscienceworld.org/gsabulletin/article-pdf/96/2/244/3444951/i0016-7606-96-2-244.pdf>. URL: [https://doi.org/10.1130/0016-7606\(1985\)96%3C244:SCOTOO%3E2.0.CO;2](https://doi.org/10.1130/0016-7606(1985)96%3C244:SCOTOO%3E2.0.CO;2).
- Simonson, B. M. 2003. "Origin and Evolution of Large Precambrian Iron Formations". Em: *Extreme Depositional Environments: Mega End Members in Geologic Time*. Geological Society of America. ISBN: 978-0-8137-2370-9. DOI: 10.1130/0-8137-2370-1.231. URL: <https://doi.org/10.1130/0-8137-2370-1.231>.
- Sleep, N. H. 2005. "Evolution of the Continental Lithosphere". Em: *Annual Review of Earth and Planetary Sciences* 33.1, pp. 369–393. DOI: 10.1146/annurev.earth.33.092203.122643.

- Snyder, D. B., Humphreys, E. & Pearson, D. G. 2017. "Construction and Destruction of Some North American Cratons". Em: *Tectonophysics* **694**, pp. 464–485. DOI: [10.1016/j.tecto.2016.11.032](https://doi.org/10.1016/j.tecto.2016.11.032).
- Souza, D., Fernandes, F., Guimaraes, J. & Lopes, J. 1979. "Projeto Colomi; Geologia Da Região Do Médio São Francisco". Em: *Relatório final, DNPM/CPRM, Salvador, Brasil. 3v.*
- Spector, A. & Grant, F. S. 1970. "STATISTICAL MODELS FOR INTERPRETING AERO-MAGNETIC DATA". Em: *GEOPHYSICS* **35.2**, pp. 293–302. DOI: [10.1190/1.1440092](https://doi.org/10.1190/1.1440092).
- Teixeira, J. B. G., Misi, A., da Glória da Silva, M. & de Brito, R. S. C. 2019. "Reconstruction of Precambrian Terranes of Northeastern Brazil along Cambrian Strike-Slip Faults: A New Model of Geodynamic Evolution and Gold Metallogeny in the State of Bahia". Em: *Brazilian Journal of Geology* **49.3**. DOI: [10.1590/2317-4889201920190009](https://doi.org/10.1590/2317-4889201920190009).
- Teixeira, W., Oliveira, E. P. & Marques, L. S. 2017. "Nature and Evolution of the Archean Crust of the São Francisco Craton". Em: *São Francisco Craton, Eastern Brazil*. Ed. por M. Heilbron, U. G. Cordani & F. F. Alkmim. Cham: Springer International Publishing, pp. 29–56. ISBN: 978-3-319-01714-3 978-3-319-01715-0. DOI: [10.1007/978-3-319-01715-0_3](https://doi.org/10.1007/978-3-319-01715-0_3).
- URL: http://link.springer.com/10.1007/978-3-319-01715-0_3 (acesso em 06/08/2023).
- Thorne, W. S., Hagemann, S. G., Sepe, D., Dalstra, H. J. & Banks, D. A. 2014. "Structural Control, Hydrothermal Alteration Zonation, and Fluid Chemistry of the Concealed, High-Grade 4EE Iron Orebody at the Paraburadoo 4E Deposit, Hamersley Province, Western Australia". Em: *Economic Geology* **109.6**, pp. 1529–1562. DOI: [10.2113/econgeo.109.6.1529](https://doi.org/10.2113/econgeo.109.6.1529).
- Trendall, A. F. 2002. "The Significance of Iron-Formation in the Precambrian Stratigraphic Record". Em: *Precambrian Sedimentary Environments*. John Wiley & Sons, Ltd, pp. 33–66. ISBN: 978-1-4443-0431-2. DOI: [10.1002/9781444304312.ch3](https://doi.org/10.1002/9781444304312.ch3). eprint: <https://onlinelibrary.wiley.com/doi/pdf/10.1002/9781444304312.ch3>. URL: <https://onlinelibrary.wiley.com/doi/abs/10.1002/9781444304312.ch3>.
- Trendall, A. 1983. "Chapter 3 the Hamersley Basin". Em: *Iron-Formation Facts and Problems*. Ed. por A. Trendall & R. Morris. Vol. 6. Developments in Precambrian Geology. Elsevier, pp. 69–129. DOI: [10.1016/S0166-2635\(08\)70042-2](https://doi.org/10.1016/S0166-2635(08)70042-2). URL: <http://www.sciencedirect.com/science/article/pii/S0166263508700422>.
- Trompette, R., Uhlein, A., Silva, M. & Karmann, I. 1992. "O Cráton Brasiliano - Uma Revisão". Em: *Rev Bras Geoc* **22.4**, pp. 481–486.

- Vale, J. A. R. d. 2018. "Caracterização Geoquímica e Geocronológica Do Complexo Granjeiro Sul, Província Borborema, NE Brasil: Implicações Para a Evolução Crustal Paleoarqueana Do Distrito Ferrífero de Curral Novo Do Piauí". Tese de dout. INSTITUTO DE GEOCIÊNCIAS.
- Vasconcelos, A. M. & Gomes, F. 1998. *Geologia e Metalogênese - Folha Iguatu SB.24-Y-B, Programa Levantamentos Geológicos Básicos Do Brasil. Estado Do Ceará, Escala 1:250.000*. CPRM - Serviço Geológico do Brasil.
- Vermeesch, P. 2012. "On the Visualisation of Detrital Age Distributions". Em: *Chemical Geology* **312–313**, pp. 190–194. DOI: [10.1016/j.chemgeo.2012.04.021](https://doi.org/10.1016/j.chemgeo.2012.04.021).
- 2018. "IsoplotR: A Free and Open Toolbox for Geochronology". Em: *Geoscience Frontiers* **9**, pp. 1479–1493. DOI: [10.1016/j.gsf.2018.04.001](https://doi.org/10.1016/j.gsf.2018.04.001).
- Wiedenbeck, M., Allé, P., Corfu, F., Griffin, W. L., Meier, M., Oberli, F., Quadt, A. V., Roddick, J. C. & Spiegel, W. 1995. "Three Natural Zircon Standards for U-Th-Pb, Lu-Hf, Trace Element and Ree Analyses". Em: *Geostandards Newsletter* **19**, pp. 1–23. ISSN: 1751-908X. DOI: [10.1111/j.1751-908X.1995.tb00147.x](https://doi.org/10.1111/j.1751-908X.1995.tb00147.x).
- Wu, F.-Y., Yang, J.-H., Xu, Y.-G., Wilde, S. A. & Walker, R. J. 2019. "Destruction of the North China Craton in the Mesozoic". Em: *Annual Review of Earth and Planetary Sciences* **47**, pp. 173–195. ISSN: 0084-6597, 1545-4495. DOI: [10.1146/annurev-earth-053018-060342](https://doi.org/10.1146/annurev-earth-053018-060342). URL: <https://www.annualreviews.org/doi/10.1146/annurev-earth-053018-060342> (acesso em 08/08/2023).
- Wyborn, L., Heinrich, C. & Jaques, A. 1994. "Australian Proterozoic Mineral Systems: Essential Ingredients and Mappable Criteria". Em: *The AusIMM Annual Conference*. Vol. 1994. AusIMM Darwin, pp. 109–115.
- Yang, C.-X. & Santosh, M. 2020. "Ancient Deep Roots for Mesozoic World-Class Gold Deposits in the North China Craton: An Integrated Genetic Perspective". Em: *Geoscience Frontiers* **11**, pp. 203–214. DOI: [10.1016/j.gsf.2019.03.002](https://doi.org/10.1016/j.gsf.2019.03.002).
- Yang, J.-H., Wu, F.-Y., Wilde, S. A., Belousova, E. & Griffin, W. L. 2008. "Mesozoic Decratonization of the North China Block". Em: *Geology* **36**, p. 467. DOI: [10.1130/g24518a.1](https://doi.org/10.1130/g24518a.1).
- Yang, J.-H., Xu, L., Sun, J.-F., Zeng, Q., Zhao, Y.-N., Wang, H. & Zhu, Y.-S. 2021. "Geodynamics of Decratonization and Related Magmatism and Mineralization in the North China Craton". Em: *Science China Earth Sciences* **64**, pp. 1409–1427. ISSN: 1674-7313, 1869-1897. DOI: [10.1007/s11430-020-9732-6](https://doi.org/10.1007/s11430-020-9732-6). URL: <https://link.springer.com/10.1007/s11430-020-9732-6> (acesso em 23/10/2023).

- Yang, L.-Q., Deng, J., Groves, D. I., Santosh, M., He, W.-Y., Li, N., Zhang, L., Zhang, R.-R. & Zhang, H.-R. 2022. “Metallogenic ‘factories’ and Resultant Highly Anomalous Mineral Endowment on the Craton Margins of China”. Em: *Geoscience Frontiers* **13**.2, p. 101339. DOI: [10.1016/j.gsf.2021.101339](https://doi.org/10.1016/j.gsf.2021.101339).
- Yoshida, M. & Yoshizawa, K. 2021. “Continental Drift with Deep Cratonic Roots”. Em: *Annual Review of Earth and Planetary Sciences* **49**.1, pp. 117–139. DOI: [10.1146/annurev-earth-091620-113028](https://doi.org/10.1146/annurev-earth-091620-113028).
- Yousefi, M., Kreuzer, O. P., Nykänen, V. & Hronsky, J. M. 2019. “Exploration Information Systems – A Proposal for the Future Use of GIS in Mineral Exploration Targeting”. Em: *Ore Geology Reviews* **111**, p. 103005. DOI: [10.1016/j.oregeorev.2019.103005](https://doi.org/10.1016/j.oregeorev.2019.103005).
- Yuan, H. & Romanowicz, B. 2010. “Lithospheric layering in the North American craton”. Em: *Nature* **466**.7310, pp. 1063–1068. ISSN: 1476-4687. DOI: [10.1038/nature09332](https://doi.org/10.1038/nature09332).
- 2018. *Lithospheric discontinuities*. Vol. 239. John Wiley & Sons.

ANEXO I

O autor alega que, dentre os trabalhos que perfazem esta tese, apenas foi submetido o artigo intitulado "*Exploring the Gravimetric and Geochronological Links in Ancient Terranes of the São Francisco Craton and Borborema Province*". Porém ainda em processo de avaliação por parte da revista:

WILEY

[My Submissions](#) Douglas ▾

The screenshot shows the Wiley manuscript submission interface. At the top, there's a button to "Start a new submission for *Terra Nova*" and a "Start submission →" button. Below this, there are filters for "My Submissions", "Journal" (set to "All Journals"), "Submission Status" (set to "All Submission Statuses"), and "Author Role" (set to "Submitting Author Only").

The main content area displays a submission for the journal "Terra Nova" (Research Article). The title of the article is "Exploring the Gravimetric and Geochronological Links in Ancient Terranes of the São Francisco Craton and Borborema Province, NE-Brazil".

Details about the submission include:

- Submission Status: Under Review
- Submitted On: 9 May 2024 by Douglas Martins
- Submission Started: 30 April 2024 by Douglas Martins

A note states: "This submission is under consideration and cannot be edited. Further information will be emailed to you by the journal editorial office." Below this is a "Submission overview →" button.

To the right, there's a sidebar with the heading "Need help choosing a journal? We've put together some resources and tools to help you find the right journal for your research." It includes a "Find a Journal" button.

ANEXO II

O autor alega que, o segundo trabalho utilizado para compor esta tese, apresentado como uma proposta de artigo, intitulado “*São Francisco Paleocontinent Construction, Fragmentation, and Reworking in the Mineral System Evolution of the Curral Novo Iron District*” não foi publicado ou submetido, até o momento, em nenhum meio científico.

ANEXO III

Sample/ Spot	206 (%)	U		Th		Pb		Th/U	Isotopic ratios					Ages (Ma)					Concor. %			
		(mg.g ⁻¹)	2s	(mg.g ⁻¹)	2s	(mg.g ⁻¹)	2s		²⁰⁷ Pb/ ²³⁵ U	2s	²⁰⁶ Pb/ ²³⁸ U	2s	Rho	²⁰⁷ Pb/ ²⁰⁶ Pb	2s	²⁰⁶ Pb/ ²³⁸ U	2s	²⁰⁷ Pb/ ²³⁵ U	2s			
SRND04																				6		
1	1	0.16	40	2	19	1	16	1	0.48	7.550	0.240	0.337	0.010	0.54	2502	34	1869	47	2171	30	75	x
2	2	0.03	115	7	76	4	119	8	0.66	16.440	0.400	0.573	0.015	0.78	2918	14	2901	60	2896	24	99	
3	3.1	0.05	146	6	84	3	86	4	0.57	7.110	0.170	0.296	0.007	0.72	2593	19	1673	37	2113	22	65	x
4	3.2	0.08	64	10	44	8	71	12	0.68	10.680	0.410	0.418	0.016	0.54	2728	37	2251	73	2477	35	83	x
5	4.1	0.05	111	7	74	2	80	3	0.67	7.110	0.190	0.378	0.010	0.60	2204	24	2072	44	2116	23	94	x
6	4.2	0.08	70	2	66	2	74	2	0.94	7.030	0.180	0.371	0.009	0.50	2192	28	2023	41	2099	22	92	x
7	5.1	0.03	180	5	72	2	109	4	0.40	14.810	0.330	0.514	0.013	0.78	2940	16	2669	55	2803	21	91	x
8	5.2	0.02	278	12	158	7	215	9	0.57	13.730	0.230	0.489	0.009	0.61	2863	14	2564	38	2724	16	90	x
9	6	0.02	237	7	153	4	185	5	0.64	13.050	0.290	0.485	0.011	0.67	2791	16	2542	47	2673	21	91	x
10	7	0.03	256	11	66	4	66	4	0.26	9.210	0.210	0.399	0.010	0.65	2563	21	2166	43	2359	21	85	x
11	8	0.02	318	18	196	12	259	17	0.62	14.010	0.310	0.504	0.013	0.75	2852	16	2616	53	2743	20	92	x
12	9	0.02	233	6	91	3	105	4	0.39	14.080	0.270	0.511	0.011	0.67	2829	16	2649	47	2751	18	94	x
13	10	0.04	141	5	76	3	90	4	0.54	13.510	0.320	0.495	0.013	0.75	2828	17	2575	53	2712	22	91	x
14	11.1	0.01	332	11	339	9	521	18	1.02	15.700	0.400	0.560	0.015	0.75	2884	16	2862	63	2848	24	99	
15	12	0.14	55	2	14	1	13	1	0.25	7.870	0.220	0.346	0.009	0.57	2519	24	1903	42	2208	25	76	x
16	13	2.26	212	13	129	8	212	13	0.61	15.030	0.380	0.525	0.014	0.69	2910	20	2710	57	2809	24	93	x
17	14	0.02	249	11	117	5	167	8	0.47	12.560	0.330	0.474	0.013	0.74	2790	21	2480	57	2642	25	89	x
18	15.1	0.02	279	7	183	4	258	6	0.66	12.540	0.290	0.466	0.013	0.72	2797	19	2476	57	2636	21	89	x
19	15.2	0.02	307	21	110	7	196	15	0.36	15.370	0.400	0.543	0.015	0.73	2872	19	2777	64	2829	24	97	
20	16.1	0.02	286	10	125	3	191	7	0.44	13.830	0.290	0.500	0.012	0.71	2836	18	2597	51	2738	20	92	x
21	16.2	0.09	73	4	52	3	80	6	0.71	10.160	0.310	0.456	0.012	0.63	2499	30	2411	52	2449	28	96	
22	17.1	0.02	270	15	192	12	282	18	0.71	15.260	0.340	0.556	0.013	0.75	2832	16	2846	52	2825	21	100	
23	17.2	0.05	123	6	59	3	76	4	0.48	13.730	0.310	0.502	0.012	0.71	2824	20	2621	52	2730	21	93	x
24	18	0.06	72	8	37	4	59	6	0.52	17.770	0.470	0.630	0.017	0.70	2888	21	3133	66	2961	24	108	
25	19	0.04	142	6	65	3	103	4	0.46	15.760	0.380	0.554	0.015	0.71	2881	18	2828	61	2855	23	98	
26	20	0.04	145	5	60	2	92	3	0.42	15.010	0.330	0.530	0.012	0.66	2894	18	2733	51	2811	21	94	x
27	21.1	0.08	68	3	40	2	47	2	0.58	17.590	0.420	0.597	0.016	0.70	2935	20	3014	63	2951	23	103	
28	21.2	0.03	165	4	126	4	178	7	0.76	16.410	0.330	0.558	0.012	0.69	2938	16	2844	48	2898	19	97	
29	22	0.02	270	11	113	5	134	6	0.42	14.140	0.290	0.502	0.012	0.72	2859	16	2631	51	2751	20	92	x
30	23	0.03	247	6	102	3	137	5	0.41	12.980	0.390	0.484	0.015	0.71	2808	25	2531	62	2674	28	90	x
31	24.1	0.03	192	8	109	5	142	7	0.57	13.600	0.330	0.496	0.012	0.71	2802	19	2585	52	2716	22	92	x
32	24.2	0.02	329	16	185	8	256	11	0.56	14.940	0.360	0.529	0.014	0.73	2864	19	2727	56	2797	23	95	x
33	25.1	0.05	148	6	81	3	82	4	0.55	14.530	0.320	0.509	0.011	0.72	2876	15	2645	48	2776	21	92	x

SRND05A																	10				
1	1.1	0.03	199	10	61	3	110	7	0.31	21.240	0.610	0.655	0.022	0.54	3106	25	3223	84	3146	29	104
2	2	1.92	176	15	69	5	173	18	0.39	16.990	0.530	0.545	0.021	0.55	3068	29	2767	87	2918	30	90
3	3	0.05	126	7	25	3	43	4	0.20	14.300	0.430	0.515	0.015	0.72	2878	23	2662	63	2770	29	92
4	4	0.03	214	14	99	6	173	14	0.46	19.250	0.630	0.617	0.025	0.64	3088	25	3037	96	3033	31	98
5	5	0.02	362	22	153	8	280	19	0.42	19.910	0.710	0.618	0.024	0.57	3113	28	3051	93	3071	34	98
6	6	0.02	251	9	109	3	150	6	0.43	20.530	0.470	0.681	0.016	0.69	2971	17	3325	61	3112	22	112
7	7	0.05	122	7	37	2	62	4	0.31	18.620	0.540	0.604	0.022	0.72	3050	23	2995	85	3008	27	98
8	8.1	0.10	70	4	28	2	38	3	0.40	18.590	0.540	0.596	0.020	0.63	3034	23	2967	79	3007	27	98
9	8.2	0.03	281	22	101	8	126	10	0.36	13.180	0.390	0.468	0.013	0.71	2844	23	2485	59	2695	27	87
10	9	0.05	329	12	56	3	50	4	0.17	7.570	0.240	0.281	0.009	0.67	2768	24	1588	43	2166	28	57
11	11	17.50	582	16	106	3	385	15	0.18	4.920	0.140	0.144	0.005	0.61	3134	33	862	28	1800	24	48
12	12	0.04	233	12	104	5	197	12	0.45	18.560	0.570	0.599	0.022	0.58	3043	29	2997	88	3013	29	98
13	13	0.05	172	9	79	4	129	9	0.46	18.320	0.680	0.583	0.023	0.68	3022	27	2906	92	2974	35	96
14	14	0.05	174	6	96	3	157	7	0.55	18.920	0.610	0.595	0.022	0.66	3060	29	2963	88	3024	31	97
15	15	0.03	339	16	140	6	272	14	0.41	19.870	0.650	0.622	0.024	0.67	3060	21	3075	93	3058	31	100
16	16	0.06	160	6	79	3	135	7	0.49	19.110	0.620	0.610	0.024	0.70	3021	27	3030	95	3035	31	100
17	18	0.03	289	16	80	6	129	11	0.28	19.280	0.720	0.639	0.024	0.66	2917	31	3126	92	3016	36	107
18	20	0.06	164	7	92	4	105	7	0.56	18.780	0.550	0.608	0.020	0.72	2989	20	3025	78	3023	27	101
19	22	0.05	207	16	70	4	112	12	0.34	16.060	0.710	0.523	0.024	0.74	2939	29	2658	98	2840	42	90
20	23	0.13	202	16	46	3	43	4	0.23	4.540	0.150	0.206	0.007	0.61	2411	30	1200	38	1736	26	69
SRND05C																	22				
1	1	0.07	131	9	49	3	81	6	0.37	15.300	0.520	0.552	0.019	0.69	2794	26	2803	79	2830	32	100
2	2	0.05	286	21	118	7	122	11	0.41	11.810	0.400	0.406	0.016	0.59	2862	29	2179	72	2572	31	76
3	3	0.16	78	3	39	2	48	3	0.50	13.010	0.460	0.499	0.018	0.72	2685	30	2578	79	2668	34	96
4	4	0.56	23	2	8	1	9	1	0.36	14.440	0.710	0.555	0.029	0.68	2744	50	2770	120	2734	48	101
5	6	0.19	189	6	100	3	37	2	0.53	5.060	0.170	0.204	0.007	0.54	2583	31	1185	36	1815	28	65
6	8	0.37	43	1	13	1	16	1	0.32	15.760	0.610	0.529	0.021	0.61	2868	35	2700	87	2830	37	94
7	9	0.26	64	2	27	1	30	2	0.42	16.110	0.610	0.496	0.019	0.62	3013	34	2575	81	2878	38	85
8	10	0.74	26	1	12	1	11	1	0.45	12.720	0.670	0.425	0.021	0.54	2924	52	2274	94	2629	53	78
9	11	0.16	178	4	63	2	32	2	0.36	7.770	0.250	0.284	0.009	0.65	2713	28	1603	46	2190	29	59
10	12.1	0.13	212	5	118	3	78	4	0.56	8.940	0.280	0.302	0.011	0.71	2839	27	1686	54	2311	28	59
11	12.2	0.68	23	1	6	0	7	1	0.26	12.550	0.660	0.520	0.028	0.53	2631	54	2620	120	2632	50	100
12	13.1	0.13	156	6	99	4	101	6	0.64	11.710	0.390	0.387	0.014	0.74	2903	25	2086	64	2569	31	72
13	13.2	0.30	133	4	79	2	34	2	0.60	3.920	0.150	0.211	0.008	0.55	2066	38	1224	39	1596	30	59
14	14.1	0.10	244	7	97	3	103	5	0.40	10.220	0.310	0.335	0.012	0.74	2875	23	1842	57	2441	28	64
15	14.2	0.37	109	3	64	2	20	2	0.59	6.120	0.280	0.215	0.010	0.70	2781	34	1243	50	1963	39	45
16	15.1	0.24	123	4	95	4	67	4	0.77	11.580	0.460	0.354	0.015	0.66	3023	32	1933	69	2538	39	64
17	15.2	0.09	214	13	107	5	182	12	0.50	21.040	0.900	0.643	0.031	0.71	3048	32	3140	120	3122	41	103

18	16.1	0.12	345	10	380	11	169	9	1.10	12.460	0.450	0.391	0.014	0.72	2959	24	2106	65	2627	35	71	
19	14	0.33	418	14	-372	15	135	11	-0.89	11.250	0.450	0.375	0.015	0.60	2913	36	2031	68	2516	37	70	
20	18	0.13	3122	87	-304	11	998	56	-0.10	12.760	0.380	0.411	0.014	0.65	2980	23	2212	63	2652	29	74	
21	19	0.17	-25300	1100	-268	8	-1750	100	0.01	9.440	0.330	0.295	0.010	0.65	2938	31	1657	51	2364	32	56	
22	20	0.25	4770	180	-253	8	-1264	82	-0.05	11.040	0.450	0.362	0.015	0.72	2939	30	1970	74	2513	39	67	
23	21	0.22	605	17	-1346	77	530	29	-2.22	13.840	0.430	0.414	0.015	0.57	3098	28	2218	67	2739	30	72	
24	22	0.29	188	6	166	6	102	6	0.88	11.650	0.410	0.380	0.014	0.65	2929	30	2049	65	2567	33	70	
25	23	0.04	195	8	92	3	145	6	0.47	20.600	0.540	0.631	0.019	0.63	3064	22	3118	72	3109	25	102	
26	24	0.02	396	15	80	2	144	6	0.20	18.580	0.620	0.598	0.025	0.65	3044	32	2964	99	3026	32	97	
27	25	0.14	47	2	20	1	22	2	0.43	15.520	0.470	0.545	0.019	0.63	2802	33	2775	78	2839	29	99	
28	26	0.02	313	17	152	9	292	18	0.49	20.300	0.700	0.625	0.027	0.62	3122	29	3080	110	3081	33	99	
29	27.1	0.06	114	7	43	2	46	3	0.38	12.010	0.280	0.498	0.012	0.69	2568	20	2597	51	2593	22	101	
30	28	0.03	161	8	57	3	102	6	0.35	19.540	0.460	0.617	0.018	0.65	3047	21	3060	71	3053	23	100	
31	29.1	3.13	203	7	63	2	92	4	0.31	12.410	0.410	0.405	0.015	0.79	3010	22	2171	67	2624	30	72	
32	30.1	0.06	89	5	51	2	62	4	0.58	20.010	0.440	0.619	0.015	0.70	3056	19	3095	58	3084	21	101	
33	30.2	0.02	286	8	216	6	395	14	0.76	20.010	0.540	0.623	0.020	0.65	3086	22	3123	77	3088	26	101	
34	31	0.13	299	11	53	2	57	4	0.18	2.469	0.089	0.100	0.004	0.65	2631	28	612	20	1252	26	49	
35	32	0.04	182	9	69	3	132	7	0.38	20.260	0.560	0.624	0.020	0.69	3094	24	3105	77	3091	27	100	
36	33	0.04	180	8	61	3	110	6	0.34	18.950	0.480	0.605	0.017	0.71	3048	21	3033	70	3032	24	100	
37	34.1	0.02	360	23	160	11	331	26	0.44	20.600	0.490	0.626	0.017	0.67	3098	20	3102	65	3108	23	100	
38	36	0.05	137	14	52	6	79	10	0.38	18.050	0.520	0.642	0.019	0.67	2861	26	3176	73	2979	28	111	
39	37.1	0.03	262	19	108	8	207	17	0.41	18.460	0.470	0.610	0.018	0.65	3010	19	3042	71	3003	24	101	
40	38	0.02	290	19	110	8	194	18	0.38	13.310	0.430	0.504	0.019	0.66	2787	28	2602	80	2696	31	93	
41	39.1	0.02	347	18	238	12	428	26	0.69	19.330	0.560	0.627	0.020	0.66	3012	24	3116	79	3034	28	103	
42	39.2	0.02	244	13	158	9	198	12	0.65	17.520	0.440	0.593	0.014	0.76	2925	17	2992	57	2960	24	102	
43	41	0.02	268	11	152	6	301	13	0.57	20.090	0.530	0.623	0.018	0.72	3079	19	3093	71	3082	25	100	
44	42	0.02	232	11	123	7	214	12	0.53	20.860	0.510	0.637	0.018	0.73	3089	18	3161	69	3124	23	102	
45	44	0.05	111	6	54	3	74	4	0.49	19.190	0.440	0.629	0.015	0.73	2985	17	3135	58	3043	22	105	
46	45	0.01	466	26	317	15	638	36	0.68	20.980	0.500	0.645	0.018	0.73	3112	17	3190	69	3127	23	103	
47	46	0.04	184	13	90	8	119	11	0.49	16.180	0.390	0.576	0.014	0.38	2846	23	2934	58	2883	24	103	
SRN-D-16																			21			
1	1.1	0.14	288	8	16	1	9	1	0.06	3.740	0.120	0.177	0.006	0.61	2391	30	1045	33	1579	27	66	x
2	2.1	0.30	58	5	39	3	47	4	0.68	6.770	0.300	0.395	0.017	0.43	2024	48	2134	77	2059	40	105	
3	2.2	0.36	49	5	74	6	78	8	1.51	6.830	0.300	0.394	0.016	0.39	2078	49	2113	75	2082	40	102	
4	3	0.13	142	3	61	2	63	3	0.43	10.730	0.300	0.392	0.013	0.59	2799	27	2122	58	2497	26	76	x
5	4	0.13	132	4	30	1	35	2	0.23	11.170	0.340	0.410	0.014	0.62	2796	28	2197	63	2529	29	79	x
6	5	0.21	123	3	110	2	81	4	0.89	3.840	0.120	0.274	0.008	0.51	1625	34	1551	41	1593	26	95	
7	6.1	0.13	132	4	145	4	155	8	1.10	12.930	0.360	0.405	0.014	0.66	3016	26	2176	62	2669	26	72	x
8	6.2	0.18	80	2	35	1	46	3	0.44	14.430	0.460	0.483	0.016	0.58	2945	31	2510	71	2766	31	85	x

9	6.3	0.28	54	2	24	1	25	2	0.45	13.230	0.420	0.480	0.015	0.46	2801	31	2516	62	2672	30	90	
10	7	0.10	335	10	273	9	71	3	0.82	4.670	0.140	0.215	0.007	0.65	2406	30	1245	38	1760	24	52	x
11	8.1	5.42	187	7	61	2	114	6	0.32	12.480	0.360	0.383	0.012	0.64	3063	24	2095	55	2632	27	68	x
12	9.1	0.08	203	12	108	5	145	10	0.53	12.660	0.390	0.441	0.015	0.59	2858	26	2339	68	2653	28	82	x
13	9.2	0.24	175	7	68	4	33	3	0.39	2.826	0.097	0.175	0.005	0.46	1930	40	1038	29	1359	26	76	x
14	11.1	0.09	139	11	97	7	148	12	0.70	16.710	0.500	0.559	0.017	0.60	2923	24	2852	70	2914	28	98	
15	11.2	0.13	135	3	43	1	47	2	0.32	11.660	0.320	0.402	0.011	0.60	2865	25	2167	53	2562	25	76	x
16	12.1	0.07	172	14	174	13	282	24	1.01	16.170	0.470	0.563	0.020	0.63	2876	29	2857	79	2877	28	99	
17	12.2	0.17	104	4	101	3	100	4	0.97	12.010	0.360	0.397	0.012	0.54	2923	29	2143	56	2590	27	73	x
18	12.3	0.12	197	5	91	2	83	3	0.46	6.810	0.190	0.298	0.009	0.58	2481	26	1671	44	2073	25	67	x
19	13.1	0.11	173	8	208	8	230	14	1.20	7.100	0.180	0.371	0.009	0.61	2166	24	2018	43	2117	22	93	
20	13.2	0.15	263	7	54	1	24	2	0.20	2.660	0.076	0.175	0.005	0.56	1759	30	1035	27	1309	21	79	x
21	14.1	0.14	105	6	80	5	77	8	0.76	11.360	0.350	0.486	0.014	0.61	2517	29	2524	61	2537	29	100	
22	14.2	0.07	285	7	189	5	163	6	0.66	5.470	0.150	0.321	0.009	0.58	1980	26	1788	43	1884	24	90	
23	14.3	0.09	230	5	151	3	136	5	0.66	5.850	0.140	0.324	0.009	0.51	2067	29	1805	46	1944	20	87	x
24	15.1	0.17	245	6	127	3	81	3	0.52	3.690	0.100	0.158	0.005	0.64	2492	28	940	26	1560	22	60	x
25	15.2	0.47	202	5	81	3	26	2	0.40	1.181	0.048	0.068	0.002	0.18	2069	53	426	14	783	22	54	x
26	16	0.32	50	2	29	1	33	2	0.58	8.170	0.250	0.420	0.012	0.48	2243	33	2243	53	2225	26	100	
27	17.1	0.04	407	21	213	9	283	16	0.52	13.860	0.410	0.447	0.015	0.69	3004	22	2371	69	2714	27	79	x
28	17.2	0.05	232	14	103	6	178	11	0.45	19.110	0.510	0.590	0.018	0.64	3057	23	2971	74	3032	25	97	
29	18.1	0.03	576	25	326	13	382	19	0.57	6.820	0.160	0.389	0.010	0.66	2013	22	2109	48	2083	20	105	
30	18.2	0.03	604	29	284	13	309	19	0.47	6.100	0.150	0.363	0.012	0.58	2011	26	1984	54	1991	22	99	
31	19.1	0.10	167	6	177	5	190	8	1.06	6.960	0.210	0.383	0.011	0.52	2101	27	2080	52	2103	26	99	
32	19.2	0.34	51	2	48	2	47	3	0.94	6.760	0.220	0.369	0.013	0.44	2137	40	2005	59	2071	29	94	
33	21.1	0.05	254	11	208	11	290	15	0.82	14.670	0.350	0.505	0.014	0.69	2885	20	2617	60	2782	22	91	
34	21.2	0.12	98	3	32	1	44	2	0.32	14.480	0.420	0.517	0.015	0.54	2787	29	2692	65	2782	28	97	
35	22	0.18	97	3	32	1	32	2	0.32	6.090	0.180	0.363	0.012	0.59	1976	30	1996	57	1978	25	101	
36	23.1	0.10	183	14	128	10	138	12	0.70	5.750	0.180	0.328	0.011	0.63	2037	32	1824	56	1929	27	90	
37	23.2	0.05	344	22	460	25	517	32	1.34	6.650	0.180	0.382	0.012	0.61	2028	30	2070	57	2056	24	102	
38	24.1	0.51	68	2	28	1	46	3	0.41	5.550	0.200	0.185	0.007	0.40	2975	45	1089	40	1902	31	57	x
39	25.1	0.14	232	5	63	2	75	3	0.27	3.860	0.120	0.193	0.006	0.59	2214	30	1134	31	1601	23	71	x
40	25.2	0.19	212	5	24	1	35	2	0.11	2.866	0.073	0.152	0.004	0.47	2148	30	915	21	1370	19	67	x
41	27.1	0.15	247	7	132	4	96	4	0.53	3.570	0.100	0.165	0.005	0.56	2374	30	984	27	1533	23	64	x
42	27.2	1.13	55	2	7	0	15	1	0.13	2.590	0.120	0.104	0.005	0.30	2714	61	638	29	1291	34	49	x
43	28.1	0.19	86	3	43	2	44	2	0.50	6.920	0.240	0.385	0.014	0.59	2147	38	2075	65	2114	33	97	
44	29	0.17	196	7	47	2	46	3	0.24	3.870	0.120	0.182	0.006	0.60	2354	34	1078	32	1592	25	68	x
45	30	0.19	250	6	30	1	25	2	0.12	1.869	0.062	0.131	0.004	0.49	1668	34	791	24	1066	22	74	x
46	31.1	0.14	102	7	36	2	50	4	0.35	10.800	0.410	0.461	0.018	0.69	2559	31	2410	77	2492	35	94	
47	31.2	0.20	112	3	8	0	7	1	0.07	4.850	0.160	0.273	0.008	0.57	2029	34	1553	42	1782	28	77	x

48	32.1	0.13	127	4	76	2	85	4	0.60	10.050	0.300	0.361	0.011	0.61	2777	27	1975	52	2428	27	71	x
49	32.2	0.15	278	9	9	0	33	2	0.03	2.562	0.078	0.149	0.005	0.52	1966	35	892	28	1286	22	69	x
SMD011																						
1	z1	0.09	43	2	29	2	49	3	0.67	26.110	0.630	0.665	0.017	0.63	3420	20	3279	64	3350	23	96	
2	z2	0.01	314	25	172	11	299	19	0.55	30.310	0.620	0.758	0.016	0.70	3427	14	3652	59	3492	20	107	
3	z3	0.01	274	10	218	7	364	11	0.80	30.290	0.600	0.761	0.016	0.67	3419	15	3646	59	3494	20	107	
4	z4	0.06	67	2	39	1	62	2	0.59	25.670	0.540	0.653	0.014	0.61	3404	16	3226	55	3323	21	95	
5	z5	0.05	74	4	72	4	123	7	0.96	28.120	0.690	0.702	0.020	0.69	3449	18	3409	75	3414	24	99	
6	z6	0.02	161	7	104	3	161	5	0.64	27.590	0.480	0.695	0.013	0.66	3417	13	3385	48	3398	17	99	
7	z7	0.03	128	3	119	3	158	4	0.93	26.460	0.470	0.667	0.013	0.58	3429	15	3302	51	3357	18	96	
8	z8	0.09	43	1	28	1	46	2	0.66	27.630	0.520	0.693	0.014	0.63	3437	14	3393	53	3399	18	99	
9	z9	0.02	194	11	229	17	355	24	1.18	27.780	0.560	0.701	0.014	0.72	3406	12	3423	53	3407	19	100	
10	z10	0.02	194	4	133	3	234	6	0.68	29.570	0.670	0.746	0.017	0.70	3402	14	3581	62	3471	22	105	
11	z11	0.04	101	2	58	2	91	3	0.57	24.500	0.570	0.635	0.015	0.56	3362	21	3154	59	3286	23	94	
12	z12	0.02	207	7	90	2	129	3	0.44	26.500	0.480	0.676	0.013	0.65	3360	14	3326	51	3358	18	99	
13	z13	0.06	70	3	67	2	105	4	0.95	27.440	0.500	0.694	0.013	0.63	3375	15	3392	50	3392	18	101	
14	z14	0.01	418	17	259	7	386	9	0.62	28.090	0.600	0.710	0.015	0.65	3366	15	3458	58	3414	21	103	
15	z15	0.02	208	11	202	11	315	17	0.97	28.360	0.570	0.720	0.015	0.65	3384	15	3492	55	3427	20	103	
16	z16	0.02	159	5	130	4	207	6	0.82	28.220	0.530	0.710	0.014	0.65	3378	14	3455	54	3424	19	102	
17	z17	0.03	120	3	84	2	140	4	0.70	29.180	0.640	0.729	0.016	0.68	3380	15	3527	61	3458	22	104	
18	z18	0.03	122	3	93	3	158	5	0.76	28.240	0.630	0.716	0.018	0.68	3359	16	3466	67	3419	21	103	
19	z19	0.04	98	2	95	3	153	5	0.96	28.640	0.560	0.729	0.015	0.62	3346	15	3530	55	3434	19	105	
20	z20	0.09	48	2	44	2	71	3	0.92	27.490	0.650	0.696	0.016	0.69	3372	18	3382	61	3394	23	100	
21	z21	0.02	180	8	170	7	289	12	0.95	28.190	0.500	0.698	0.013	0.66	3395	13	3411	50	3423	17	100	
22	z22	0.05	82	5	57	4	93	6	0.69	27.630	0.550	0.701	0.015	0.57	3361	16	3426	57	3402	19	102	
23	z23	0.02	178	10	81	9	134	15	0.46	27.370	0.500	0.703	0.013	0.65	3347	14	3426	50	3393	18	102	
24	z24	0.05	73	2	67	3	112	4	0.91	28.310	0.590	0.714	0.015	0.63	3390	15	3478	58	3423	21	103	
25	z25	0.08	53	3	26	2	43	3	0.48	24.840	0.570	0.650	0.016	0.62	3333	19	3218	63	3297	23	97	
26	z26	0.06	77	5	40	2	68	4	0.52	27.630	0.510	0.698	0.014	0.64	3418	15	3408	53	3402	18	100	
27	z27	0.02	235	6	162	3	275	5	0.69	28.040	0.500	0.700	0.013	0.66	3416	12	3418	49	3420	17	100	
28	z28	0.03	140	3	83	2	141	3	0.59	28.200	0.570	0.707	0.015	0.63	3422	15	3466	57	3427	20	101	
29	z29	0.09	49	2	43	1	75	3	0.87	27.970	0.720	0.709	0.019	0.63	3422	21	3456	71	3411	25	101	
30	z30	0.02	179	9	155	9	261	14	0.87	27.400	0.580	0.695	0.017	0.63	3404	17	3403	65	3397	21	100	
31	z31	0.06	75	2	43	1	68	2	0.57	27.940	0.600	0.696	0.017	0.61	3424	19	3397	62	3414	21	99	
32	z32	0.07	66	3	34	1	57	3	0.51	25.370	0.560	0.650	0.015	0.63	3372	18	3210	57	3318	22	95	
33	z33	0.15	29	1	16	1	27	1	0.56	27.500	0.600	0.697	0.017	0.60	3398	19	3386	64	3396	21	100	
34	z34	0.03	136	7	83	4	139	7	0.62	27.970	0.610	0.707	0.017	0.70	3390	16	3451	65	3419	22	102	
35	z35	0.02	413	37	155	13	235	18	0.38	17.730	0.390	0.482	0.011	0.66	3262	17	2536	48	2972	22	78	
36	z36	0.05	99	4	69	2	112	4	0.70	27.720	0.490	0.700	0.014	0.61	3392	14	3405	54	3400	17	100	

37	z37	0.04	126	3	71	2	116	3	0.57	21.140	0.510	0.588	0.015	0.64	3228	18	2973	60	3137	24	92
38	z38	0.03	163	4	88	2	181	5	0.54	30.640	0.800	0.752	0.020	0.72	3398	18	3594	71	3499	25	106
39	z39	0.02	214	8	6	0	12	1	0.03	24.060	0.520	0.636	0.014	0.69	3281	16	3183	56	3264	21	97
40	z40	0.02	194	14	84	6	144	10	0.43	29.270	0.550	0.741	0.016	0.68	3396	13	3555	57	3464	18	105
41	z41	0.04	133	9	64	4	101	6	0.48	23.460	0.470	0.642	0.014	0.67	3256	16	3184	53	3248	19	98
42	z42	0.02	256	11	79	5	127	8	0.31	27.080	0.450	0.691	0.012	0.63	3388	13	3373	47	3384	16	100
43	z43	0.07	62	3	58	3	92	4	0.94	27.940	0.660	0.704	0.017	0.62	3411	18	3432	65	3414	23	101
44	z44	0.04	113	5	54	3	99	5	0.48	28.510	0.490	0.728	0.013	0.60	3388	14	3528	48	3429	17	104
45	z45	0.03	196	16	39	3	56	5	0.20	19.910	0.380	0.554	0.011	0.61	3261	16	2829	47	3088	18	87
46	z46	0.03	174	8	174	8	276	13	1.00	27.750	0.660	0.717	0.018	0.70	3386	17	3469	66	3402	23	102
47	z47	0.04	111	5	64	3	106	5	0.57	28.120	0.590	0.706	0.017	0.63	3419	17	3429	64	3420	20	100
48	z48	0.05	101	4	65	3	123	6	0.64	29.330	0.530	0.743	0.014	0.67	3408	15	3569	52	3463	18	105
49	z49	0.02	222	9	269	14	427	22	1.21	27.960	0.510	0.710	0.015	0.65	3392	14	3460	56	3414	18	102
50	z50	0.02	205	4	176	4	280	6	0.86	28.090	0.490	0.700	0.012	0.67	3404	12	3424	45	3411	17	101
51	z51	0.02	234	8	129	4	213	6	0.55	28.430	0.630	0.713	0.015	0.67	3380	15	3464	59	3434	22	102

RPE27

7

1	z1	0.01	310	12	216	10	288	12	0.70	13.400	0.140	0.520	0.006	0.69	2715	9	2696	26	2707	10	99
2	z2	0.01	371	10	303	7	387	9	0.82	12.400	0.150	0.482	0.006	0.70	2724	10	2537	27	2635	11	93
3	z3	0.01	754	18	684	11	1019	20	0.91	12.820	0.160	0.497	0.007	0.73	2709	10	2599	32	2661	12	96
4	z4	0.01	521	10	444	10	493	11	0.85	11.830	0.140	0.466	0.006	0.73	2695	9	2466	26	2590	11	92
5	z5	0.01	356	10	298	7	399	10	0.84	12.850	0.150	0.502	0.007	0.65	2708	11	2617	29	2672	11	97
6	z6	0.02	193	5	169	3	236	6	0.87	12.860	0.190	0.500	0.007	0.71	2730	11	2612	32	2670	14	96
7	z7	0.02	196	6	155	4	199	5	0.79	12.260	0.140	0.479	0.006	0.66	2717	10	2524	26	2625	11	93
8	z8	0.04	116	2	57	1	93	3	0.49	12.280	0.190	0.462	0.008	0.58	2772	15	2446	35	2626	15	88
9	z9	0.01	437	17	330	10	461	17	0.76	12.620	0.120	0.485	0.005	0.67	2723	8	2552	22	2651	9	94
10	z10	0.01	357	13	217	6	306	9	0.61	10.350	0.150	0.413	0.007	0.68	2670	14	2226	30	2468	14	83
11	z11	0.02	175	3	115	2	173	3	0.66	12.560	0.180	0.486	0.008	0.69	2725	12	2550	34	2645	14	94
12	z12	0.03	249	7	93	2	96	2	0.37	5.889	0.086	0.270	0.004	0.64	2439	12	1540	19	1959	12	63
13	z13	0.05	80	3	52	2	71	3	0.66	12.610	0.220	0.491	0.008	0.66	2716	15	2573	35	2642	16	95
14	z14	0.01	635	15	435	12	649	15	0.69	13.050	0.140	0.498	0.006	0.69	2734	9	2604	27	2680	10	95
15	z15	0.03	109	2	72	2	101	3	0.66	13.400	0.170	0.524	0.008	0.60	2733	11	2712	32	2704	12	99
16	z16	0.04	97	2	64	1	93	2	0.66	13.210	0.140	0.514	0.006	0.53	2729	10	2671	25	2692	10	98
17	z17	0.01	326	11	264	10	367	13	0.81	12.680	0.170	0.503	0.007	0.74	2676	9	2622	28	2656	13	98
18	z18	0.01	1383	39	866	15	756	19	0.63	5.339	0.069	0.263	0.004	0.70	2317	12	1505	18	1874	11	65
19	z19	0.02	219	5	120	2	136	3	0.55	11.620	0.140	0.462	0.006	0.64	2686	11	2449	27	2577	12	91
20	z20	0.01	320	8	197	4	283	7	0.61	11.740	0.160	0.464	0.007	0.63	2682	10	2453	31	2582	13	91
21	z21	0.02	234	8	194	6	248	8	0.83	13.060	0.140	0.507	0.006	0.68	2726	9	2636	27	2685	10	97
22	z22	0.02	285	7	207	4	220	6	0.73	10.090	0.120	0.407	0.005	0.70	2654	10	2197	22	2442	12	83
23	z23	0.01	286	4	231	3	308	5	0.81	13.210	0.150	0.519	0.006	0.62	2701	11	2693	27	2693	11	100

24	z24	0.02	214	6	109	2	162	4	0.51	13.260	0.170	0.519	0.008	0.68	2719	11	2687	32	2699	12	99		
25	z25	0.02	217	8	176	6	243	8	0.81	13.280	0.140	0.521	0.007	0.71	2701	9	2700	28	2702	10	100		
26	z26	0.04	172	5	65	1	56	2	0.38	6.472	0.096	0.287	0.005	0.60	2492	14	1620	24	2039	13	65		
27	z27	0.04	90	3	52	2	71	3	0.57	13.290	0.170	0.520	0.007	0.63	2712	11	2699	29	2700	12	100		
28	z28	0.01	811	40	596	29	571	34	0.73	7.710	0.099	0.335	0.005	0.67	2521	11	1861	21	2196	11	74		
29	z29	0.03	126	4	84	2	109	2	0.66	13.410	0.150	0.523	0.006	0.57	2704	10	2711	26	2709	11	100		
30	z30	0.01	375	15	248	10	357	16	0.66	13.540	0.150	0.530	0.006	0.70	2700	9	2742	25	2720	10	102		
31	z31	0.01	1073	16	692	13	692	8	0.64	7.370	0.110	0.328	0.005	0.73	2476	11	1825	22	2158	13	74		
32	z32	0.04	123	4	97	3	105	3	0.79	11.280	0.170	0.441	0.007	0.70	2692	11	2353	30	2545	14	87		
33	z33	1.31	235	12	236	14	356	23	1.00	14.600	0.180	0.550	0.007	0.66	2761	11	2824	30	2792	12	102		
RPW04																							12
1	z1	0.02	320	7	157	6	222	7	0.49	12.920	0.280	0.511	0.012	0.70	2681	17	2654	52	2674	20	99		
2	z2	0.05	132	2	85	2	114	5	0.65	12.800	0.230	0.510	0.011	0.63	2696	16	2653	46	2666	17	98		
3	z3	0.07	217	4	176	4	76	3	0.81	5.260	0.120	0.225	0.006	0.64	2583	19	1302	31	1862	18	50		
4	z4	0.03	238	6	99	3	149	6	0.42	13.000	0.220	0.518	0.010	0.65	2668	13	2686	42	2678	16	101		
5	z5	0.04	212	7	73	2	105	4	0.34	12.700	0.250	0.510	0.011	0.53	2657	18	2651	46	2651	18	100		
6	z6	0.03	260	9	306	10	428	15	1.18	13.050	0.220	0.519	0.009	0.60	2686	15	2686	39	2683	16	100		
7	z7	0.03	231	11	160	6	253	9	0.69	13.440	0.220	0.537	0.009	0.58	2664	14	2768	39	2710	15	104		
8	z8	0.04	221	4	91	2	107	3	0.41	10.210	0.250	0.410	0.010	0.59	2655	22	2208	47	2442	22	83		
9	z9	0.02	513	19	310	11	430	16	0.60	13.060	0.220	0.517	0.009	0.62	2672	15	2686	39	2681	16	101		
10	z10	0.04	323	8	350	9	226	6	1.08	6.370	0.130	0.286	0.006	0.65	2475	18	1615	31	2028	18	65		
11	z11	0.05	174	4	97	3	95	3	0.55	11.430	0.210	0.468	0.009	0.58	2634	18	2471	37	2560	18	94		
12	z12	0.04	195	4	521	11	737	18	2.67	11.260	0.270	0.464	0.013	0.63	2621	21	2454	56	2543	22	94		
13	z13	0.04	203	10	135	10	131	9	0.67	11.770	0.200	0.483	0.009	0.57	2631	14	2544	38	2585	15	97		
14	z14	0.10	86	2	42	1	59	2	0.48	11.370	0.280	0.469	0.011	0.63	2650	21	2466	49	2548	23	93		
15	z15	0.03	256	8	134	5	209	8	0.52	12.990	0.200	0.512	0.009	0.61	2690	14	2659	36	2673	14	99		
16	z16	0.04	202	9	88	5	120	7	0.43	12.360	0.210	0.500	0.009	0.54	2659	16	2610	39	2629	16	98		
17	z17	0.02	425	12	573	18	756	27	1.35	12.810	0.180	0.510	0.008	0.56	2667	16	2652	35	2665	13	99		
18	z18	0.02	490	12	232	15	313	20	0.47	12.540	0.260	0.505	0.011	0.63	2677	16	2625	48	2640	20	98		
19	z19	0.03	250	9	95	2	137	4	0.38	12.370	0.220	0.496	0.010	0.61	2665	16	2594	43	2637	16	97		
20	z20	0.01	506	13	478	17	735	25	0.94	13.250	0.260	0.544	0.013	0.63	2610	19	2794	55	2693	19	107		
21	z21	0.03	386	8	329	13	157	7	0.85	7.650	0.150	0.337	0.007	0.55	2516	18	1869	32	2195	17	74		
22	z22	0.05	167	8	117	7	145	8	0.70	13.180	0.220	0.520	0.009	0.50	2694	16	2695	39	2686	16	100		
23	z23	0.05	146	4	81	3	108	3	0.55	12.800	0.230	0.514	0.010	0.58	2675	16	2673	41	2660	16	100		
24	z24	0.03	251	10	101	3	129	3	0.40	11.360	0.200	0.461	0.009	0.58	2645	16	2441	40	2551	16	92		
25	z25	0.02	305	20	195	15	283	21	0.64	12.800	0.180	0.514	0.008	0.62	2669	13	2664	35	2664	13	100		
26	z26	0.03	294	14	240	13	221	14	0.82	10.710	0.180	0.456	0.008	0.60	2556	15	2424	36	2493	16	95		
27	z27	0.03	289	14	69	1	94	3	0.24	12.090	0.210	0.491	0.009	0.55	2634	18	2570	37	2610	17	98		
28	z28	0.03	276	6	67	1	97	3	0.24	12.310	0.220	0.486	0.011	0.63	2693	17	2556	46	2630	16	95		

29	z29	0.03	296	5	94	5	133	7	0.32	12.470	0.260	0.501	0.011	0.69	2673	16	2612	48	2646	19	98	
RPB22																						53
1	z1	0.03	83	3	68	2	66	2	0.82	6.000	0.088	0.363	0.006	0.57	2003	16	1991	28	1974	13	99	
2	z2	0.02	114	4	111	4	95	4	0.97	4.895	0.081	0.327	0.006	0.59	1823	18	1826	27	1799	14	100	
3	z3	0.90	257	6	87	3	86	3	0.34	5.910	0.083	0.351	0.005	0.59	2017	14	1936	26	1964	12	96	
4	z4	2.02	134	6	117	5	153	7	0.88	8.220	0.170	0.416	0.009	0.64	2304	19	2243	40	2246	18	97	
5	z5	0.01	189	7	47	2	42	2	0.25	5.661	0.079	0.347	0.005	0.65	1960	14	1919	25	1924	12	98	
6	z6	0.02	164	9	118	5	110	5	0.72	4.987	0.076	0.329	0.005	0.64	1817	15	1831	26	1813	13	101	
7	z7	0.04	58	2	58	2	58	2	1.00	5.950	0.100	0.356	0.006	0.57	2006	18	1963	30	1965	15	98	
8	z8	0.04	58	3	36	1	35	1	0.61	7.550	0.120	0.405	0.007	0.54	2206	17	2186	33	2174	15	99	
9	z9	0.03	98	3	49	2	43	2	0.50	6.644	0.099	0.376	0.006	0.63	2082	14	2054	28	2063	13	99	
10	z10	0.05	48	2	37	1	33	1	0.77	7.110	0.120	0.387	0.007	0.60	2167	17	2110	34	2120	15	97	
11	z11	0.01	208	8	210	6	228	8	1.01	10.340	0.140	0.463	0.007	0.66	2498	13	2444	32	2462	12	98	
12	z12	0.03	93	5	75	4	58	4	0.81	4.789	0.078	0.316	0.005	0.56	1820	16	1772	27	1786	13	97	
13	z13	0.03	115	5	85	3	68	3	0.74	4.661	0.085	0.316	0.006	0.62	1790	17	1766	29	1759	15	99	
14	z14	0.02	129	2	98	2	86	2	0.76	5.260	0.081	0.334	0.006	0.68	1889	15	1852	26	1857	13	98	
15	z15	0.04	99	4	50	2	33	1	0.51	2.970	0.059	0.242	0.005	0.57	1450	19	1397	24	1396	15	96	
16	z16	0.03	106	2	83	2	80	2	0.78	5.273	0.096	0.331	0.007	0.72	1912	16	1837	31	1862	15	96	
17	z17	1.63	265	10	99	2	87	2	0.37	4.221	0.085	0.239	0.005	0.65	2073	20	1380	28	1676	16	67	x
18	z18	0.02	125	3	82	2	78	2	0.66	5.147	0.078	0.331	0.005	0.60	1829	15	1838	26	1840	13	100	
19	z19	0.07	50	2	34	1	27	1	0.68	3.738	0.082	0.275	0.006	0.56	1593	23	1563	28	1579	17	98	
20	z20	0.04	65	3	66	4	66	4	1.01	5.166	0.097	0.329	0.006	0.53	1847	19	1829	31	1848	16	99	
21	z21	3.10	73	3	75	4	41	2	1.03	5.610	0.140	0.267	0.006	0.68	2348	19	1523	31	1909	21	65	x
22	z22	0.02	133	4	119	3	122	3	0.89	6.450	0.100	0.368	0.006	0.58	2045	16	2018	30	2039	14	99	
23	z23	0.04	100	3	49	1	40	1	0.49	3.717	0.076	0.276	0.006	0.61	1581	22	1573	30	1571	16	99	
24	z24	0.02	186	8	133	5	132	5	0.71	5.920	0.078	0.355	0.005	0.59	1955	13	1956	25	1961	11	100	
25	z25	0.02	179	7	71	2	76	3	0.40	6.080	0.130	0.358	0.008	0.64	1997	20	1973	38	1989	18	99	
26	z26	3.07	81	4	51	2	55	3	0.64	5.680	0.100	0.286	0.006	0.49	2271	23	1618	28	1926	16	71	x
27	z27	0.01	207	7	81	3	98	3	0.39	6.830	0.120	0.365	0.007	0.63	2178	18	2008	35	2086	15	92	
28	z28	0.04	47	2	21	1	36	2	0.45	18.970	0.360	0.568	0.014	0.64	3135	18	2888	55	3038	19	92	
29	z29	0.03	99	3	31	1	41	1	0.31	5.910	0.140	0.319	0.008	0.68	2162	19	1790	39	1960	19	83	x
30	z30	0.13	34	1	22	1	16	1	0.64	3.083	0.080	0.217	0.005	0.48	1738	30	1261	27	1426	20	73	x
31	z31	0.04	71	3	30	1	33	1	0.43	5.584	0.097	0.348	0.006	0.63	1934	16	1922	29	1921	15	99	
32	z32	4.15	82	2	30	1	44	1	0.37	4.990	0.120	0.249	0.006	0.54	2316	29	1429	33	1809	21	62	x
33	z33	0.05	62	5	29	1	31	2	0.47	5.520	0.110	0.354	0.007	0.58	1868	21	1943	34	1891	17	104	
34	z34	0.02	110	5	62	2	94	4	0.56	12.840	0.180	0.515	0.008	0.65	2699	13	2670	36	2667	13	99	
35	z35	0.01	932	24	301	6	353	10	0.32	7.040	0.110	0.375	0.007	0.62	2169	16	2054	32	2115	14	95	
36	z36	0.07	212	4	159	6	164	5	0.75	5.110	0.120	0.263	0.008	0.59	2255	25	1500	38	1837	21	67	x
37	z37	0.09	120	3	71	2	67	3	0.59	5.500	0.110	0.341	0.007	0.50	1948	23	1887	34	1896	17	97	

38	z38	0.10	100	4	32	1	35	2	0.32	6.670	0.140	0.380	0.008	0.58	2077	22	2071	38	2069	18	100		
39	z39	0.04	249	7	149	2	154	4	0.60	5.761	0.088	0.345	0.006	0.59	1981	16	1909	26	1936	13	96		
40	z40	0.09	120	3	124	2	120	3	1.03	4.790	0.110	0.319	0.008	0.43	1804	25	1785	36	1778	19	99		
41	z41	0.10	111	4	45	2	42	2	0.41	4.830	0.120	0.307	0.008	0.54	1892	22	1719	37	1788	21	91		
42	z42	0.06	176	7	123	5	120	5	0.70	5.036	0.089	0.326	0.006	0.44	1830	21	1814	28	1824	15	99		
43	z43	0.21	70	2	28	1	25	1	0.41	3.980	0.120	0.271	0.007	0.41	1779	34	1542	34	1623	24	87	x	
44	z44	0.08	103	3	93	2	133	4	0.90	10.320	0.200	0.459	0.010	0.54	2504	22	2435	45	2458	18	97		
45	z45	0.13	89	4	63	3	60	3	0.71	5.510	0.130	0.327	0.007	0.44	2003	24	1818	34	1899	19	91		
46	z46	0.04	281	9	171	3	180	5	0.61	4.925	0.072	0.325	0.005	0.54	1804	16	1810	25	1809	12	100		
47	z47	0.06	184	5	128	2	135	4	0.69	6.180	0.100	0.362	0.006	0.56	2008	15	1995	27	2003	14	99		
48	z48	0.03	329	8	50	1	70	3	0.15	10.380	0.180	0.444	0.008	0.66	2552	16	2371	35	2464	16	93		
49	z49	0.10	84	4	26	1	38	2	0.30	10.970	0.240	0.442	0.011	0.56	2649	23	2349	47	2517	20	89	x	
50	z50	3.51	253	7	69	2	114	6	0.27	6.660	0.130	0.331	0.007	0.59	2297	24	1840	34	2069	17	80	x	
51	z51	0.36	32	1	29	1	29	1	0.91	5.690	0.210	0.334	0.010	0.29	2058	41	1850	47	1890	31	90		
52	z52	0.08	148	5	25	1	33	2	0.17	6.080	0.140	0.350	0.007	0.52	2027	22	1933	32	1982	20	95		
53	z53	3.21	401	11	63	2	98	4	0.16	2.864	0.053	0.189	0.003	0.50	1812	22	1118	19	1372	14	81	x	
54	z54	0.02	647	22	188	4	213	5	0.29	7.160	0.120	0.385	0.007	0.68	2160	14	2096	33	2132	15	97		
55	z55	0.04	290	8	154	4	164	6	0.53	5.451	0.086	0.337	0.006	0.61	1911	15	1868	27	1892	13	98		
56	z56	1.96	352	10	172	3	197	7	0.49	5.350	0.110	0.322	0.007	0.53	1968	23	1791	33	1870	18	91		
57	z57	0.03	408	12	193	3	201	6	0.47	6.000	0.084	0.359	0.005	0.55	1960	14	1972	26	1974	12	101		
58	z58	0.03	375	13	296	8	292	11	0.79	5.688	0.091	0.339	0.006	0.62	1970	16	1883	30	1926	14	96		
59	z59	0.09	125	4	116	2	116	4	0.93	5.440	0.120	0.341	0.007	0.57	1874	23	1889	33	1886	18	101		
60	z60	0.06	183	5	131	2	142	4	0.72	6.130	0.100	0.362	0.007	0.50	2009	18	1988	31	1992	14	99		
61	z61	0.09	132	5	63	2	68	2	0.48	5.860	0.120	0.345	0.007	0.55	1993	20	1907	32	1951	17	96		
62	z62	0.03	353	11	261	7	270	8	0.74	5.960	0.110	0.351	0.007	0.61	2006	16	1936	31	1965	15	97		
63	z63	0.08	102	4	70	3	87	3	0.68	10.380	0.180	0.446	0.009	0.53	2547	18	2381	40	2468	17	93		
64	z64	0.11	102	5	37	2	36	2	0.37	5.550	0.130	0.333	0.007	0.41	1964	27	1848	32	1904	21	94		
RPB25																							6
1	z1	0.03	205	9	76	3	58	3	0.37	6.860	0.110	0.360	0.006	0.64	2169	14	1978	27	2090	14	91		
2	z2	0.01	370	11	33	1	41	1	0.09	12.960	0.190	0.468	0.007	0.72	2789	11	2472	29	2672	14	89		
3	z3	0.32	27	1	29	1	23	1	1.05	3.900	0.120	0.285	0.008	0.33	1628	41	1614	39	1603	26	99		
4	z4	0.03	269	7	86	1	86	2	0.32	6.371	0.097	0.359	0.006	0.57	2055	15	1975	29	2026	13	96		
5	z5	0.01	863	26	644	12	558	15	0.75	4.656	0.052	0.315	0.004	0.68	1730	10	1762	19	1758	9	102		
6	z6	0.07	90	3	63	1	60	2	0.70	6.170	0.100	0.360	0.006	0.42	1980	19	1983	29	1999	15	100		
7	z7	0.20	45	1	51	1	42	2	1.15	3.950	0.100	0.282	0.007	0.29	1713	35	1591	35	1625	22	93		
8	z8	0.08	110	3	95	4	73	3	0.87	3.800	0.085	0.274	0.006	0.50	1641	24	1556	31	1590	18	95		
9	z9	0.19	45	1	36	1	29	1	0.80	3.947	0.083	0.284	0.006	0.37	1663	24	1606	27	1616	17	97		
10	z10	0.14	61	3	48	2	38	2	0.79	3.942	0.075	0.283	0.005	0.40	1656	22	1605	25	1624	16	97		
11	z11	0.18	46	1	53	1	48	1	1.17	4.610	0.110	0.308	0.007	0.35	1773	27	1727	33	1744	20	97		

12	z12	0.02	264	15	79	2	91	4	0.30	7.250	0.120	0.392	0.007	0.56	2130	16	2126	32	2138	15	100	
13	z13	0.01	719	22	247	6	263	8	0.34	6.974	0.083	0.382	0.006	0.64	2111	12	2089	26	2107	11	99	
14	z14	0.03	248	7	267	4	230	5	1.08	4.654	0.058	0.310	0.004	0.57	1753	13	1744	20	1754	10	99	
15	z15	0.03	184	7	186	8	181	8	1.01	6.450	0.100	0.372	0.006	0.59	2014	16	2032	29	2036	14	101	
16	z16	0.03	302	7	139	2	139	3	0.46	5.912	0.096	0.344	0.006	0.65	2016	15	1907	30	1960	14	95	
17	z17	0.04	168	6	132	4	130	4	0.78	5.922	0.088	0.344	0.005	0.55	2003	14	1905	24	1963	13	95	
18	z18	0.20	46	1	37	1	30	1	0.80	4.010	0.110	0.288	0.008	0.37	1705	35	1627	38	1630	23	95	
19	z19	0.02	340	11	36	1	37	1	0.10	6.500	0.068	0.368	0.004	0.65	2066	9	2016	20	2045	9	98	
20	z20	0.06	154	4	107	2	94	3	0.70	4.597	0.086	0.307	0.006	0.55	1754	19	1729	27	1749	16	99	
21	z21	0.02	348	9	48	2	57	3	0.14	6.200	0.097	0.353	0.007	0.63	2063	15	1954	32	2009	14	95	
22	z22	0.03	255	8	25	1	20	1	0.10	5.407	0.076	0.306	0.004	0.59	2053	14	1718	22	1888	12	84	
23	z23	0.07	98	4	111	3	106	3	1.14	6.150	0.120	0.354	0.007	0.55	2009	20	1956	31	1995	17	97	
24	z24	0.02	334	12	245	12	258	12	0.73	6.798	0.093	0.382	0.006	0.59	2062	14	2082	27	2085	12	101	
25	z25	0.04	183	8	43	1	45	1	0.23	7.560	0.120	0.400	0.006	0.53	2180	14	2166	29	2177	14	99	
26	z26	0.06	99	3	53	1	51	1	0.53	7.640	0.100	0.393	0.006	0.44	2233	15	2132	25	2187	12	95	
27	z27	0.04	165	6	142	5	139	4	0.86	6.750	0.120	0.376	0.007	0.54	2102	18	2053	34	2073	15	98	
28	z28	0.01	681	12	275	5	237	4	0.40	6.480	0.083	0.361	0.005	0.67	2078	12	1981	25	2045	11	95	
29	z29	0.20	47	2	75	2	57	2	1.60	3.844	0.082	0.275	0.005	0.38	1660	25	1560	24	1598	17	94	
30	z30	0.05	128	5	132	5	129	5	1.03	6.470	0.110	0.377	0.006	0.50	2023	16	2060	28	2039	14	102	
31	z31	0.05	123	3	51	2	67	3	0.41	9.000	0.150	0.401	0.007	0.63	2448	13	2171	31	2336	16	89	
32	z32	0.03	223	3	193	8	209	8	0.86	6.900	0.120	0.376	0.007	0.60	2134	18	2055	33	2097	15	96	
33	z33	0.11	74	2	96	2	77	2	1.30	4.593	0.081	0.309	0.005	0.40	1764	22	1736	24	1747	14	98	
34	z34	0.07	95	2	31	1	29	1	0.33	6.150	0.100	0.337	0.006	0.53	2100	18	1874	28	1997	15	89	
35	z35	0.03	198	10	94	5	120	5	0.48	12.130	0.200	0.453	0.009	0.74	2767	12	2404	38	2610	15	87	
36	z36	0.05	147	5	40	2	38	2	0.27	6.840	0.120	0.372	0.007	0.56	2112	19	2034	31	2091	15	96	
37	z37	0.05	123	4	57	1	61	2	0.46	7.420	0.100	0.387	0.006	0.54	2212	14	2102	25	2163	12	95	